



National Library  
of Canada

Bibliothèque nationale  
du Canada

Canadian Theses Service

Services des thèses canadiennes

Ottawa, Canada  
K1A 0N4

## CANADIAN THESES

### NOTICE

The quality of this microfiche is heavily dependent upon the quality of the original thesis submitted for microfilming. Every effort has been made to ensure the highest quality of reproduction possible.

If pages are missing, contact the university which granted the degree.

Some pages may have indistinct print especially if the original pages were typed with a poor typewriter ribbon or if the university sent us an inferior photocopy.

Previously copyrighted materials (journal articles, published tests, etc.) are not filmed.

Reproduction in full or in part of this film is governed by the Canadian Copyright Act, R.S.C. 1970, c. C-30. Please read the authorization forms which accompany this thesis.

**THIS DISSERTATION  
HAS BEEN MICROFILMED  
EXACTLY AS RECEIVED**

## THÈSES CANADIENNES

### AVIS

La qualité de cette microfiche dépend grandement de la qualité de la thèse soumise au microfilmage. Nous avons tout fait pour assurer une qualité supérieure de reproduction.

S'il manque des pages, veuillez communiquer avec l'université qui a conféré le grade.

La qualité d'impression de certaines pages peut laisser à désirer, surtout si les pages originales ont été dactylographiées à l'aide d'un ruban usé ou si l'université nous a fait parvenir une photocopie de qualité inférieure.

Les documents qui font déjà l'objet d'un droit d'auteur (articles de revue, examens publiés, etc.) ne sont pas microfilmés.

La reproduction, même partielle, de ce microfilm est soumise à la Loi canadienne sur le droit d'auteur, SRC 1970, c. C-30. Veuillez prendre connaissance des formules d'autorisation qui accompagnent cette thèse.

**LA THÈSE A ÉTÉ  
MICROFILMÉE TELLE QUE  
NOUS L'AVONS REÇUE**

244

0-315-26975-8

National Library  
of CanadaBibliothèque nationale  
du Canada

Canadian Theses Division Division des thèses canadiennes

Ottawa, Canada  
K1A 0N4**PERMISSION TO MICROFILM — AUTORISATION DE MICROFILMER**

• Please print or type — Écrire en lettres moulées ou dactylographier

Full Name of Author — Nom complet de l'auteur

ROBERT L. SUTHERBY

Date of Birth — Date de naissance

22/07/54

Country of Birth — Lieu de naissance

CANADA

Permanent Address — Résidence fixe

21 Adamic Cres.  
Leduc, Alberta  
T9E 3N9

Title of Thesis — Titre de la thèse

CORROSION BEHAVIOR OF SURGICAL  
— IMPLANT MATERIALS.

University — Université

THE UNIVERSITY OF ALBERTA

Degree for which thesis was presented — Grade pour lequel cette thèse fut présentée

M.Sc. (METALLURGICAL ENGINEERING)

Year this degree conferred — Année d'obtention de ce grade

1984

Name of Supervisor — Nom du directeur de thèse

DR. S.A. BRADFORD.

Permission is hereby granted to the NATIONAL LIBRARY OF  
CANADA to microfilm this thesis and to lend or sell copies of  
the film.The author reserves other publication rights, and neither the  
thesis nor extensive extracts from it may be printed or other-  
wise reproduced without the author's written permission.L'autorisation est, par la présente, accordée à la BIBLIOTHÈ-  
QUE NATIONALE DU CANADA de microfilmer cette thèse et de  
prêter ou de vendre des exemplaires du film.L'auteur se réserve les autres droits de publication; ni la thèse  
ni de longs extraits de celle-ci ne doivent être imprimés ou  
autrement reproduits sans l'autorisation écrite de l'auteur.

Date

April 12/84

Signature

---

THE UNIVERSITY OF ALBERTA

CORROSION BEHAVIOR OF SURGICAL IMPLANT MATERIALS

by

ROBERT L. SUTHERBY

A THESIS

SUBMITTED TO THE FACULTY OF GRADUATE STUDIES AND RESEARCH  
IN PARTIAL FULFILMENT OF THE REQUIREMENTS FOR THE DEGREE

OF MASTER OF SCIENCE

IN

METALLURGICAL ENGINEERING

DEPARTMENT OF MINERAL ENGINEERING

EDMONTON, ALBERTA

SPRING 1984

THE UNIVERSITY OF ALBERTA

RELEASE FORM

NAME OF AUTHOR ROBERT L. SUTHERBY

TITLE OF THESIS

CORROSION BEHAVIOR OF SURGICAL IMPLANT  
MATERIALS

DEGREE FOR WHICH THESIS WAS PRESENTED MASTER OF SCIENCE

YEAR THIS DEGREE GRANTED SPRING 1984

Permission is hereby granted to THE UNIVERSITY OF  
ALBERTA LIBRARY to reproduce single copies of this thesis  
and to lend or sell such copies for private, scholarly or  
scientific research purposes only.

The author reserves other publication rights, and  
neither the thesis nor extensive extracts from it may be  
printed or otherwise reproduced without the author's written  
permission.

(SIGNED) .....  .....

PERMANENT ADDRESS:

21 Adanic Cres.

Leduc, Alberta

T9E 3N9

DATED: April 12, 1984

THE UNIVERSITY OF ALBERTA  
FACULTY OF GRADUATE STUDIES AND RESEARCH

The undersigned certify that they have read, and recommend to the Faculty of Graduate Studies and Research, for acceptance, a thesis entitled CORROSION BEHAVIOR OF SURGICAL IMPLANT MATERIALS submitted by ROBERT L. SUTHERBY in partial fulfilment of the requirements for the degree of MASTER OF SCIENCE in METALLURGICAL ENGINEERING.

*Samuel A. Bradford*

Supervisor

*Thomas H. Eitel*  
*Michael L. Wayman*  
*Shelley A. Newman*

External Examiner

Date *Feb. 2, 1984*

## DEDICATION

---

I dedicate this thesis  
to my parents

# ABSTRACT

A study has been made of the corrosion and corrosion fatigue behavior of the surgical implant materials 316L stainless steel and the cobalt alloy, Vitallium, in simulated

---

physiological solutions, both with and without organics.

In solutions containing no organics 316L stainless steel was found to be highly susceptible to crevice and pitting corrosion. Under these same conditions, however, Vitallium remained completely passive.

In tests on Vitallium in solutions containing organics it was found that, while glucose had minimal effects on the polarization behavior, serum shifted the corrosion potential in the negative direction. Fortunately, the potential shift occurred wholly within the passive range, so that no increase in the corrosion rate resulted. These tests have also indicated that where Vitallium is involved a saline solution containing serum more closely approximates in vivo conditions, at least in the short term, than does an inorganic saline solution.

In the corrosion fatigue experiments it was determined, with a high degree of probability, that serum reduces the corrosion fatigue life of Vitallium. However, the means by which this reduction occurs, without changing the basic fracture mechanism, was not determined.

## ACKNOWLEDGEMENTS

---

The author expresses his appreciation and thanks to:

Dr. Samuel A. Bradford for his supervision, encouragement,  
and patience over the past five years,

Mr. Bob Konzuk, Mr. Tom Forman, Mrs. Tina Barker,

Mr. Dave Skrastins, and Mr. S. Merali for their  
individual expertise in the preparation of this  
thesis,

The Royal Alexandra, University of Alberta, and Misericordia  
Hospitals for their donations of used prostheses,  
from which the test materials were machined, and  
The Howmedica Co. for casting and donating the Vitallium  
fatigue specimens.

Special thanks are also extended to my wife, Eleanor,  
and to my parents; without their prodding and patience this  
thesis would never have been completed.



## Table of Contents

| Chapter   | Page |
|---|------|
| 1. INTRODUCTION .....   | 1    |
| 1.1 Problem Statement .....   | 4    |
| <hr/>   |      |
| 2. SERVICE CONDITIONS .....   | 5    |
| 2.1 Fluids .....  | 5    |
| 2.2 Structural Members .....  | 8    |
| 2.2.1 Loading .....   | 8    |
| 3. THEORY .....   | 10   |
| 3.1 Thermodynamics - The Driving Force .....                        | 10   |
| 3.2 Corrosion Kinetics .....  | 12   |
| 3.2.1 The General Rate Equation .....                               | 14   |
| 3.2.2 Redox Reactions at Equilibrium Conditions .....               | 15   |
| 3.2.3 Non-Equilibrium Conditions .....                              | 16   |
| 3.2.4 Concentration Polarization .....                              | 18   |
| 3.3 Mixed Potential Theory .....                                    | 19   |
| 3.3.1 Passivity .....   | 20   |
| 3.3.2 Breakdown of Passivity .....                                  | 21   |
| 3.3.3 Corrosion Inhibition .....                                    | 22   |
| 3.3.4 Potentiostatic Polarization .....                             | 25   |
| 3.4 Corrosion Fatigue .....   | 28   |
| 3.4.1 The Fatigue Aspect .....                                      | 28   |
| 3.4.2 The Corrosion Aspect .....                                    | 31   |
| 3.4.3 Variables Affecting Corrosion Fatigue<br>Cracking Rates ..... | 32   |
| 3.4.3.1 Mechanical Variables .....                                  | 33   |
| 3.4.3.2 Metallurgical Variables .....                               | 34   |
| 4. LITERATURE REVIEW .....  | 37   |

|         |   |    |
|---------|---|----|
| 4.1     | Stainless Steel .....   | 37 |
| 4.1.1   | Clinical Findings .....   | 37 |
| 4.1.2   | Corrosion Studies .....   | 38 |
| 4.2     | Cobalt Alloys .....   | 42 |
| 4.2.1   | Clinical Findings .....   | 42 |
| 4.2.2   | Corrosion Studies .....   | 42 |
| 4.3     | Effects of Organics on Other Alloy Systems .....                  | 46 |
| 4.4     | Corrosion Fatigue of Cast CoCrMo .....                            | 47 |
| 5.      | MATERIALS AND PROCEDURES .....                                    | 51 |
| 5.1     | Test Materials .....  | 51 |
| 5.1.1   | Stainless Steel .....   | 54 |
| 5.1.1.1 | Metallographic Examination .....                                  | 54 |
| 5.1.1.2 | Hardness Results .....  | 55 |
| 5.1.2   | Cast Vitallium .....  | 56 |
| 5.1.2.1 | Metallographic Examination .....                                  | 58 |
| 5.1.2.2 | Hardness Results .....  | 60 |
| 5.1.2.3 | Tensile Results .....   | 60 |
| 5.1.3   | Water .....   | 62 |
| 5.1.4   | Simulated Physiological Solutions .....                           | 62 |
| 5.1.5   | Gases .....   | 64 |
| 5.2     | Polarization Studies .....  | 64 |
| 5.2.1   | Development of Experimental Procedure .....                       | 64 |
| 5.2.1.1 | Test Apparatus .....  | 65 |
| 5.2.1.2 | Procedures .....  | 69 |
| 5.2.2   | Polarization Studies in Simulated<br>Physiological Solution ..... | 72 |
| 5.2.2.1 | Procedures .....  | 72 |

|   |     |
|---|-----|
| 5.3 Corrosion Fatigue .....   | 73  |
| 5.3.1 Apparatus .....   | 73  |
| 5.3.1.1 The Load Frame .....  | 73  |
| 5.3.1.2 The Cell .....  | 75  |
| 5.3.1.3 Solution Conditioning And<br>Circulation .....  | 75  |
| 5.3.2 Samples .....   | 75  |
| 5.3.3 Test Solutions .....  | 77  |
| 5.3.4 Procedures .....  | 77  |
| 5.4 Conventions .....   | 79  |
| 6. RESULTS AND DISCUSSION .....   | 80  |
| 6.1 Technique Development .....   | 80  |
| 6.2 316L Stainless Steel and Cast Vitallium in<br>Serum-Free and Glucose-free Solution .....          | 80  |
| 6.2.1 Stainless Steel .....   | 80  |
| 6.2.2 Cast Vitallium .....  | 87  |
| 6.2.3 316L vs. Vitallium .....  | 89  |
| 6.3 The Effects of Organics on the Corrosion of Cast<br>Vitallium .....                               | 92  |
| 6.3.1 Preliminary Tests on the Effects of<br>Organics .....   | 93  |
| 6.3.1.1 The Effects of Glucose in the<br>Absence of Serum .....                                       | 93  |
| 6.3.1.2 Solution pH .....   | 97  |
| 6.3.2 The Effects of Glucose and Serum on the<br>Cathodic Polarization Behavior of<br>Vitallium ..... | 100 |
| 6.3.2.1 No Glucose and No Serum - NG/NS ..  | 100 |
| 6.3.2.2 Glucose With and Without Serum -<br>G/S and G/NS .....  | 104 |

|  |     |
|--|-----|
| 6.3.2.3. Glucose-Free Solution Containing Serum - NG/S .....                           | 115 |
| 6.3.3 The Effects of Organic Additions on the Polarization Behavior of Vitallium ..... | 117 |
| 6.4 Corrosion Fatigue .....  | 119 |
| 6.4.1 Fractographic Results .....  | 121 |
| 6.4.1.1 Flat Fracture .....  | 121 |
| 6.4.1.2 Mixed-Mode Fracture .....  | 124 |
| 6.4.2 The Effects of Organics on the Corrosion Fatigue Behavior of Vitallium .....     | 124 |
| 7. CONCLUSIONS .....   | 126 |
| 7.1 Potentiostatic Polarization Tests .....  | 126 |
| 7.2 Corrosion Fatigue Tests .....  | 127 |
| 8. RECOMMENDATIONS .....   | 128 |
| REFERENCES .....   | 130 |
| APPENDIX A .....   | 140 |
| APPENDIX B .....   | 142 |
| APPENDIX C .....   | 144 |

## List of Tables

| Table   | Page |
|---|------|
| 2.1 Static Composition of Interstitial Fluid.....                                 | 7    |
| 3.1 Examples of Organic Corrosion Inhibitors.....                                 | 25   |
| 4.1 Results Reported by Hughes et al.....   | 49   |
| <hr/>   |      |
| 5.1 Chemical Composition of Stainless Steel<br>Test Material.....                 | 54   |
| 5.2 Hardness of Stainless Steel Test Material.....                                | 56   |
| 5.3 Chemical Composition of Vitallium Test Materials....                          | 57   |
| 5.4 Hardness of Vitallium Test Materials.....                                     | 60   |
| 5.5 Tensile Properties of Vitallium Fatigue Specimens...                          | 61   |
| 5.6 Composition of Simulated Physiological Solution....                           | 63   |
| 5.7 Gas Compositions.....   | 64   |
| 5.8 Decade Resistor Values.....   | 69   |
| 6.1 Polarization Parameters for 316L in<br>Saline Solution.....                   | 83   |
| 6.2 Corrosion Parameters for 316L without a Crevice.....                          | 85   |
| 6.3 Polarization Parameters for Vitallium in<br>Glucose-Free Saline Solution..... | 87   |
| 6.4 Anodic Polarization Parameters.....   | 91   |
| 6.5 Corrosion Parameters in Solution<br>Containing Glucose but no Serum.....      | 94   |
| 6.6 Preliminary Corrosion Parameters for<br>Glucose and Serum.....                | 97   |
| 6.7 pH Readings.....  | 98   |
| 6.8 Corrosion Potentials at the Four<br>Glucose-Serum Combinations.....           | 117  |
| 6.9 Corrosion Fatigue Lives.....  | 119  |
| 6.10 Results of Statistical Analyses of<br>Corrosion Fatigue Life Data.....       | 120  |

Table

Page

A.1 Compositions of Various Inorganic Test Solutions....141

C.1 Fatigue Life Data in Natural Logarithm Form.....146

## List of Figures

| Figure | Page   |
|--------|--|
| 2.1    | Diagram of Joint Structure.....6   |
| 2.2    | Hip Joint Load Profile During Walking.....9  |
| 3.1    | Energies Associated with a Spontaneous Reaction.....13   |
| 3.2    | Evans Diagram for Two Simultaneous Redox Reactions..17   |
| 3.3    | Variations in the Form of the<br>Polarization Curve During Reverse Scanning.....23   |
| 3.4    | Anodic Inhibition.....26   |
| 3.5    | Cathodic Inhibition.....26   |
| 3.6    | Plastic Blunting Fatigue Crack<br>Propagation Mechanism.....30   |
| 5.1    | Initial System Components.....66   |
| 5.2    | Operational Amplifier Characteristic Curve.....68  |
| 5.3    | Second Potentiostat and Current Measuring System....71   |
| 6.1    | Experimental Polarization Plot for 430<br>Stainless Steel in 1N H <sub>2</sub> SO <sub>4</sub> .....81   |
| 6.2    | Standard Potentiostatic Anodic<br>Polarization Plot for 430 Stainless Steel<br>in 1N H <sub>2</sub> SO <sub>4</sub> . Taken from ASTM G5-78.....82 |
| 6.3    | Polarization Curves for 316L in<br>Glucose-Free and Serum-Free Simulated<br>Physiological Solution.....84  |
| 6.4    | Polarization Curve for 316L in<br>Semi-Submerged Position.....86   |
| 6.5    | Polarization Curves for Vitallium in<br>Glucose-Free and Serum-Free Solution.....88  |
| 6.6    | Current-Time Traces for 316L and Vitallium.....90  |
| 6.7    | Preliminary Polarization Curves for<br>Vitallium in Solution Containing Glucose<br>but no Serum.....95   |

| Figure  | Page |
|---|------|
| 6.8 Preliminary Polarization Curves for<br>Vitallium in Solution Containing Glucose<br>and Serum.....               | 96   |
| 6.9 Variation of Corrosion Potential of<br>Vitallium in Oxygenated Solution<br>Containing Glucose but no Serum..... | 99   |
| 6.10 Polarization Behavior of Vitallium in<br>Glucose-Free and Serum-Free Solution.....                             | 101  |
| 6.11 Cathodic Polarization of Vitallium in<br>Serum-Free Solution.....  | 105  |
| 6.12 Polarization Behavior of Vitallium in<br>Solution Containing 0.01% Serum.....                                  | 106  |
| 6.13 Polarization Behavior of Vitallium in<br>Solution Containing 0.1% Serum.....                                   | 107  |
| 6.14 Cathodic Polarization Behavior of<br>Vitallium in Solution Containing 5% Serum.....                            | 108  |
| 6.15 Polarization Behavior of Vitallium in<br>Solution Containing 15% Serum.....                                    | 109  |
| 6.16 The Variation in the Corrosion Potential<br>of Vitallium with Serum Concentration.....                         | 111  |
| 6.17 Incomplete Cathodic Polarization Curve<br>for Vitallium obtained with 0.001% Serum.....                        | 113  |
| 6.18 Polarization Curves for Vitallium in<br>Glucose-Free Solution Containing Serum.....                            | 116  |



## List of Plates

| Plate  | Page |
|--|------|
| 1.1 Assorted Orthopaedic Implants.....   | 2    |
| 5.1 Fractured Stainless Steel Implant.....   | 52   |
| 5.2 Intact Vitallium Implant.....  | 52   |
| 5.3 Typical Microstructure of the 316L<br>Stainless Steel (100X).....                                | 54   |
| 5.4 Typical Microstructure of Vitallium Hip<br>Implant (100X).....                                   | 59   |
| 5.5 Typical Microstructure of Cast Vitallium<br>Fatigue Specimen (100X).....                         | 59   |
| 5.6 Equipment Used in Later Potentiostatic<br>Polarization Testing.....                              | 70   |
| 5.7 Equipment Arrangement for Corrosion<br>Fatigue Testing.....                                      | 74   |
| 5.8 The Corrosion Fatigue Cell.....  | 76   |
| 5.9 Fatigue Specimens showing the Typical<br>Location of the Notch.....                              | 78   |
| 5.10 Notch Geometry (50X).....   | 78   |
| 6.1 Fracture Surface Adjacent to the Notch on<br>a Specimen Tested in Serum-Free Solution (1000X)... | 122  |
| 6.2 Cleavage in Two Adjacent Grains (1200X).....   | 123  |
| 6.3 Typical Cleavage Fracture near the Final<br>Fracture Zone (900X).....                            | 123  |

## 1. INTRODUCTION

Implants, or prostheses, are devices surgically placed in the body to carry out either an active or a passive function which the body cannot naturally perform. It may be to replace a damaged or worn part as is the case for joint or heart valve replacements; to rectify the mode of operation of an organ, for instance a pacemaker; to correct a structural deformity, for instance, a spinal brace; or to simulate an absent or disfigured part of the anatomy, as are the cases in breast and facial reconstructions. Materials for these roles include metals, polymers, and recently, ceramics and modified transplanted materials, such as collagen and bone. Figure 1.1 shows several types of metallic orthopaedic implants, including total hip and knee replacements, a shoulder prosthesis and various bone nails and pins.

Regarding metallic surgical materials, Venable and Stuck wrote the following in 1947:

The effort to find strong materials attracted the interest of many different surgeons in the past and then, as now, they adopted the most immediately available metallic materials and modified them to their use.'

Before the electrochemical aspects of implant degradation were fully appreciated the above philosophy was responsible for the use of such materials as bronze and iron for external suture, lead shot to hold internal silver sutures, and magnesium as resorbable suture and bone plates.

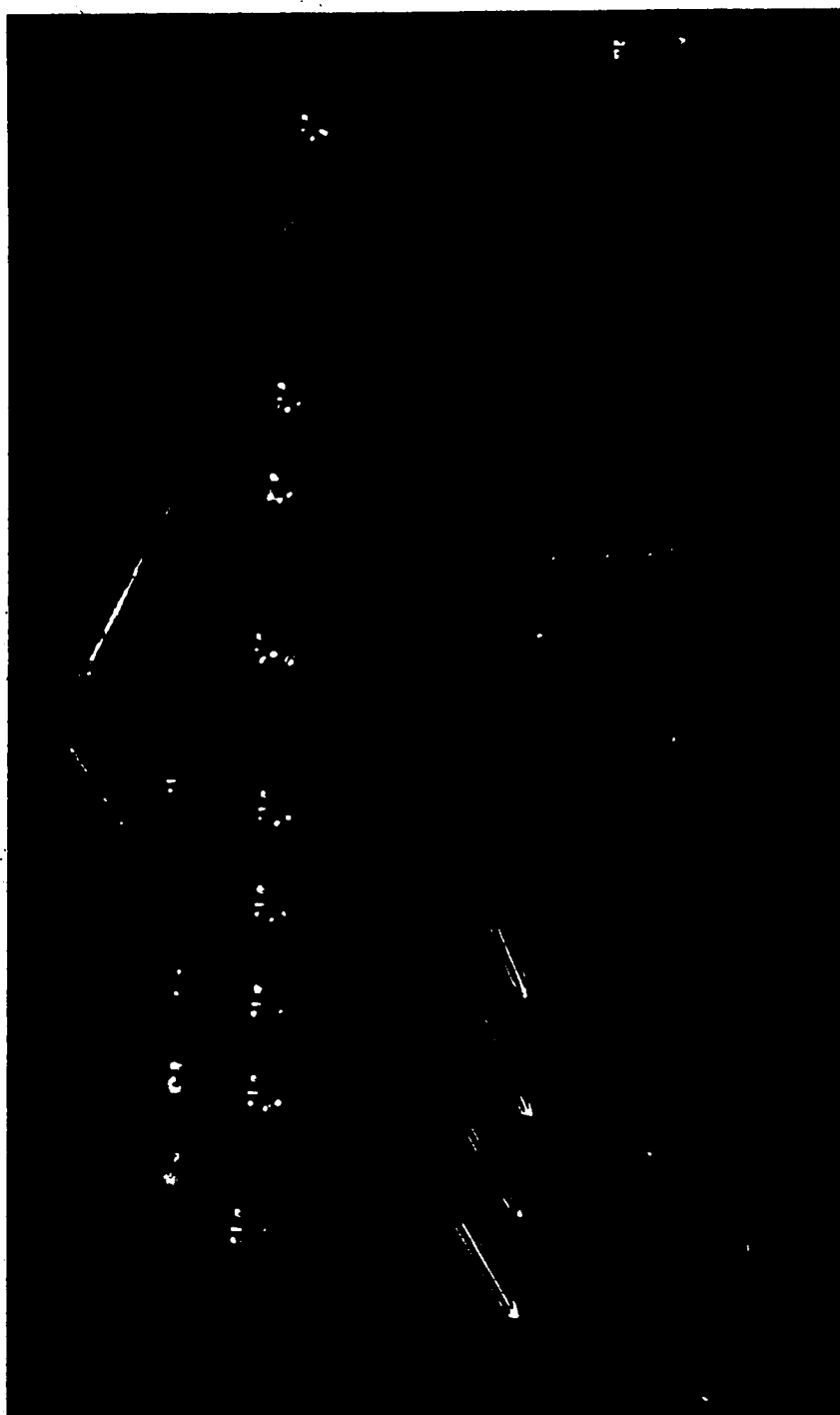


Plate 1.1 Assorted Orthopaedic Implants

According to Williams and Roaf<sup>2</sup>, in 1906 John B. Murphy recommended the use of stove pipe wire and carpenter nails and screws for bone fixation.

---

In response to a flood of new alloys in the early years of this century, tests were conducted to determine their biocompatibilities. In 1926, Austenal Laboratories patented a CoCrMo alloy to be used for dental purposes; they named it 'Vitallium'. Seven years later, after conducting in vivo and clinical tests, Venable and Stuck reported that this material was "completely inert in body fluids". It appears that it was their recommendations based on these findings that initiated the long and extensive use of this alloy group in orthopaedic and other surgical applications.

Some time after 1926 Krupp "18-8 stainless steel" (roughly equivalent to AISI 302) was found to exhibit greater resistance to the body than the widely used vanadium steel, even though it was known to experience pitting corrosion. Later, molybdenum-modified "18-8 SMO" (an early version of AISI 316) with greater resistance to pitting displaced the earlier version.

Such an improvement were these new implant materials over their predecessors that, over forty years later, they continue to be the two most widely used. However, they have not been totally without failure for, in addition to infection and loosening of devices, excessive wear and fracture still claim a number of implants each year. For this reason, research and development into new materials is

ongoing.

---

### 1.1 Problem Statement

One of the major criteria for the acceptance of a prospective material is its resistance to corrosion in the human body. Since it is impractical or dangerous to make all the necessary tests in vivo (animal or human), simulated, in vitro, conditions are substituted. In the past, most researchers used solutions similar in content to the inorganic fraction of body fluids, based on the conventional wisdom that the extent of damage increases with the chloride ion concentration.

Recent findings, however, indicate that physiological organics can significantly affect the corrosion behavior of some materials. It is, therefore, the aim of this research to investigate the effects of organics on the corrosion and corrosion fatigue of one of the most often used implant materials, the cast cobalt alloy, Vitallium. Preliminary work will also involve the use of AISI 316L stainless steel.

## 2. SERVICE CONDITIONS

Surrounding a prosthesis is a dynamic system of flowing electrolytes, together with living and moving muscle and bone. The following is a brief description of the in vivo conditions in which orthopaedic implants must perform<sup>1</sup>.

### 2.1 Fluids

About 56% of the body weight is made up of fluids. Of this, 38% exists outside the cells as extracellular fluids which include plasma, cerebrospinal, gastrointestinal, synovial, and interstitial fluids. It is primarily with the latter two of these that prostheses interact.

Synovial fluid, contained within the joints, is basically a dialysate of blood plasma. With the addition of hyaluronic acid, the fluid is responsible for the lubrication and nutrition of the adjacent articular cartilage joint surfaces. When hips, elbows, or knee joints are involved this fluid is in contact with the prosthesis, Figure 2.1.

Interstitial fluid, or physiological saline solution, lies in the spaces between the cells of both soft tissue and bone. Its major physiological roles are in the maintenance of constant conditions in the internal environment, and as a medium for the transport of nutrients, oxygen, and carbon dioxide between the cells and the capillaries. As with all extracellular fluids, the ionic and nonionic components are constantly being mixed throughout the body by various

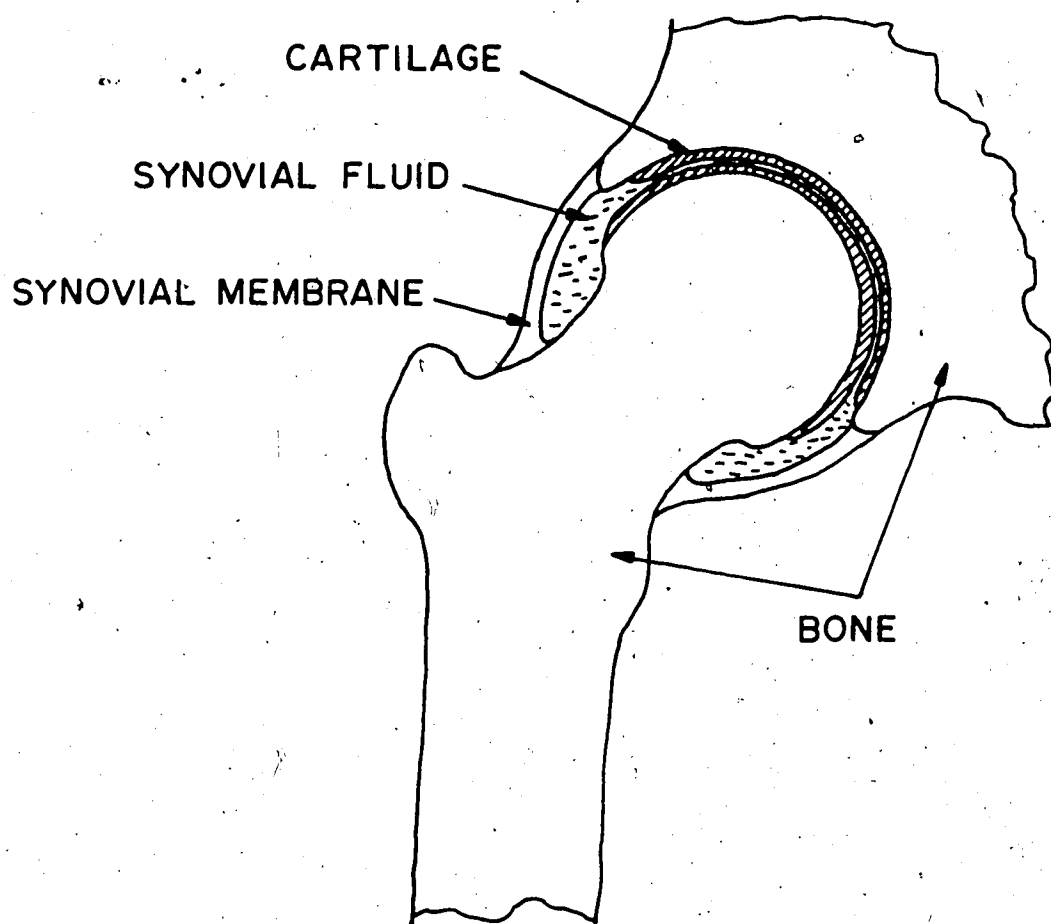


Figure 2.1 Diagram of Joint Structure

transport mechanisms. The normal static concentrations of the fluid components<sup>3</sup> are given in Table 2.1.

Table 2.1  
Static Composition of Interstitial Fluid

| <u>Component</u>  | <u>Interstitial<br/>(mg/L. of water)</u> |
|---|--|
| Na <sup>+</sup>   | 3150                                     |
| K <sup>+</sup>  | 184                                      |
| Ca <sup>++</sup>  | 96                                       |
| Mg <sup>++</sup>  | 34                                       |
| Cl <sup>-</sup>   | 4000                                     |
| HCO <sub>3</sub> <sup>-</sup>   | 1726                                     |
| HPO <sub>4</sub> <sup>-</sup> , H <sub>2</sub> PO <sub>4</sub> <sup>-</sup> | 194                                      |
| SO <sub>4</sub> <sup>-</sup>  | 48                                       |
| Amino Acids   | 0.3                                      |
| Creatine  | 26                                       |
| Lactate   | 108                                      |
| Glucose   | 1000                                     |
| Protein   | 20                                       |
| Urea  | 240                                      |

Arterial blood is regulated by several buffer and transport systems to within a few percentiles of pH 7.4. Due to a higher carbon dioxide concentration gradient interstitial fluid is maintained closer to pH 7.35.

The temperature of the body is rigorously maintained at 37°C.



## 2.2 Structural Members

The structural members of the body consist mainly of muscle and bone; muscle developing and supporting the tensile loads, and bones supporting the tensile and compressive loads.

Bone can be described as a biological tissue consisting of long and highly oriented fibres of collagen, densely packed with small crystallites of hydroxyapatite. When reacting to short term loads, bone behaves in a viscoelastic manner, and in response to long term static and dynamic stresses the bone fibres become reoriented to facilitate support of the load.

### 2.2.1 Loading

Loading on the bones and joints varies between that produced by the minor postural changes during sleep, to that developed during the more strenuous activities of walking, running, and jumping. Rydell<sup>4</sup> showed that loads on the hip can be as high as two to three times the body weight while walking, and, according to Paul<sup>5</sup>, can reach seven times body weight for young people. Figure 2.2 shows a typical load profile developed on the hip during one walking cycle.

As walking produces between 1 and 2.5 million cycles per year, and because the average age of implant recipients is falling, there is a growing need for prosthesis materials with longer fatigue lives.

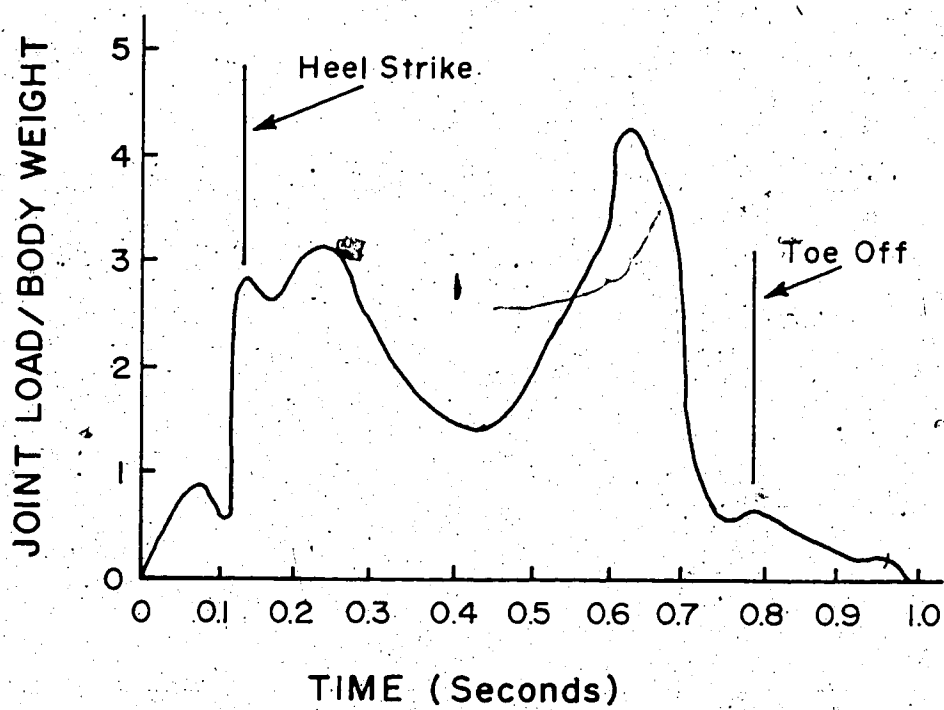


Figure 2.2 Hip Joint Load Profile During Walking

### 3. THEORY

This section will deal with the theory of corrosion commencing with the thermodynamics and kinetics. With the aid of the general rate equation, potential-current plots, or Evans' Diagrams, will be presented and used to discuss mixed potential theory.

#### 3.1 Thermodynamics - The Driving Force

In electrochemistry, the free energy of a reactant or product is given by the addition of its chemical free energy and an electrical energy term, as follows:

$$G_{ec} = G_c + q\Phi \quad \text{.....(1)}$$

where

$G_{ec}$  = the electrochemical free energy,

$G_c$  = the chemical free energy,

$q\Phi$  = the electrical energy given by the product of the charge and the electric potential at that point.

When molar quantities are in use, the electrochemical free energy of a substance is given by:

$$G_{ec} = G_c + zF\Phi \quad \text{.....(2)}$$

where

$zF$  = the charge transferred in the reaction.

According to the second law of thermodynamics, a reaction will be spontaneous if there is a net loss of free energy as the reactants form products. Thus, in terms of the above expressions, the condition for spontaneity is given

by:

$$\Delta G_{ec} + zFE < 0 \quad \dots\dots(3)$$

where

$E$  = the potential difference, or voltage.

From this last expression it is evident that a corollary to the second law is that at electrochemical equilibrium, the magnitudes of the chemical free energy and the electrical energy are equal:

$$\Delta G_{ec} = -zFE \quad \dots\dots(4)$$

When conditions are other than standard, and when the reaction is written in the reduction form, the change in free energy varies with the chemical activities or concentrations according to the van't Hoff isotherm:

$$\Delta G = \Delta G^\circ + RT \ln ([REDUCED]/[OXIDIZED]) \quad \dots\dots(5)$$

where

$\Delta G^\circ$  = the chemical free energy at standard conditions.

By inserting equation (4) into (5) the equilibrium conditions can be expressed in terms of the readily measurable electric potential difference. Thus:

$$\begin{aligned} E_r &= E^\circ - (RT/zF) \ln ([Re]/[Ox]) \quad \dots\dots(6) \\ &= E^\circ - (0.0591/z) \log ([Re]/[Ox]) \text{ at } 25^\circ\text{C} \end{aligned}$$

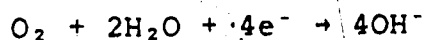
where

$E^\circ$  = the equilibrium redox potential at standard conditions.

This relationship, known as the Nernst Equation, defines the equilibrium redox potential at a given

temperature and concentrations of reactants and products.

Consider, for example, the following cathodic reaction:



According to equation (6) the equilibrium potential at 25°C is:

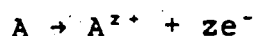
$$\begin{aligned} E_r &= 0.40 + (0.0591/4) \log(p\text{O}_2) - 0.0591 \log[\text{OH}^-] \\ &= 1.227 + 0.0148 \log(p\text{O}_2) - 0.0591\text{pH} \end{aligned}$$

If potential,  $E$ , is plotted against pH, this equation would describe a series of parallel lines of slope -0.0591, and position depending on the oxygen partial pressure.

More generally, if the reactions involving a metal and an aqueous solution are plotted, a potential-pH, or Pourbaix, diagram could be constructed showing the domains of stability of all reactants and products, and would, therefore, define the conditions under which the metal should thermodynamically be either free from corrosion, or should corrode.

### 3.2 Corrosion Kinetics

Although a spontaneous reaction will, by definition, reduce the energy of the system, some minimum activation energy is required before the reaction can proceed. This notion of activation energy is illustrated in Figure 3.1 for the following hypothetical reaction:



Although the reaction involves a reduction in energy, a quantity of energy at least equal to  $\Delta G^*$  must be supplied to

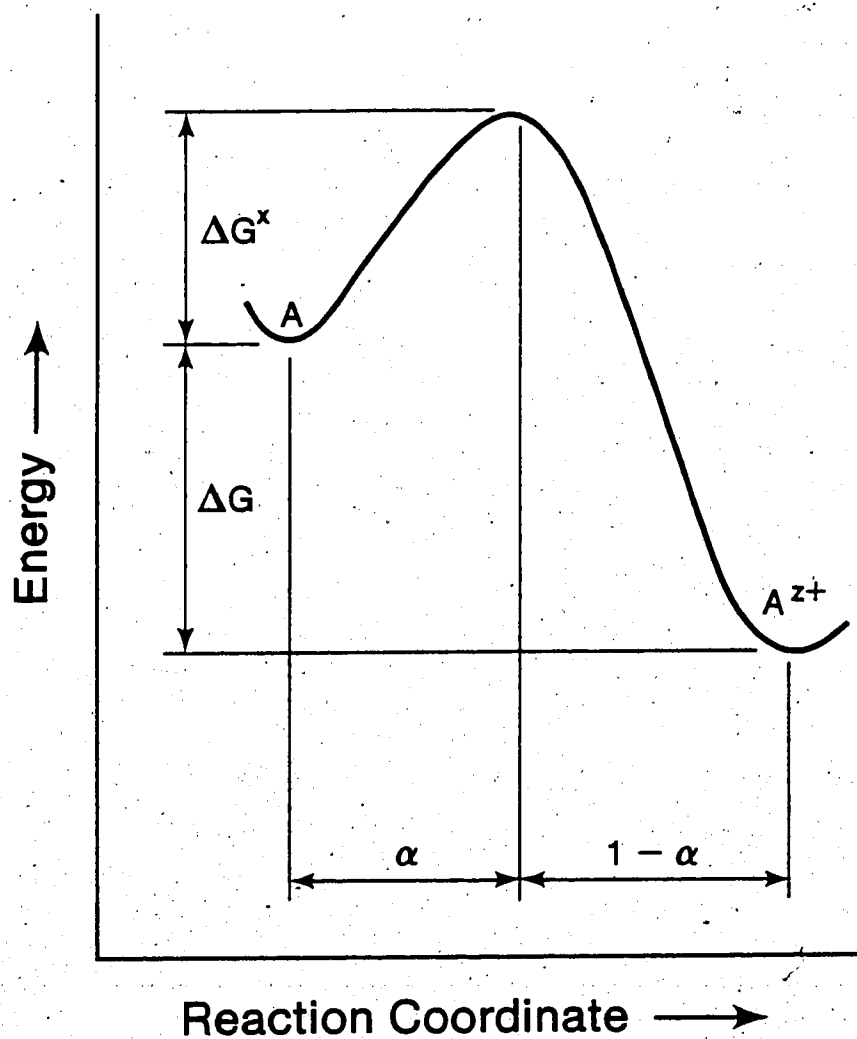


Figure 3.1 Energies Associated with a Spontaneous Reaction

overcome the energy barrier. Where corrosion reactions are involved this 'activation energy' results from the inherent, random, thermal vibration among the atoms.

---

### 3.2.1 The General Rate Equation

According to Maxwell's Distribution Law the number of particles,  $N$ , in a total population,  $M$ , having an energy at least equal to a value,  $E$ , is given by:

$$N = M \exp(-E/kT) \quad \dots\dots(7)$$

where

$k$  = Boltzmann's constant,

$T$  = absolute temperature.

In corrosion,  $N$  is proportional to the rate of the reaction, and the equation, on a molar basis, takes on the following form:

$$\text{Rate} = K [A] \exp(-\Delta G^\circ/RT) \quad \dots\dots(8)$$

where

$[A]$  = the concentration of reactant A,

$R$  = the universal gas constant,

$K$  = a constant of proportionality which

includes the rate of thermal vibration,

a measure of the reversibility of

the reaction, etc.

If the rate of the reaction is expressed in moles/second, the rate of the corrosion process can be expressed in terms of electrical current using Faraday's Law:

$$\text{rate} = i/(zF) \quad \text{.....(9)}$$

where

$i$  is the current density, or the electrical  
current involved per unit area.

---

### 3.2.2 Redox Reactions at Equilibrium Conditions

When a metal is placed in a solution of its ions the activation energy changes as a charge separation occurs across the interface. Because this electrified interface has an associated electric field any particle crossing the region will be acted upon by the field, and the height of the activation energy barrier will be altered. Substituting the new activation energy term into the basic anodic rate equation gives the following expression for the equilibrium corrosion rate:

$$\begin{aligned} i_a &= KzF \exp[-(\Delta G^\circ - azFE_r)/RT] \\ &= K' zF \exp[azFE_r/RT] \end{aligned} \quad \text{.....(10)}$$

The cathodic reaction has a similar form:

$$i_c = K'' zF \exp[-(1-a)zFE_r/RT] \quad \text{.....(11)}$$

where

$a$  is a measure of the symmetry of the  
energy barrier with respect to the peak.

$i_a$ ,  $i_c$  are the anodic and cathodic  
current densities, respectively.

As the magnitudes of the anodic and the cathodic  
reactions are equal at equilibrium the net current flow is



zero. The magnitude of the current flowing in either direction is referred to as the exchange current density,  $i_0$ .

### 3.2.3 Non-Equilibrium Conditions

If a potential is supplied from an external power source the electrode reactions will deviate from the equilibrium state. If, for example, the metal is made more positive (noble), the activation energy for dissolution will be reduced while that for oxidation will be increased.

Substituting the new value of the activation energy gives the following equations:

$$\text{Anodic } i_a = i_0 \exp[azF\eta/RT] \quad \dots\dots(12)$$

$$\text{Cathodic } i_c = i_0 \exp[-(1-a)zF\eta/RT] \quad \dots\dots(13)$$

and a net rate (in this case anodic) of:

$$\begin{aligned} i_{\text{net}} &= i_a - i_c \\ &= i_0 [\exp(azF\eta/RT) - \exp(-(1-a)zF\eta/RT)] \quad \dots\dots(14) \end{aligned}$$

where

$\eta$  is the overpotential, or difference between the electrode potential and the corrosion potential, thus  $E - E_r$ .

A visual summary of the corrosion kinetics can be obtained by plotting this latter equation, in terms of potential,  $E$ , versus the logarithm of the reaction current density,  $i$ , as shown in Figure 3.2 for two redox reactions involving species 'A' and 'B'. This is sometimes referred to as an 'Evans Diagram'.

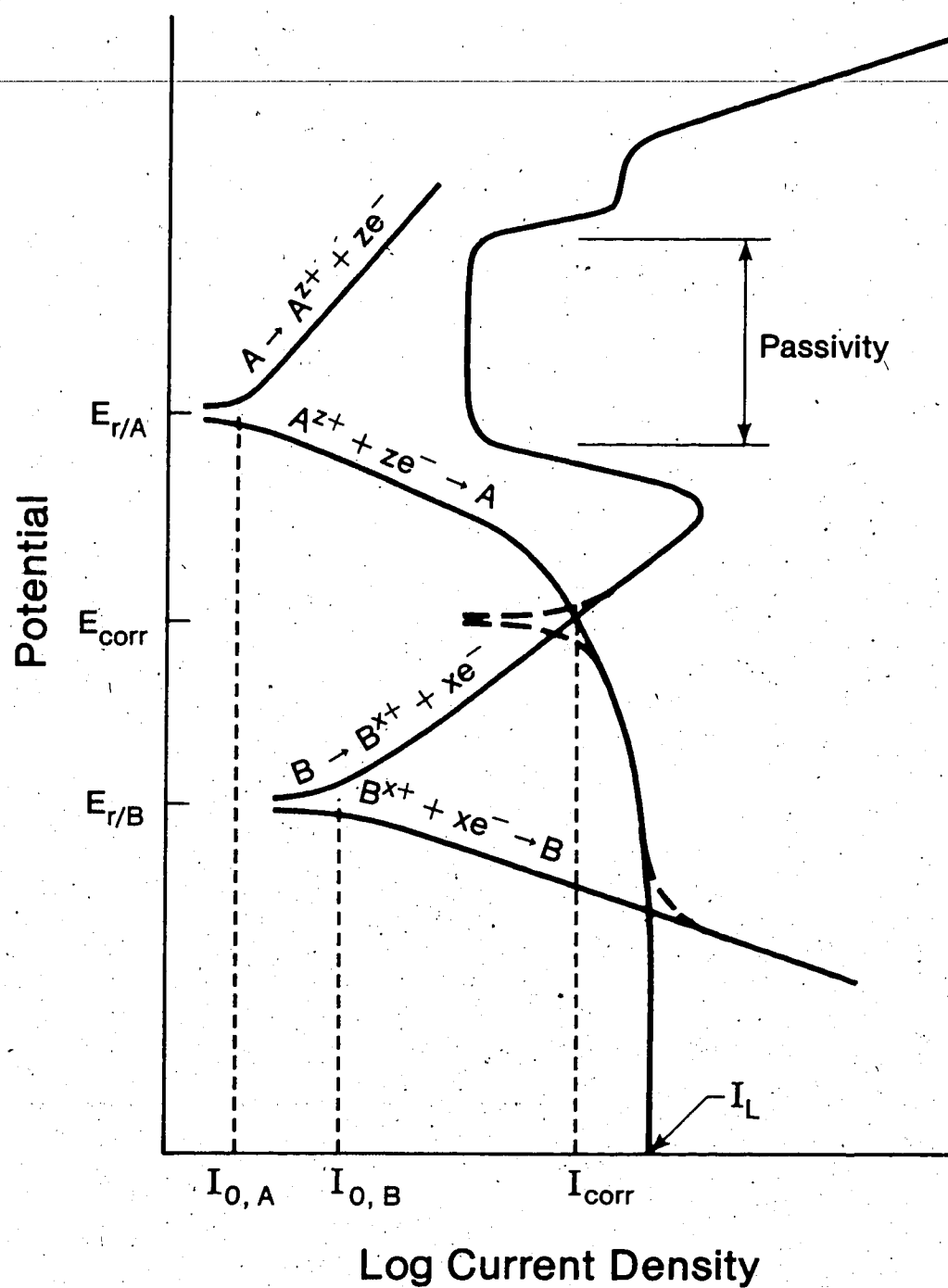


Figure 3.2 Evans Diagram for Two Simultaneous Redox Reactions

Considering the reactions involving 'A' and 'B', it is noted that as the electrodes are polarized in the positive (noble) direction the cathodic currents become zero, and the net currents (equation (14)) are equal to the anodic currents as given by equation (12). However, in terms of the semi-log plot, the relationship is expressed in the so-called Tafel Equation form:

$$\eta_a = 2.303(RT/azF) \log i_a - 2.303(RT/azF) \ln i_o \dots\dots(15)$$

As the figure implies, and as this equation states the overpotential has a linear relationship with the logarithm of the current density; this slope is referred to as the anodic Tafel slope and is written:

$$b_a = 2.303 RT/(azF) \dots\dots(16)$$

A similar argument applies when the electrodes are polarized in the negative (active) direction, which results in a cathodic Tafel Equation and slope, as follows:

$$\eta_c = -2.303(RT/(1-a)zF) \log i_c - 2.303(RT/(1-a)zF) \log i_o \dots\dots(17)$$

$$b_c = -2.303 RT/((1-a)zF) \dots\dots(18)$$

As would be expected, the intersection of the extensions of the linear anodic and cathodic Tafel regions occurs at the point given by  $(E_r, \log i_o)$  for each reaction.

### 3.2.4 Concentration Polarization

As the cathodic overpotential is increased the rate of the reduction reaction approaches the diffusion rate of reducible species to the electrode, and the cathodic current

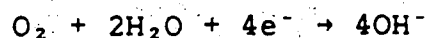
line deviates from the linear Tafel slope. When the diffusion rate becomes the rate determining step, that is when the reduction reaction consumes the reducible species as fast as it can arrive, the current reaches a limiting value,  $i_L$ .

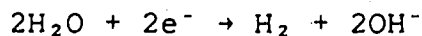
### 3.3 Mixed Potential Theory

When the sites of the two redox reactions are connected through electric and ionic conductors, the redox reactions may proceed concurrently and the total current at any given potential will be the algebraic sum of the currents for the individual reactions. Thus at very negative potentials, in Figure 3.2, the cathodic current will be primarily the cathodic current resulting from the reduction reaction involving 'B'. However, as the intersection of the cathodic curves is approached the contribution from the other reduction reaction will become significant, shown by the dashed line, and finally dominant. A similar situation exists where the total anodic curve crosses the cathodic curve; the total currents become equal at the equilibrium corrosion potential,  $E_{\text{corr}}$ . The intersection of the two partial curves defines the corrosion current density,

$i_{\text{corr}}$ .

Typical cathodic reactions that interact with anodic processes in neutral aerated solutions are as follows:





### 3.3.1 Passivity

~~In terms of oxidation behavior beyond the linear Tafel~~  
region, metals are divided into two groups: those abnormal metals, such as chromium, nickel, iron, aluminum, and titanium, whose corrosion rates fall significantly with further increase in anodic overpotential, and those normal metals whose corrosion rates continue to increase with overpotential. The idealized form of the Evans Diagram for the former of these is shown in Figure 3.2 for material 'B'.

While it is appreciated that the passive metal owes its low corrosion rates to a protective film on the surface, the exact nature of the film is still a subject of controversy. Two theories, however, have wide acceptance today: the adsorption theory and the oxide film theory.

The adsorption theory credits the low corrosion rates with the presence of an array of an adsorbed species, in some cases less than a monolayer thick, on the surface. The presence of such a layer has been demonstrated by Langmuir<sup>6</sup> and Frankenthal<sup>7</sup>, among others, and its passivating effect has been reported by Agius and Siejka<sup>8</sup>.

The oxide film theory credits a three dimensional metal oxide layer with reducing the further dissolution of the metal. DeG: moboy and Shreir<sup>9</sup>, in anodic polarization studies on nickel in sulphuric acid, found current arrests

at potentials which corresponded with several metal oxide/metal reversible potentials. Verink<sup>10</sup> has also demonstrated agreement of polarization data, at several pH values, with the respective thermodynamic E-pH diagrams.

---

### 3.3.2 Breakdown of Passivity

At the noble end of the passive range a sharp increase in current is usually observed. This current rise is associated with a disruption or breakdown of the passive film. Although several mechanisms have been proposed and controversy continues, all the theories involve some damaging species, such as the chloride ion. Whatever the mechanism, it is agreed that surface imperfections, such as inclusions, lattice defects, and micro-pores in the film become initial sites for breakdown and localized attack in the form of pitting corrosion or grain boundary attack.

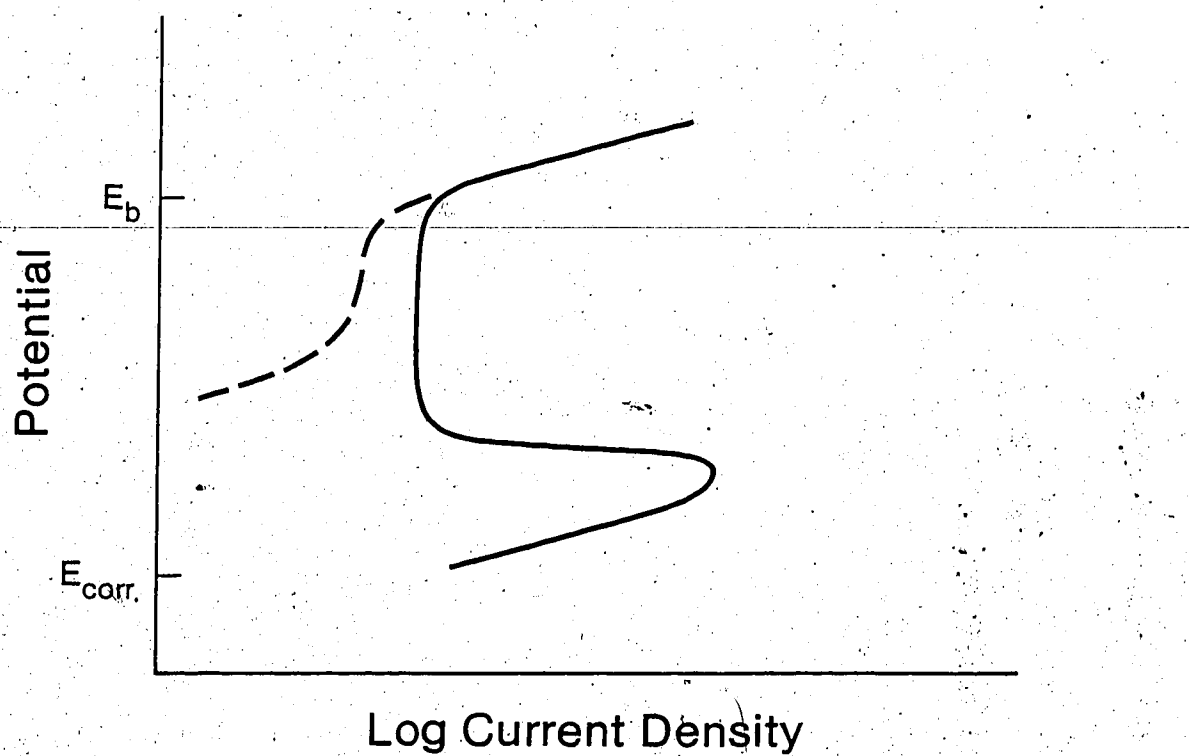
Polarization studies also reveal a phenomenon which mimics breakdown, however, at potentials below the breakdown potential. Crevice corrosion is a form of localized attack which is limited to regions which have become depleted of the primary oxidizing agent, such as oxygen, and continue to corrode by means of another cathodic reaction, such as hydrogen ion reduction, which depolarizes the anode to a high anodic current regime. The new potential difference, or driving force, can be determined by applying the Nernst Equation to the conditions of the anodic and cathodic half cells. Hydrolysis within the crevice causes the pH to fall

and the reaction to become self propagating, with severe localized attack.

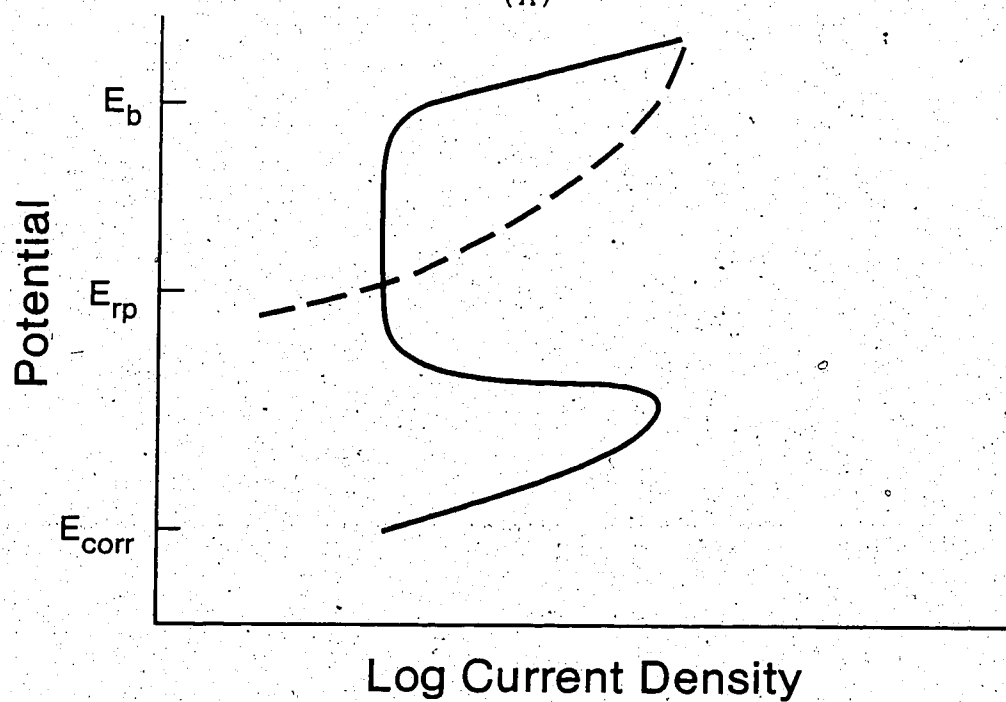
The sensitivity of a material to suffer localized attack can be determined qualitatively by reversing the potential scan after film breakdown has occurred. The form of the polarization curve thus produced can have one of the two forms shown in Figure 3.3. In Figure 3.3(A) the current is seen to fall to values lower than those reached on the forward scan. This indicates that the surface film has become even more protective, a very desirable situation. On the other hand, the current may remain high and exhibit a hysteresis effect. According to Wilde<sup>11</sup> the size of the hysteresis is a qualitative measure of the susceptibility of the material to locally corrode. It has been demonstrated<sup>12</sup> that when potentials are held above the crossover, or repassivation potential,  $E_{rp}$ , localized attack will continue at any pre-existing pits or crevices. Below the repassivation potential all pitting and crevice attack should cease. A more quantitative assessment of the susceptibility to localized attack can, therefore, be made by comparing the corrosion, breakdown, and repassivation potentials.

### 3.3.3 Corrosion Inhibition

In order for corrosion to occur, three conditions must be met:



(A)



(B)

Figure 3.3 Variations in the Form of the Polarization Curve During Reverse Scanning



1. There must be a potential difference, given by the Nernst Equation,
2. There must exist mechanisms for the transfer of charge between the electronic and electrolytic conductors, and
3. There must exist a continuous electronic conductor between the anode and cathode.

Corrosion inhibitors act on the first two of these requirements. The former involves neutralization of the corrodent, while the latter involves the action of a barrier layer former.

Neutralization of the corrodent is achieved by adding a reducing agent to react with the oxidizer which is responsible for the high corrosion rates. An example is the use of hydrazine ( $N_2H_4$ ) against oxygen in acid and neutral solutions.

Two of the most common types of barrier layer formers are oxidizing inhibitors and surface-active inhibitors. The former of these are used with passive metals when the addition of the inhibitor polarizes the metal into its passive region, for example, the nitrite inhibition of steel, as described by Dean et al.<sup>13</sup>.

Surface-active inhibitors adsorb on the metal surface and interfere with the anodic reaction, cathodic reaction, or both. The mechanism of the inhibitor may be to physically block a site, preventing diffusion of reactants, to alter the electrified interface thus changing the kinetics, or to block specific high energy sites, such as surface defects.

and grain boundaries where dissolution may be concentrated.

Organics make up a large proportion of adsorbed layer formers, and have found uses in a wide variety of environmental conditions, as the following examples show:

Table 3.1  
Examples of Organic Corrosion Inhibitors

| <u>Metal</u> | <u>Reagent</u>                 | <u>Inhibitor</u>     |
|--------------|--------------------------------|----------------------|
| Fe           | H <sub>2</sub> SO <sub>4</sub> | Amines,<br>thioureas |
| Al, Zn       | NaOH                           | Glucose              |

Depending on the action of the inhibitor it may be classified as either an anodic or a cathodic inhibitor, or both. An anodic inhibitor, as the name implies, inhibits the anodic reaction and reduces the corrosion rate as illustrated in Figure 3.4.

Similarly a cathodic inhibitor reduces the rate of corrosion, Figure 3.5, by interfering with the cathodic reaction.

#### 3.3.4 Potentiostatic Polarization

The E-log I plots, discussed above, are generated with a potentiostat, an instrument which maintains a known potential between a working electrode (the metal sample) and a reference electrode, and monitors the corrosion rate in terms of electrical current. By changing the potential, or

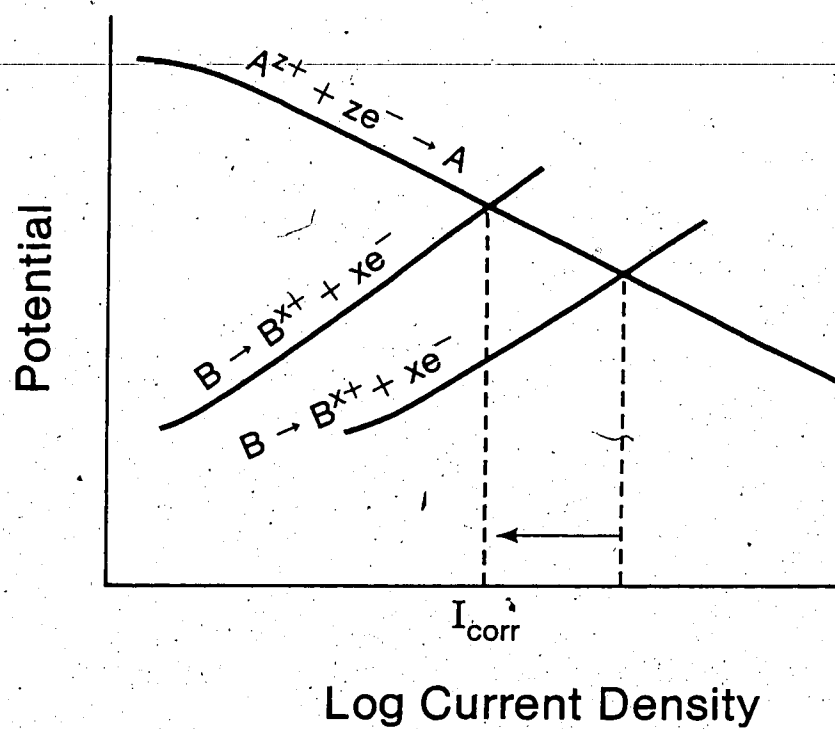


Figure 3.4 Anodic Inhibition

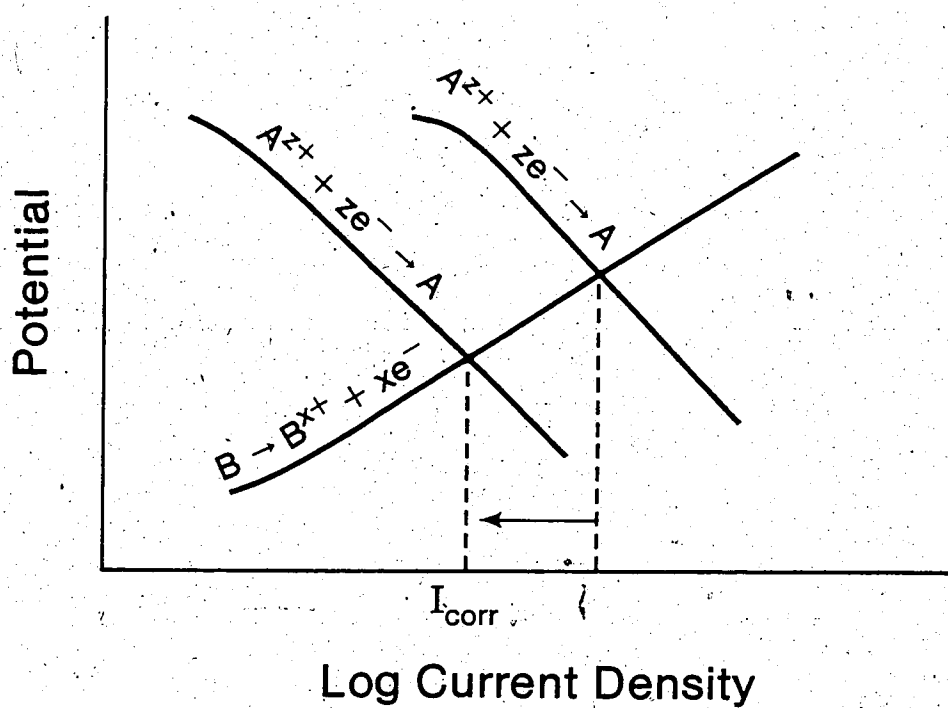


Figure 3.5 Cathodic Inhibition

strictly speaking, the overpotential, on the working electrode in a stepwise manner (potentiostatic polarization), or scanning at a preset rate (potentiodynamic polarization), the corrosion behavior of a material can be evaluated over a wide range of potentials. The former of these methods will be used to examine the implant materials in the subsequent tests.

### 3.4 Corrosion Fatigue

Corrosion fatigue, or more generally, environmentally assisted fatigue can be defined as the cracking of a material in response to combined cyclic loading and chemical attack. Significant reductions below expected life can be caused by cyclic loads well below the ultimate tensile stress and, in many cases, below the average yield stress. Often the chemical environment is not excessively aggressive toward the material in the absence of the loading; however, in the presence of a cyclic stress service life may be significantly reduced. It has been demonstrated for an aluminum alloy that the crack growth rate increases as the relative humidity of the air is increased'. For reasons such as this, some consider that any fatigue testing performed in other than a high vacuum is actually environmentally-assisted-fatigue testing.

To state that corrosion fatigue is simply a superposition of corrosion and fatigue is a gross over-simplification. However, some insight into the phenomenon can be obtained by considering the two components separately, but in the context of the overall problem.

#### 3.4.1 The Fatigue Aspect

The fatigue process has been divided into three stages. Stage I involves crack initiation and the subsequent propagation of the crack through the two to five surface grains. Initiation is considered to have occurred when

dislocations accumulate at the metal surface in such a configuration as to be equivalent to irreversible extrusions and intrusions of layers of metal. If such deformation continues, the intrusions, particularly, will become initiation sites for cracks.

In response to the applied stresses cracks will propagate into the metal following slip planes in the surface grains which are under the highest critical resolved shear stress. Because the surface grains may have a random orientation in the metal, Stage I fracture surfaces will tend to be at  $45^\circ$  to the direction of the applied stress.

According to Laird's Stage II fracture occurs by a plastic blunting process; Figure 3.6 illustrates the steps involved. As the tensile stress is increased toward the ultimate, slip becomes concentrated at the crack tip, in the lobes of the stress field, resulting in irreversible plastic deformation and finally in an incremental extension of the crack. When the load is reversed the crack faces are forced together where the blunt tip partly folds to form a resharpened tip. Thereafter, the cycle is repeated. As illustrated, cracking is usually straight, transgranular and perpendicular to the axis of the applied stress.'

Another theory for Stage II crack growth, called crack closure, has been proposed by Elber''. While this mechanism does not offer a radical alternative for the extension mechanism occurring at the tip of a propagating fatigue crack, it argues that residual tensile stresses, remaining

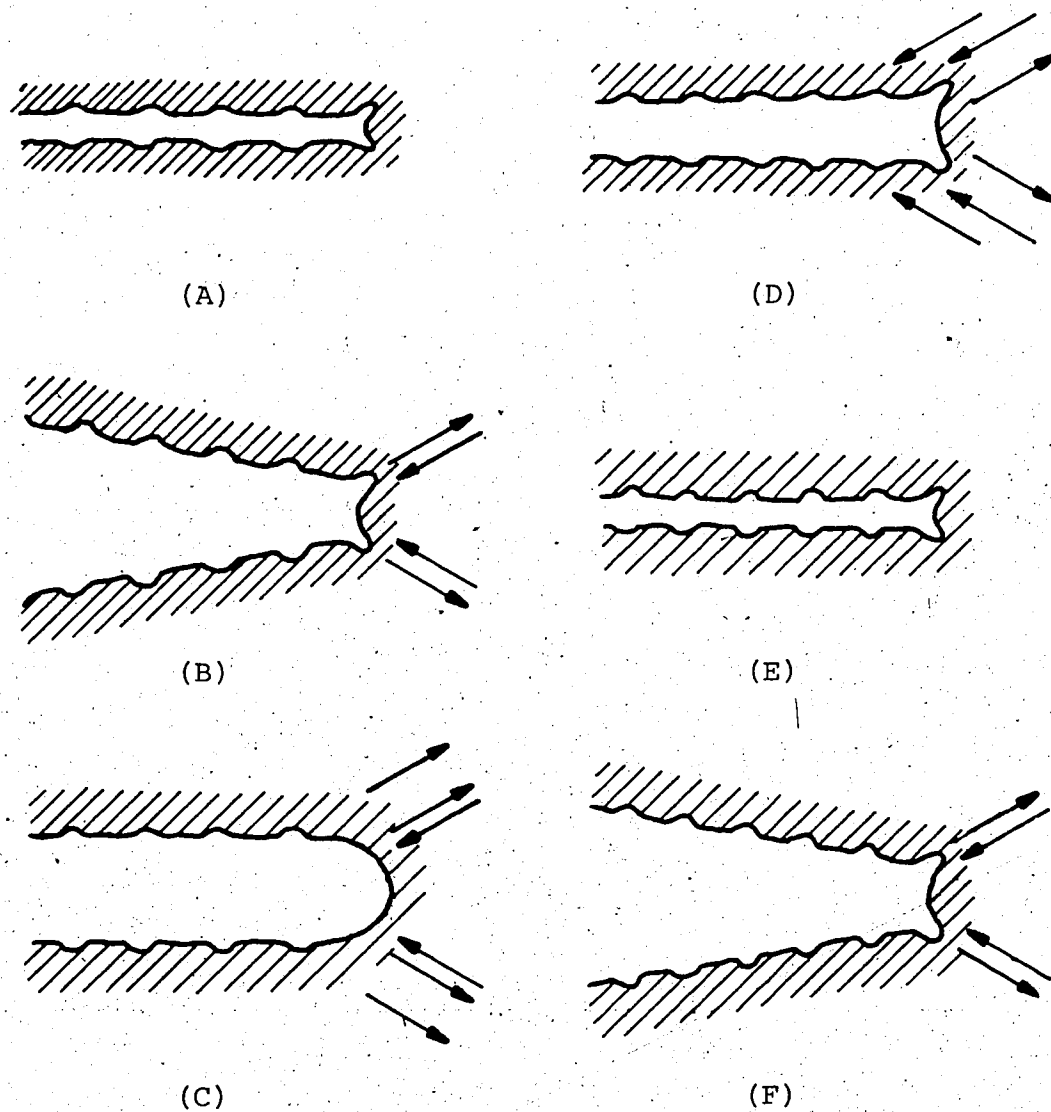


Figure 3.6 Plastic Blunting Fatigue Crack Propagation Mechanism

after tensile deformation, play a significant role in the kinetics of propagation. "As a consequence of the permanent tensile plastic deformation left in the wake of a fatigue crack, one should expect partial crack closure after unloading." The crack should also be expected to remain closed for at least a portion of the tensile part of the load cycle. This mechanism means, therefore, that rather than the crack propagation rate being a function of the total amplitude of the stress waveform, or the 'R' value, only that portion of the cycle during which the crack is open actually contributes to propagation. In addition to its use in situations where loading is known to be regular (constant amplitude and frequency), this theory also gives insight into crack retardation and acceleration following low and high loading blocks, and in the propagation rate during random loading.

Finally, Stage III involves the final rupture when the crack length exceeds a critical value and the crack growth rate becomes exceedingly rapid. The advancing crack becomes highly dependent upon inherent weaknesses in the remaining ligament, and is typically characterized, therefore, by a rough surface composed of regions of brittle and/or ductile fracture.

#### 3.4.2 The Corrosion Aspect

In the simplest case, preferential anodic dissolution at the highly stressed crack tip may be the only



contribution made by corrosion to the overall mechanism. However, the contribution may be more subtle and devastating. For example, the anodic dissolution reaction may produce a chemical species which embrittles the material by either absorption and accumulation within the metal lattice, or it may adsorb at the high energy crack tip, presumably reducing the surface energy, and leading to decohesion of the metal.

On the other hand, if the species is an effective corrosion inhibitor, the effect of the environment may be significantly reduced, possibly returning the situation to one resembling pure fatigue.

### 3.4.3 Variables Affecting Corrosion Fatigue Cracking Rates

Wei and Speidel<sup>20</sup> have outlined a large number of variables which can affect the corrosion fatigue cracking rate. These have been divided into three groups, as follows.

#### Mechanical Variables

- Maximum stress or stress ratio,  $R$ .
- Cyclic loading frequency.
- Cyclic load waveform (e.g. square or sinusoidal waves).
- Stress state (e.g. bi- or triaxial).
- Residual stress.
- Notch or crack size.
- Specimen geometry.

#### Metallurgical Variables

- Alloy composition.
- Distribution of alloying elements.
- Crystal structure and microstructure.
- Prior heat treatment.
- Mechanical properties.

#### Environmental Variables.

- Temperature.
- Concentration of damaging species.
- Electrochemical potential.
- Coatings, inhibitors, etc.

Fundamental to all theories of fatigue and corrosion fatigue crack propagation is the involvement of slip in plastic deformation and work hardening. Variables, therefore, which limit the number and movement of the dislocations will have a major effect on the cracking mechanism.

#### 3.4.3.1 Mechanical Variables

Slip occurs in response to shearing stresses. Load configurations, therefore, which tend to produce low shear stress zones, such as under triaxial stress conditions, will result in the accumulation of dislocations and possibly in the formation of a crack. This sequence of events can occur in thick materials in response to external loads, or at the roots of cracks or notches.

Just as the applied stress is a major concern, the presence of residual stresses from prior forming and heat treating practice can also have a significant effect.

---

Of particular importance in corrosion fatigue is the cyclic loading frequency and waveform. Barsom<sup>21</sup> has demonstrated that the crack propagation rate often increases as the loading frequency falls. Furthermore, the loading waveform is also seen to be a controlling factor<sup>22</sup>. Crack rates are highest when the rise-time of the tensile waveform is longest; a sinusoidal loading curve is, therefore, more destructive than a square wave.

These phenomena, unique to corrosion fatigue, appear to be the results of synergistic combinations of the fatigue and corrosion mechanisms.

#### 3.4.3.2 Metallurgical Variables

As the generation and movement of dislocations has a fundamental dependence on the particular material, the metallurgical condition has a profound effect on crack initiation and growth. In addition to its crystal structure, one of the most important fundamental properties of a material is the relative magnitude of its stacking fault energy (SFE). This energy term is simply the surface energy of a plane of atoms in the solid which is stacked in a pattern out of sequence from the ideal. As the energy term falls, the length of the stacking fault increases as does the force required to make it cross slip.

With regard to low cycle fatigue crack propagation behavior, face centre cubic (FCC) alloys can be grouped according to relative magnitudes of SFE, which bear directly on the dislocation structures generated in those materials in response to cyclic loading. Low SFE alloys, such as austenitic stainless steels and cobalt-chromium alloys, having high resistances to cross slip form fine planar dislocation structures; high SFE materials, for example copper and aluminum, form cell-like dislocation structures owing to their low resistance to cross slip.

A consequence of the higher resistance to cross slip, in low SFE materials, is the formation of fine persistent slip bands, which cause the material to reach its saturation hardness at a higher number of cycles than the high SFE materials. This capacity to retain the reversible nature of slip prolongs the time required for crack initiation. Furthermore, fine slip more evenly distributes plastic deformation at the crack tip, which leads to lower stress concentrations and slower crack propagation rates than for high SFE alloys.

Two other factors which are considered to have significance in fatigue crack propagation are grain size and ductility. Whereas in high cycle fatigue, where life increases with decreasing grain size, the same is not considered to be the case for low cycle fatigue. According to Feltner and Laird<sup>23</sup> the grain size has no effect on the rate of crack growth in high SFE alloys, presumably as a

consequence of the dislocation cell structures. Concerning low SFE materials, on the other hand, it has been hypothesized by Laird<sup>24</sup> that fatigue cracks propagating by plastic blunting should be slowed with decreasing grain size.

The effects of ductility vary according to whether the fatigue is strain-, or stress-controlled. In strain-controlled, low cycle fatigue, the greater the ductility the greater the capacity for deformation and blunting<sup>25</sup>, therefore, the lower the propagation rate.

In stress-controlled, low cycle fatigue, high ductility is especially important for cold-worked materials, which fatigue soften<sup>26</sup>. If the material possesses insufficient ductility the initiation time will be short, and propagation rates will be high. For annealed alloys the importance of ductility will increase with the level of the stress.

#### 4. LITERATURE REVIEW

This chapter reviews the relevant clinical and scientific literature on the corrosion and corrosion fatigue behavior of 316L stainless steel and cobalt alloys. A review is also made of the literature dealing with the effects of organics on these and other materials.

##### 4.1 Stainless Steel

###### 4.1.1 Clinical Findings

Clinical reports<sup>27-36</sup> indicate that the fracture of 316L stainless steel implants is usually accompanied by metallurgical defects in the form of porosity, manufacturing defects such as grinding marks, and various design problems. However, the actual fracture mechanisms generally fall into three groups: fatigue, corrosion fatigue, and stress corrosion cracking. While it is sometimes equivocal whether the responsible mechanism is actually fatigue or corrosion fatigue, some cases have been reported where two mechanisms were clearly active during the life of a single component<sup>30,32</sup>.

Some form of corrosion is usually associated with used stainless steel implants. In one study by Colangelo and Greene<sup>35</sup> corrosion was observed on 91% of all retrieved components, and crevice corrosion was present at 42% of the possible sites. In a number of cases, reported by Cahoon and Paxton<sup>28</sup>, crevice corrosion was credited with causing such

severe tissue irritation that implant removal was required.

#### 4.1.2 Corrosion Studies

---

Considerable research has been conducted on the corrosion behavior of austenitic stainless steels under saline conditions. While some reports have dealt with stainless steel as an implant material, much of the published results deal with material selection for use in seawater, chemical process lines, and recently, geothermal power plants. Fortunately, these latter service conditions are similar enough to the inorganic fraction of body fluids to make, at least, a first approximation to the behavior of these materials in vivo.

It has been known since the earliest applications of the material that it suffers from localized attack. In 1943 Venable and Stuck<sup>37</sup> reported that '18-8' stainless steel experienced "pit corrosion" in body fluids, but the addition of molybdenum reduced this tendency.

Recent tests in various other media have indicated similar problems. Streicher<sup>38</sup> studied the corrosion of twenty-five different alloys in seawater and found that the high Cr-Mo alloys, such as Hastelloy C-276 and Inconel 625, had the greatest resistance to localized attack, while AISI 316 had one of the worst. In similar tests Hack<sup>39</sup> found that crevice corrosion on 316 was variable.

Susceptibility to localized attack has also been demonstrated by electrochemical means. Bennett et al.<sup>40</sup>

using cyclic anodic polarization compared the relative resistances of AISI 304, 316, and 317 stainless steels in pulp mill white water; 316 was rated between the other two.

---

Bandy and Cahoon<sup>41</sup> studied the effect of alloy composition on the resistance of austenitic stainless steels to localized attack in Ringer's Solution. In the case of 316L the repassivation potential was below the corrosion potential; increasing the molybdenum content, however, produced a higher breakdown potential, and a very small hysteresis loop.

While polarization tests usually give corrosion potentials in the vicinity of  $-0.2$  V (Mueller and Greener<sup>42</sup>) to  $0.065$  V (Bandy and Cahoon<sup>41</sup>), long term tests indicate that the corrosion potential generally drifts in the positive direction to an average value, after twenty days, of approximately  $0.14$  V (Levine and Staehle<sup>43</sup>). Brettle and Hughes<sup>44</sup> also show a similar trend; however, the potential after 100 days, in their test, was only about  $0.014$  V. Because they did not report if the solution had been oxygenated, this potential value may reflect ~~deoxygenated~~ conditions. Regardless of the source, however, all potential-time plots show frequent potential fluctuations, similar to the results of Levine and Staehle<sup>43</sup>, which Hoar and Mears<sup>45</sup> suggest are caused by passive film breakdown and pitting.

Hoar and Mears<sup>45</sup>, who conducted both potentiostatic polarization and potential monitoring tests, report that



after 480 hours a corrosion potential of 0.26 V was reached. Because they also recorded breakdown potentials of 0.116 V to 0.24 V, they concluded that spontaneous film breakdown is possible if the stainless steel remains in aerated saline for long periods.

Some confusion appears to be associated with the value of the breakdown potential. Anodic polarization curves generated by Mueller and Greener<sup>45</sup> and Bandy and Cahoon<sup>41</sup> for annealed 316 in aerated Ringer's Solution show breakdown in the vicinities of 0.35 V and 0.55 V. Mueller and Greener<sup>45</sup> suggest that the difference is due to a variation in oxygen partial pressure, an explanation which is consistent with another of their findings, that breakdown under deaerated conditions occurs at 0.16 V. In similar tests using cold worked 316L, however, Syrett<sup>46</sup> found that the breakdown potential was independent of oxygen content.

Concerning Bandy and Cahoon's<sup>41</sup> results, no mention is made of varying oxygen concentrations. However, it is reported that in the early tests, possibly referring to those giving lower breakdown potentials, crevice attack occurred at the gasket-sample interface. As the breakdown potential for crevice corrosion is lower than that for pitting, it is possible that this phenomenon was responsible for the lower values in the cases of both the annealed and cold worked materials.

A few papers have been published recently dealing with the effects of physiological organics on the corrosion

behavior of 316 stainless steel; however, the results appear to be contradictory.

Samitz and Katz<sup>47</sup> compared nickel dissolution from 316L in various solutions including isotonic saline (0.17M NaCl), pooled sweat, whole blood, and plasma. After one week, they found nickel concentrations to be greater, for the most part, in the physiological solutions than in the isotonic saline.

In 1980, Brown and Merritt<sup>48</sup> reported results which supported those of Samitz and Katz<sup>47</sup>. 316L coupons were immersed in solutions of saline, saline plus 1% serum, and saline plus 10% serum. After maintaining an anodic potential of 5 V for thirty minutes, the samples were compared. Samples in solutions containing serum were attacked more than those in saline, and the extent of damage increased with serum content. Anodic polarization curves in the same solutions showed that the critical current for passivation was increased in saline containing serum.

Contrary to the results of the two reports above, however, another series of tests, also reported by Brown and Merritt<sup>48</sup>, on fretting corrosion of 316L, indicated that the serum may have actually been beneficial; weight losses were over seven times greater in isotonic saline than in 10% serum. As a side note, their results showed a more negative corrosion potential in serum than in saline.

## 4.2 Cobalt Alloys

### 4.2.1 Clinical Findings

In a survey of ten reports<sup>2,3,4</sup> dealing with both stainless steel and CoCrMo implants, the only failure mechanism reported for the latter was fatigue. In one paper, by Cahoon and Paxton<sup>2</sup>, however, this mechanism was assumed simply on the basis that the implant failed in a brittle manner and because it had been cyclically loaded. This case emphasizes a caution stated by White et al.<sup>3</sup> on the identification of fracture mechanisms; while fracture surfaces are often obliterated subsequent to failure, they note, it is important to consider that the necessary conditions for corrosion fatigue and stress corrosion cracking, and other mechanisms also exist, and that the identification of all brittle failures as fatigue will only "lead to complete ignorance of the root cause of the problem."

As was the case with the stainless steel implants, all the CoCrMo fractures had associated defects. However, unlike the stainless steels, no corrosion of any type was reported.

### 4.2.2 Corrosion Studies

Compared to the volume of literature on the corrosion of stainless steels, relatively little is available on the ambient temperature corrosion of CoCrMo alloys. Most of what is available, however, deals with the use of the material in

surgical implants..

The anodic polarization of cast CoCrMo has been studied by several teams in solutions simulating the physiological milieu. Cahoon et al.<sup>50</sup> performed potentiodynamic polarization on a cast CoCrMo in Ringer's Solution containing physiological pressures of oxygen and carbon dioxide. The anodic curves, thus produced, were similar to those for the stainless steel in that the material self-passivated with a current of approximately  $10^{-6}$  A/cm<sup>2</sup>. On reversing the potential scan, however, unlike the 316L, the material repassivated and exhibited only a small hysteresis. This behavior agrees with the results of Sury<sup>51</sup>, who studied Vitallium in 10% HCl, and Uhlig and Asphahani<sup>52</sup>, who examined HS-21 in 4% NaCl at 70°C, all without experiencing localized attack. In fact, this material is so resistant to localized attack that it took Pugh et al.<sup>53</sup> 74 days to detect crevice corrosion on Vitallium in 10% HCl plus 1% FeCl<sub>3</sub>, and of 40 samples tested only two showed evidence of the attack.

While Hoar and Mears<sup>45</sup> did not study reverse polarization behavior, they found forward anodic curve forms similar to those reported by the authors mentioned above in Hank's Solution, human blood, and in NaCl solutions.

Depending on the source, breakdown potentials are reported from approximately 0.3 V, in the case of Mueller and Greener<sup>45</sup>, who used aerated Ringer's, to 0.87 V for Brettle and Hughes<sup>44</sup> where 0.17 M NaCl was the test solution. While

there are several cases when high breakdown potentials arise (such as high potentiodynamic scanning rates), Hoar and Mears<sup>45</sup> report that the potentials in 0.17 M NaCl are always higher than in balanced saline solutions, such as Hank's Solution.

As was the case with 316L, corrosion potentials of CoCrMo rise with time. Lucas et al.<sup>54</sup> reported a corrosion potential after a number of hours in 0.9% saline to be -0.24 V, while Hoar and Mears<sup>45</sup> reported an average value of 0.26 V, between 20 and 200 days in 0.17 M NaCl, and 0.07 V, after 71 days in vivo. Because these long term values, and particularly that for the in vivo situation, are lower than the breakdown potential, Hoar and Mears<sup>45</sup> consider spontaneous film breakdown to be highly unlikely.

Regarding the interactions between implant materials and physiological organics, research has continued, to varying degrees, from two standpoints: the effects of body organics on the implant metal, and the effects of the dissolved metal ions on the body. Work on the first of these has been relatively sparse.

Samitz and Katz<sup>57</sup>, in addition to working with stainless steel, also studied Vitallium and found the concentrations of nickel to be greatest in physiological solutions, as was the case for the steel.

Hoar and Mears<sup>45</sup> monitored corrosion potentials in vivo and in vitro and found the former to be up to 200 mV more negative after 71 days.

In a test reported by Clark and Williams<sup>55</sup>, a CoCrMo alloy was immersed in a saline solution containing serum albumin. They found that the cobalt and molybdenum were being selectively removed from the surface, possibly by the formation of stable complexes with the surrounding organics.

Perhaps the first unifying theory relating the role of physiological organics to the corrosion of an implant material was made recently by Woodman et al.<sup>56</sup>. In tests on Vitallium total finger prostheses implanted into cats they learned that the concentrations of dissolved cobalt and nickel increased exponentially over the one year test period. Furthermore, both ions were only detected bound to serum proteins. It was hypothesized that the continued increase in the metal ion levels was due to an autocatalytic mechanism directly involving the serum proteins: the presence of dissolved metal ions stimulates the immune system which results in a supply of proteins; metal ions complex with the proteins, diminishing the ion concentration adjacent to the metal, which leads to continued dissolution.

In comparison, a greater number of studies have considered the interactions between metal ions and physiological organics. Among the information gathered to date are the following points:

- Cr, Co, and Ni tend to circulate in the body and become stored in various organs,<sup>57</sup>
- at least Co forms complexes with serum proteins, and possibly other organics,<sup>58</sup>

- Cr levels are highest near the implant,<sup>11</sup>
- the metal-protein bond may grow stronger with time<sup>10</sup>.

---

#### 4.3 Effects of Organics on Other Alloy Systems

In addition to the research performed on the effects of organics on stainless steel and CoCrMo, work has also been made on other alloy groups.

While testing candidate materials for implantable electrodes, Niazy et al.<sup>11</sup> studied the effects of various organics on the anodic polarization behavior of aluminum and zinc. While none of the test solutions had any visible effect on the passivation of aluminum, solutions containing bovine plasma protein, and a mixture of chondroitin sulphate and arginine produced passivity on zinc where none existed in isotonic saline.

Similarly, in anodic polarization experiments on copper, nickel, cobalt, and titanium in Ringer's Solution, Svare et al.<sup>12</sup> found that solutions containing the amino acid cystine enhanced the passivity of copper, while for nickel passivity was inhibited.

The effects of amino acids were also investigated by Solar et al.<sup>13</sup> on Ti-6Al-4V. In anodic polarization tests arginine and methionine shifted the reversible potential in the negative direction, while proline, tyrosine, glycine, and cystine shifted it in the positive sense. No effects were noted in the passive regions.

---

Ti-6Al-4V was also the material examined by Aragon and Hulbert<sup>44</sup>. In tests similar to those conducted by Solar et al.<sup>43</sup>, lower current densities were attained using plasma than with isotonic saline. Furthermore, while lactated Ringer's Solution shifted the corrosion potential in the negative direction by over 300 mV, the corrosion current increased by approximately one order of magnitude over the value in isotonic saline.

#### 4.4 Corrosion Fatigue of Cast CoCrMo

As was indicated above no corrosion related fracture mechanisms have been reported in the clinical literature for CoCrMo. However, this may not reflect the actual mechanisms, for when faced with equivocal data, one may choose to identify the fracture mode as fatigue, based on previous experience with the material, rather than the more debatable mode of corrosion fatigue.

A corrosion fatigue study was conducted by Luckey<sup>45</sup> using deaerated lactated Ringer's Solution. Samples were sinusoidally loaded in reversed bending at a rate of 30 Hz. The endurance limit at  $10^7$  cycles was reported to be 419 MPa (60.8 ksi); however, he remarked that the endurance curve was still decreasing at this point. While he did not discuss his findings in detail, he concluded that his work "... has shown potential environmental effects on the high cycle corrosion fatigue behavior of cast Co-Cr-Mo ...".



Corrosion fatigue tests were also conducted by Miller et al.<sup>66</sup>. Cast CoCrMo samples were sinusoidally loaded in an aerated tissue-culture medium at a rate of 2500 Hz. They justified their use of this high loading frequency by stating that "... the work of Bowers and Staehle and Devine and Wulff indicate that corrosion fatigue has a relatively small effect on this alloy." (the works referred to are unpublished). From their results, however, they calculate an allowable design stress of 321 MPa (46.5 ksi), such that there is a 95% confidence of less than one failure in one thousand after  $5 \times 10^7$  cycles, assuming no manufacturing defects.

Fatigue testing in air was performed by Ducheyne et al.<sup>67</sup>. In a four point bending jig, intact hip prostheses were loaded at 30 Hz to various stress levels. They reported a fatigue limit of 424 MPa (61.5 ksi) at  $10^7$  cycles.

Gilbertson<sup>68</sup>, also using intact hip prostheses, studied the relationship between fatigue strength and the loading orientation. He found that the endurance limit at  $10^7$  cycles increased from 1054 to 2122 N (237 to 477 lbs), or approximately 1 to 3 body weights, as the loading axis approached the long axis of the device.

In a review of the fatigue strengths of various cobalt-based implant alloys manufactured by Sulzer Brothers Ltd., Lorenz et al.<sup>69</sup> discuss the microstructures, the fatigue resistance, and the fatigue fracture morphologies of cast CoCrMo tested in air. From the basic fatigue strength

of 190 - 280 MPa (27.6 - 40.6 ksi) in the as-cast condition, the strength increases to 280 - 350 MPa (40.6 - 50.8 ksi) following a homogenizing anneal. Solution annealing, however, while increasing the impact and tensile strengths, produces fatigue strengths of only 220 - 280 MPa (31.9 - 40.6 ksi). This lower fatigue strength is blamed on the presence of voids, termed "Kirkendall holes", which remain after the carbides are dissolved.

The relative effects of notching and cyclic loading in a corrosive environment were investigated by Hughes et al.'. Cast CoCrMo samples were tested as both smooth and notched specimens in air and in saline, and the endurances at  $10^8$  cycles were compared. Their results are listed below:

Table 4.1  
Results Reported by Hughes et al.

| <u>Endurance Limit at <math>10^8</math> Cycles, MPa (ksi)</u> |                                   |                                |                                   |
|---|-----------------------------------|--------------------------------|-----------------------------------|
| <u>Smooth Specimens</u>                                       |                                   | <u>Notched Specimens</u>       |                                   |
| <u>Tested in</u><br><u>Air</u>                                | <u>Tested in</u><br><u>Saline</u> | <u>Tested in</u><br><u>Air</u> | <u>Tested in</u><br><u>Saline</u> |
| 248   | 234                               | 138                            | 48                                |
| (36.0)  | (33.9)                            | (20.0)                         | (7.0)                             |

Based on these findings, they calculated that the total effect of notching and testing in saline was to reduce the endurance limit by 81%. Of this the presence of the notch had the greatest effect accounting for 55% of the total reduction, while the chemical effect only accounted for 7%.

Finally, an interaction effect, defined as the difference between the total effect and the individual contributions of the notch and the environment, was calculated to contribute over 30% to the total. Therefore, although the individual

---

effect of the saline was small, the combination of it with the notch was very significant, and may have even been greater if the loading frequency were less than 100 Hz.

Regarding fractographic features, most sources, including the clinical reports, agree that fatigue crack propagation in cast CoCrMo is characterized by cleavage fracture resembling Stage I crack growth. Both Gilbertson<sup>11</sup> and Lorenz et al.<sup>12</sup> suggest that this is related to the low stacking fault energy, which makes cross slip difficult. Ducheyne et al.<sup>13</sup>, on the other hand, suggest that a deformation-induced martensite phase transformation from FCC to HCP may be responsible.

## 5. MATERIALS AND PROCEDURES

The research was divided into four sections according to the objectives. The first section was the development of an experimental procedure which could be used to generate reliable potentiostatic polarization curves. The second and third parts dealt mainly with the polarization behavior of a cast cobalt alloy in solutions containing combinations of glucose and other physiological organics, in the form of calf blood serum. The fourth, and last part, was a study of the effect of physiological organics on the corrosion fatigue crack propagation rate and fracture morphology in a cast cobalt alloy.

The following section will review the chemical compositions, metallurgical conditions, and mechanical properties of the three materials studied, and will describe the equipment used and the procedures followed.

### 5.1 Test Materials

In addition to the 430 stainless steel used in the procedure development runs, the three materials involved in the tests were: 316L stainless steel and cast Vitallium both machined from used total hip implants, and Vitallium cast into the form of round tensile specimens. Plate 5.1 shows that the stainless steel implant, used as the source of material, had fractured in service. The Vitallium implant, similar to the one shown in Plate 5.2, was, on the other hand, intact. It is assumed that it was removed because of

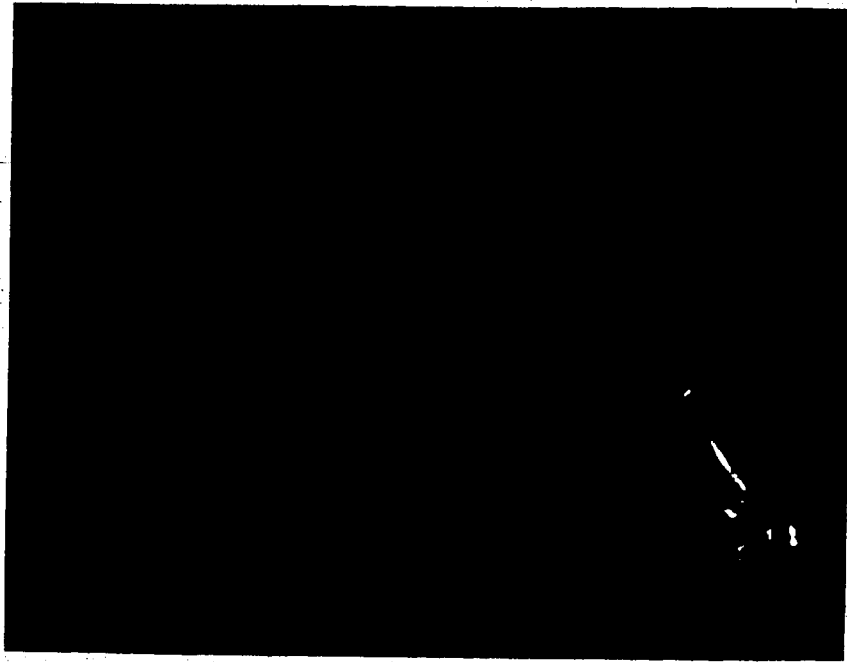


Plate 5.1 Fractured Stainless Steel Implant

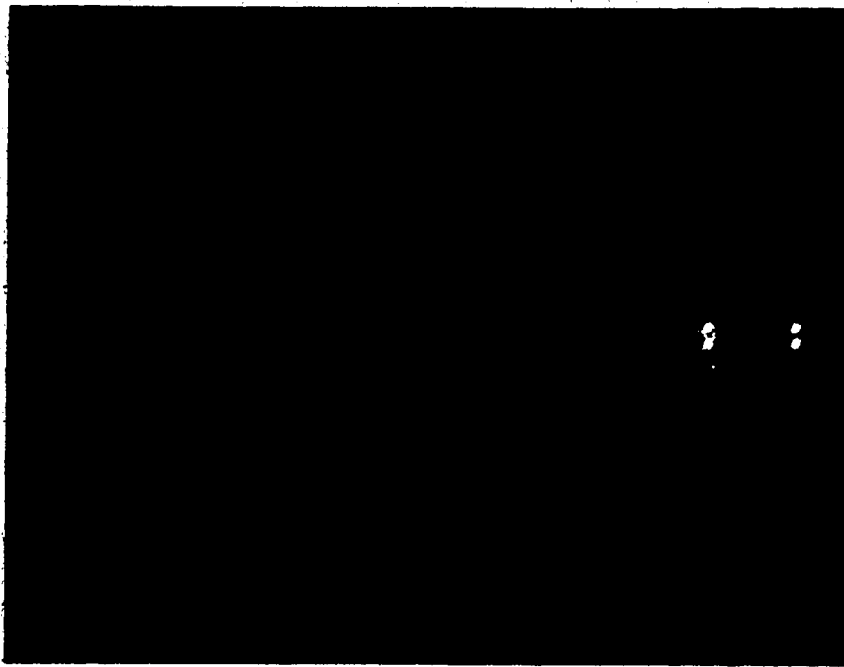


Plate 5.2 Intact Vitallium Implant

infection or loosening.

The Vitallium fatigue specimens, produced and supplied by Howmedica Inc. of Rutherford, New Jersey, were purported to be in the same metallurgical condition as the "Vitallium" prostheses that they manufacture.

Analysis of the test materials consisted of determining their chemical compositions, hardnesses, microstructures, and in the case of the fatigue specimens, tensile properties. Chemical analysis was performed by the Alberta Research Council (ARC) using their Induction Coupled Plasma (ICP) spectroscopy equipment, and in the Department of Mineral Engineering using the Leco carbon analyser. Among the results reported by ARC the compositions given for manganese, phosphorus, and sulphur were all high, in most cases, several times the maximum specified limits. In the case of the stainless steel the concentrations reported were much higher than the levels readily obtainable in even the lowest steel grades. It was, therefore, considered that the values for these elements did not reflect actual concentrations, but, rather, erroneous analyses on the part of the laboratory. While these results are not included in the following summary of results, they are attached as Appendix B.

All other analyses were carried out in the Department of Mineral Engineering.

### 5.1.1 Stainless Steel

One grade of stainless steel currently used in the manufacture of implants is 316L. In North America this material is often required to conform to the minimum requirements of ASTM F55-82. The compositional requirements of this standard and the assay of the test material are given below.

Table 5.1  
Chemical Composition of Stainless Steel Test Material

| Element | ASTM F55-82<br>Grade 2 | Test Material |
|---------|------------------------|---------------|
| C       | 0.030%(max)            | <0.01%        |
| Cr      | 17.0-19.0%             | 18.0%         |
| Ni      | 12.0-14.0%             | 14.0%         |
| Mo      | 2.0-3.0%               | 2.55%         |
| Cu      | 0.50%(max)             | 0.21%         |
| N       | 0.10%(max)             | Not Analysed  |

These results indicate that the material conformed to the chemical requirements of ASTM F55-82.

#### 5.1.1.1 Metallographic Examination

Longitudinal and transverse sections were cut from the stem of the hip prosthesis. Plate 5.3 shows a transverse cross section to have an equiaxed grain structure with an ASTM size of approximately #5. These features together with the absence of any deformed twins indicate that this

austenitic material was in the annealed condition.

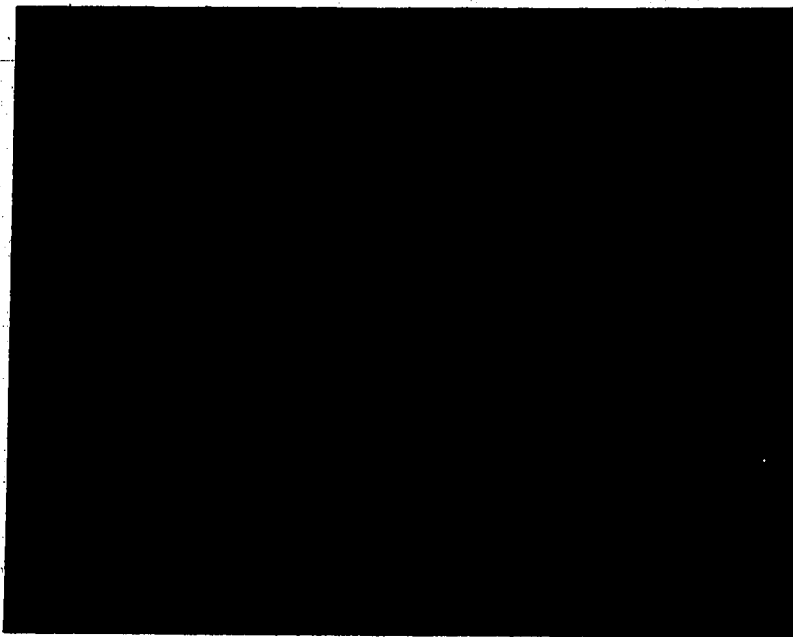


Plate 5.3 Typical Microstructure of the 316L Stainless Steel  
(100X)

#### 5.1.1.2 Hardness Results

Rockwell hardness and Vickers microhardness measurements were made on a transverse section of the implant with these results:



Table 5.2  
Hardness of Stainless Steel Test Material

| Test Sample                 | Rockwell Hardness<br>HRB 75<br>(average of 5 readings) | Vickers Microhardness<br>HV 162<br>(average of 5 readings) |
|-----------------------------|--|--|
| Typical Values <sup>1</sup> | HRB 85 - 95  | Not Given  |
| Dead Soft <sup>2</sup>      | HRB 80   | Not Given  |

Although the hardness specification was not obtained from the manufacturer, the literature values would indicate that the material was in the fully annealed condition.

Although a failure analysis was not performed on the implant, it is probable that the mechanism of fracture was aggravated by the low hardness and, therefore, a low tensile strength. However, based on the chemical composition, it is considered that the corrosion properties would have been similar to material in a harder condition.

### 5.1.2 Cast Vitallium

Of the several cast CoCrMo prostheses on the market the one used in this research was manufactured by Howmedica Inc. and is referred to by them as 'Vitallium'. Similar, if not identical alloys are also produced by other manufacturers

under other proprietary names, such as: Haynes 21 (Cabot Co.), Zimaloy (Zimmer Co.), Stellite (Union Carbide), and Protasul-2 (Sulzer Brothers Ltd.).

In North America the materials for CoCrMo implants are usually produced in conformance with the minimum requirements of ASTM F75-76. The chemical composition required for that specification, and the assays for the two alloys studied are as follows:

Table 5.3  
Chemical Composition of Vitallium Test  
Materials

| Elements | ASTM<br>F75-76   | Implant<br>Sample | Fatigue<br>Sample |
|----------|------------------|-------------------|-------------------|
| C        | 0.35%(max)       | 0.21%             | 0.03%             |
| Si       | 1.00%(max)       | 0.82%             | 0.99%             |
| Cr       | 27.0-30.0%       | 27.1%             | 24.0%             |
| Ni       | 2.5%(max)        | 2.10%             | 0.16%             |
| Mo       | 5.0-7.0%         | 6.05%             | 5.35%             |
| Fe       | 0.75%(max)       | 0.18%             | 0.17%             |
| Cu       | Not<br>Specified | 0.05%             | 0.05%             |

Of these two alloys only the implant material conforms to the ASTM specification; the fatigue sample does not conform as a result of the low chromium content. While this discrepancy means that the average corrosion properties of the fatigue sample material would be inferior to that of the

implant material, it cannot be said that the alloy is unacceptable for use in the body as it is not known if ~~conformance to the quoted specification is required in this~~ instance.

#### 5.1.2.1 Metallographic Examination

Transverse sections were cut from the neck of the prosthesis and from the gage length of a fatigue specimen. In Plates 5.4 and 5.5 the microstructures of the two samples appear to be different; the prosthesis material contains more interdendritic carbide than the fatigue test material. It is believed that the only cause for this was the lower carbon content in the latter.

Common to both materials was the large dendritic grain structure (ASTM size 0), and only a single layer of fine surface grains. These features are typical of castings which were poured into heated molds and slowly cooled.

Both materials also contained porosity. In the case of the prosthesis material it was predominantly present at the grain boundaries, while in the fatigue specimen the porosity was located both within the grains, usually associated with carbides, and at the grain boundaries.

Based on these observations, in addition to the lack of extensive coring it is likely that both materials were in the cast and homogenized conditions. In the case of the fatigue specimen, the annealing temperature may have been somewhat high and resulted in a partial dissolution of the



Plate 5.4 Typical Microstructure of Vitallium Hip Implant  
(100X)

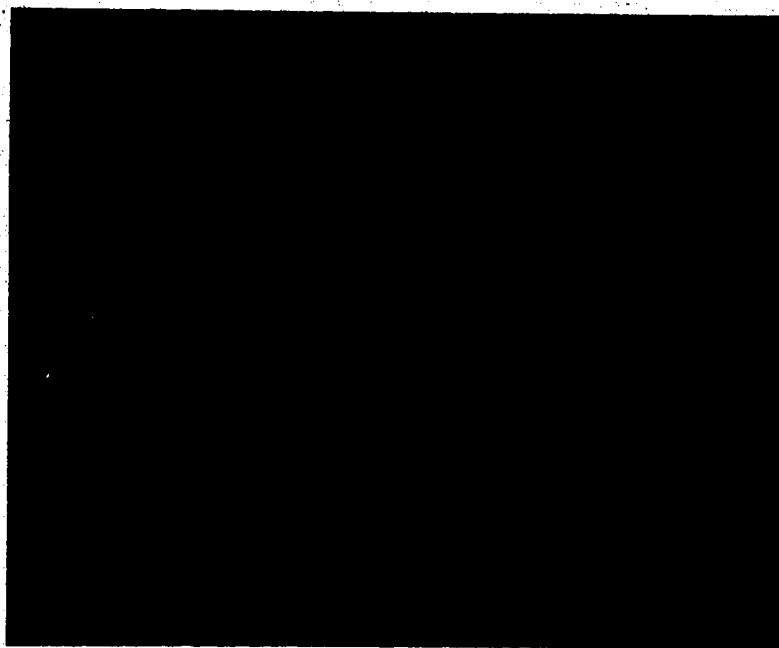


Plate 5.5 Typical Microstructure of Cast Vitallium Fatigue  
Specimen (100X)

interdendritic carbides and the formation of porosity.

#### 5.1.2.2 Hardness Results

Rockwell 'C' hardness tests and Vickers microhardness tests were made on both materials with the following results.

Table 5.4  
Hardness of Vitallium Test Materials

|                          | ASTM<br>F75-76   | Implant<br>Sample | Fatigue<br>Sample |
|--------------------------|------------------|-------------------|-------------------|
| Rockwell 'C'<br>Hardness | 25-34            | 27                | 25                |
| Vickers<br>Microhardness | Not<br>Specified | 295               | 322               |

Although the hardnesses are near the lower limit of the specified hardness range, both materials conform to the specification.

The discrepancy between the microhardnesses and the Rockwell hardnesses of the two samples is likely a result of a variation in hardnesses among various heats.

#### 5.1.2.3 Tensile Results

Three of the fatigue samples were tensile tested with the following results:

Table 5.5  
Tensile Properties of Vitallium Fatigue  
Specimens

|                                 | ASTM F75-76               | Samples               |                       |                        |
|---------------------------------|---------------------------|-----------------------|-----------------------|------------------------|
| Tensile Strength                | 655 MPa (min)<br>(95 ksi) | 630 MPa<br>(91.4 ksi) | 663 MPa<br>(96.2 ksi) | 727 MPa<br>(105.5 ksi) |
| Yield Strength<br>(0.2% Offset) | 450 MPa (min)<br>(65 ksi) | 418 MPa<br>(60.6 ksi) | 397 MPa<br>(57.6 ksi) | 272 MPa<br>(39.4 ksi)  |
| Elongation                      | 8% (min)                  | 8.6%                  | 9.4%                  | 10%                    |

These results show the tensile strengths of the fatigue samples to be highly variable (from -3% to 11% based on the minimum specified) as well as only marginally acceptable. Furthermore, the yield stresses are even more variable, and below the specified minimum values. While conformance to this specification may not be required, it is almost certain that the variability is unacceptable.

Although the corrosion behavior of the fatigue specimens would be almost identical to the prosthesis material, the endurance limit may be somewhat low as a result of the marginally acceptable tensile strength, and low, but acceptable, ductility.

### 5.1.3 Water

Common to all tests was the water used to prepare the test solutions. It was assumed that the building's purified water would be suitable. However, analysis showed the resistivity to be well below the value given in the system specifications. Since maintenance was scheduled on the order of weeks per interval, a fluctuation in water quality was expected. This source was, therefore, judged not to be sufficiently consistent, or dependable for the research. This judgement was reinforced when, during early experimentation, the deionizer resin was changed and, for several days thereafter, the water had a strong organic odor and a surfactant quality.

To ensure consistent quality, water from the building's system was first passed through a series of ion exchange columns. Any organics present were then oxidized during a single distillation from a potassium permanganate solution. Water produced by this means had an average resistivity of 10K ohms-cm.

### 5.1.4 Simulated Physiological Solutions

The ingredients of the basic simulated physiological solution were as follows:

Table 5.6  
Composition of Simulated Physiological  
Solution

---

| Component  | Weight<br>(g/l) |
|--|-----------------|
| NaCl   | 6.30            |
| KCl  | 0.374           |
| NaHCO <sub>3</sub>                                 | 2.76            |
| Na <sub>2</sub> HPO <sub>4</sub>                   | 0.071           |
| NaH <sub>2</sub> PO <sub>4</sub> ·H <sub>2</sub> O | 0.069           |
| Glucose  | 1.000           |
| MgCl <sub>2</sub> ·6H <sub>2</sub> O               | 0.203           |
| MgSO <sub>4</sub>                                  | 0.060           |

The dry ingredients for simulated physiological solutions (SPS) were prepared in batch quantities of up to thirty times the nominal composition. To ensure homogeneity, all ingredients were first pulverized with an agate mortar and pestle, and to avoid precipitation of magnesium salts during dissolution, all components bearing magnesium were segregated into a separate vial.

Besides the glucose, organics were also added in the form of calf serum, prepared by Flow Laboratories. Primarily concentrations of 0.01%, 0.1%, 5%, and 15% were used; however, in one test 0.001% serum was used.

Solutions were prepared in a one litre volumetric flask. First the serum was diluted, then the



non-magnesium-bearing salts were dissolved, followed by those containing magnesium. The solutions were mixed with a magnetic stirrer.

---

### 5.1.5 Gases

The gases used in the testing of the cobalt alloys were prepared by Matheson of Canada Ltd. and had the following compositions:


Table 5.7  
Gas Compositions

|                           |                 |                           |
|---------------------------|-----------------|---------------------------|
| Interstitial <sup>3</sup> | O <sub>2</sub>  | 40 mm (Hg)<br>(0.056 atm) |
|                           | CO <sub>2</sub> | 45 mm<br>(0.063 atm)      |
| Bottle 1                  | O <sub>2</sub>  | 6.65 molar percent        |
|                           | CO <sub>2</sub> | 6.11 "                    |
|                           | Ar              | Balance                   |
| Bottle 2                  | O <sub>2</sub>  | 6.47 molar percent        |
|                           | CO <sub>2</sub> | 6.11 "                    |
|                           | N <sub>2</sub>  | Balance                   |

## 5.2 Polarization Studies.

### 5.2.1 Development of Experimental Procedure

Before potentiostatic polarization testing could begin it was necessary to develop a standardized experimental procedure that would yield reproducible results. For this purpose ASTM designation G5-78 was used. This practice involves the generation of anodic polarization curves for



430 stainless steel in deaerated 1N  $H_2SO_4$ . It provides standard curves with which to compare results, and discusses experimental problems that may be encountered.

---

Instructions for solution and sample preparation were generally adhered to, with the following exceptions:

1. It was recommended that the working electrode be degreased in boiling benzene; this was not done. Rather, samples were ultrasonically rinsed in acetone.
2. Argon replaced hydrogen as the purging gas. According to Chance et al.<sup>1,2</sup>, when all other factors remain the same, this does not affect the results.
3. The platinum counter electrodes were not platinized.
4. The starting potential was below the corrosion potential.

#### 5.2.1.1 Test Apparatus

Figure 5.1 gives an illustration of the equipment used in this initial work. The system has four main units: the polarization cell, the gas purification and monitoring system, the potentiostat, and the current measuring and recording system:

##### The Cell

The cell and the glassware for the five electrodes were similar in design to those described by Greene<sup>7,8</sup>. The temperature of the test solution was maintained at 37°C by partial immersion in an oil bath.

##### The Gas System

As mentioned, argon was used as the purging gas. Because it was found to contain oil, which accumulated in

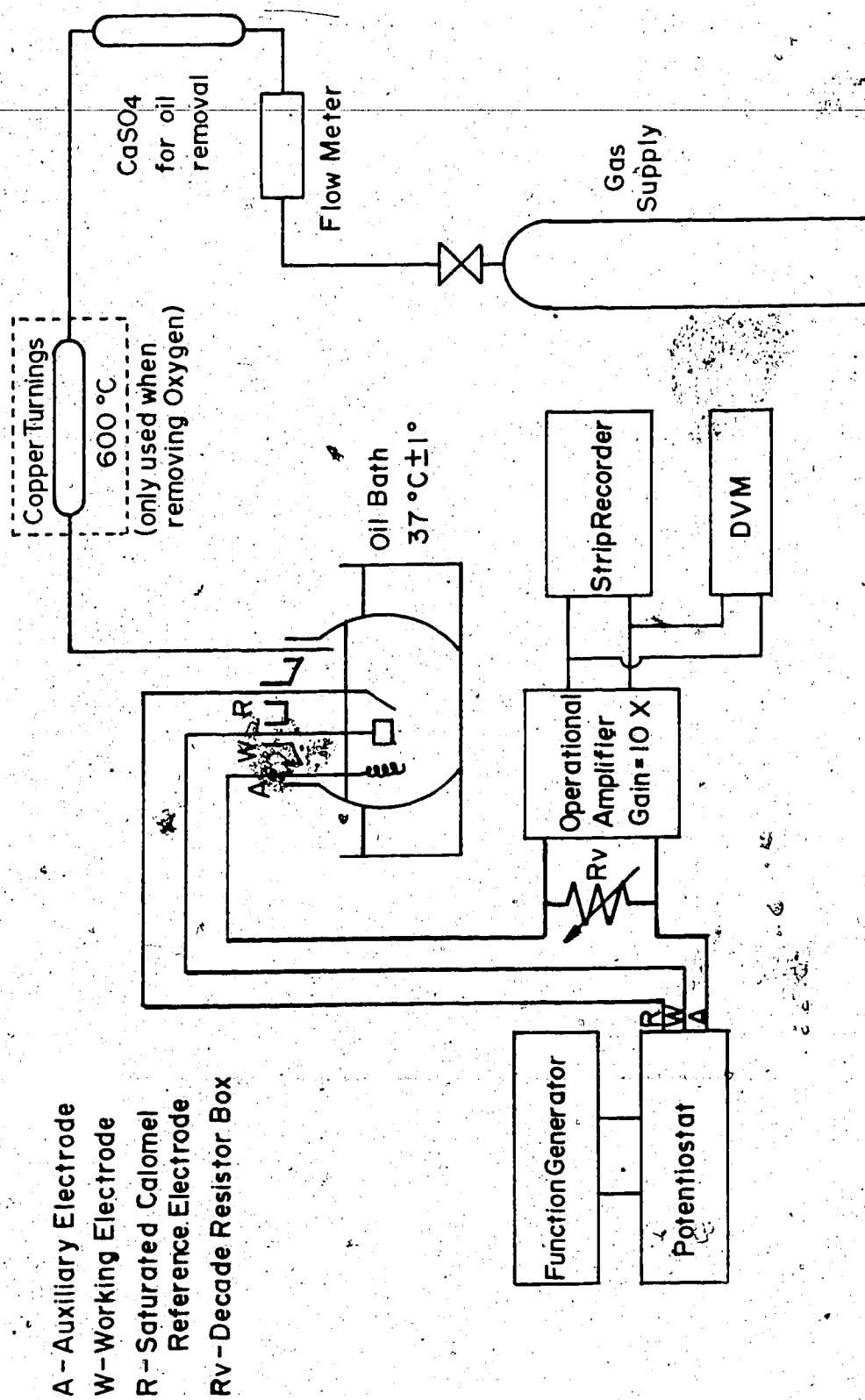


Figure 5.1 Initial System Components

the Tygon tubing, an effort was made to remove the oil by passing the gas through calcium sulphate chips at a rate of 20 mL/min. Any residual oxygen was removed by passing the gas over copper turnings or titanium powder at 600°C.

#### The Potentiostat and Current Measuring Systems

During the course of the experimentation two potentiostats and current measuring systems were utilized. Initially, an AMEL 549 potentiostat was used. Current was determined by measuring the voltage drop across a decade resistance box, placed in series between the counter electrode and the potentiostat. A strip recorder and voltmeter were isolated from the cell by an operational amplifier wired as a voltage follower with a gain of 10:1. The strip recorder monitored corrosion current with time.

This system had a number of problems and limitations. As Figure 5.2 shows, the characteristic curve for the amplifier deviates from linearity below 0.03 volts output, and gives negative output for input potentials below  $2 \times 10^{-4}$  V. These features of the amplifier became important as currents in this range were often encountered as the corrosion potential was approached.

One other limitation resulted from the fact that resistors of greater value than 10K $\Omega$  were found to affect cell reactions. The decade resistance box, therefore, could only contain five ranges; the resistor values are given below.

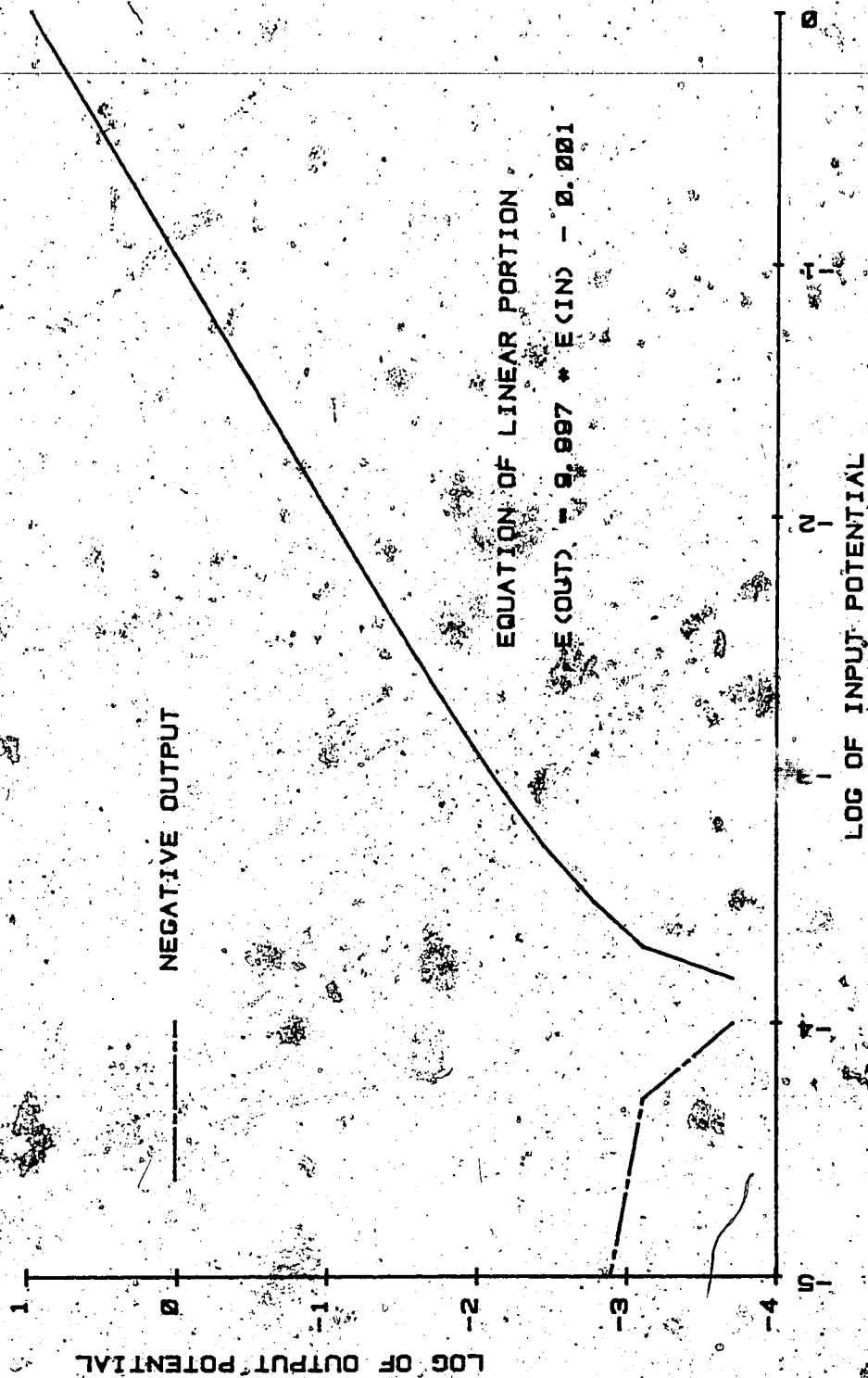


Figure 5.2 Operational Amplifier Characteristic Curve

Table 5.8  
Decade Resistor Values

| Nominal Value<br>(Ohms) | Measured Value<br>(Ohms) |
|-------------------------|--------------------------|
| 1                       | 1.0                      |
| 10                      | 10.0                     |
| 100                     | 99.6                     |
| 1K                      | 980.3                    |
| 10K                     | 8826.0                   |

The second system consisted of an AMEL 551 potentiostat with an AMEL 560 log interface. As before, the strip recorder monitored current with time and an electrometer was used to digitize the analog current values. The experimental arrangement for this system is illustrated in Plate 5.6 and in Figure 5.3.

#### 5.2.1.2 Procedures

Samples were prepared by wet abrasion down to 600 grit, with SiC paper. They were stored in acetone during transport from room to room. Prior to immersion they were rinsed in the building's purified water, then dipped in test solution.

Before the test began, the solution was purged of oxygen for at least one-half hour prior to the introduction of the sample, then the system was allowed to equilibrate for one-half to one hour.

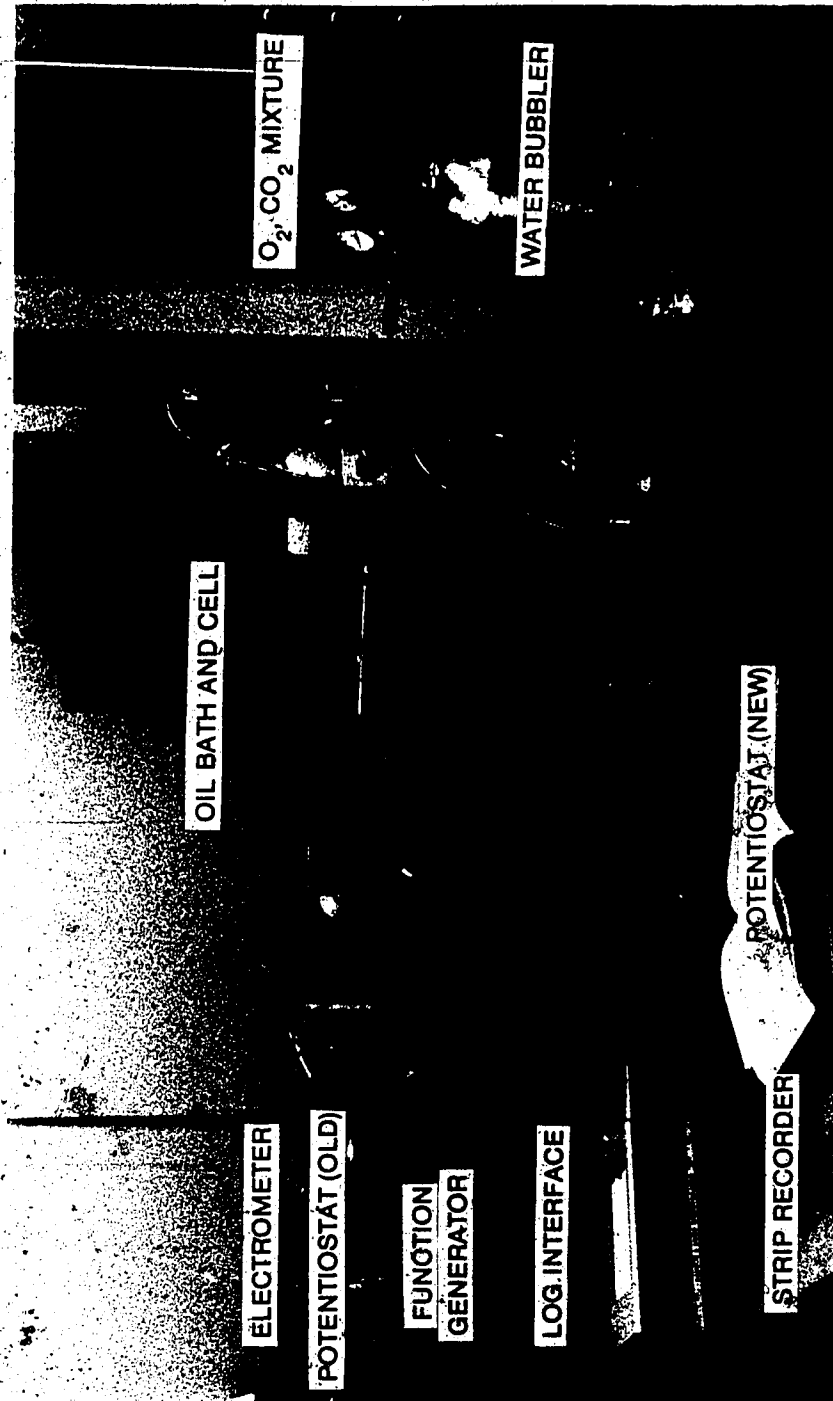


Plate 5.6 Equipment Used in Later Potentiostatic

Polarization Testing

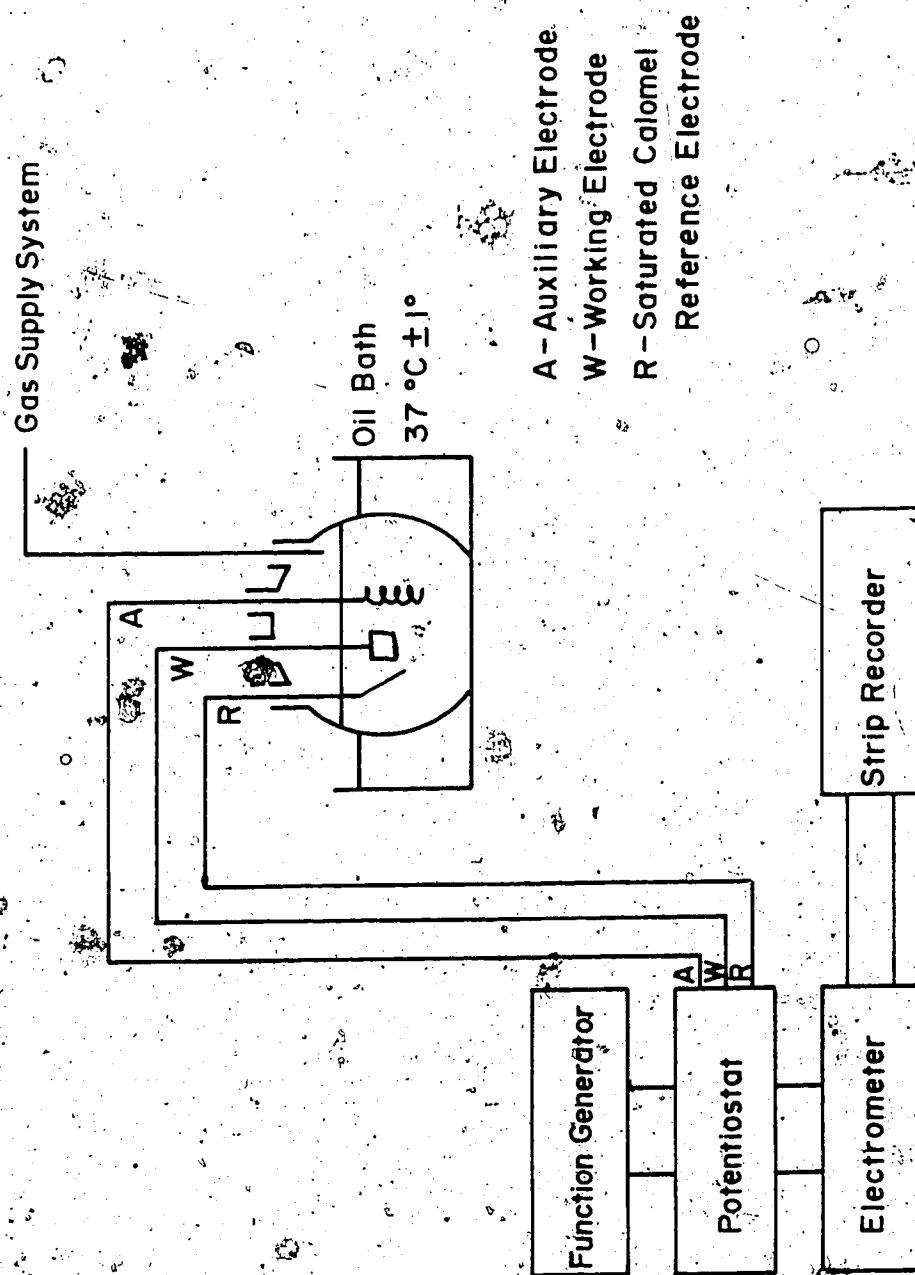


Figure 5.3 Second Potentiostat and Current Measuring System



At startup, a potential below the corrosion potential was set on the potentiostat, and a maximum level and stepping rate were set on the function generator. Finally, the cell was switched into the potentiostatic circuit, and the strip recorder turned on.

### 5.2.2 Polarization Studies in Simulated Physiological Solution

When it was found that the experimental methods could be used to generate reproducible results, work began on testing the stainless steel and cobalt alloy in simulated physiological solution.

#### 5.2.2.1 Procedures

The solution was prepared by first diluting the serum, where it was used, followed by the dissolution of the magnesium-free salts, and the magnesium salts.

As it was found that aeration of solutions containing serum, by bubbling, produced large quantities of stable foam, another method was required. This new method involved producing a vortex with a magnetic stirrer such that a swirling mass of bubbles and solution was formed. Any foam produced by this method was immediately broken by the turbulence. This process lasted approximately twenty minutes prior to the introduction of the sample.

Concurrent with solution aeration, the samples were prepared. They were first wet abraded to a 600 grit finish, then immersed in acetone while being transported, washed

with a mild detergent, rinsed in tap water, and, finally, ultrasonically degreased, again in acetone. Before the samples were placed in the cell, they were rinsed in distilled water and dipped in test solution.

---

With the stirrer rotating at about 40 rpm, the system was allowed to equilibrate for one hour. After this period, the corrosion potential was measured, the starting potential set, and the cell switched into the potentiostatic circuit.

Where applicable, the reverse scan was made at the same scan rate. The value of the current just before the next potential step was recorded.

### 5.3 Corrosion Fatigue

#### 5.3.1 Apparatus

These tests used a system composed of three units: the load frame, the cell, and the solution conditioning and circulation unit. The experimental arrangement is illustrated in Plate 5.7.

##### 5.3.1.1 The Load Frame

All fatigue tests were performed on the MTS 810 Load Frame. This is a versatile closed-loop hydraulic system with adjustable cycle frequencies and waveforms, and a maximum load capacity of twenty-five metric tons.

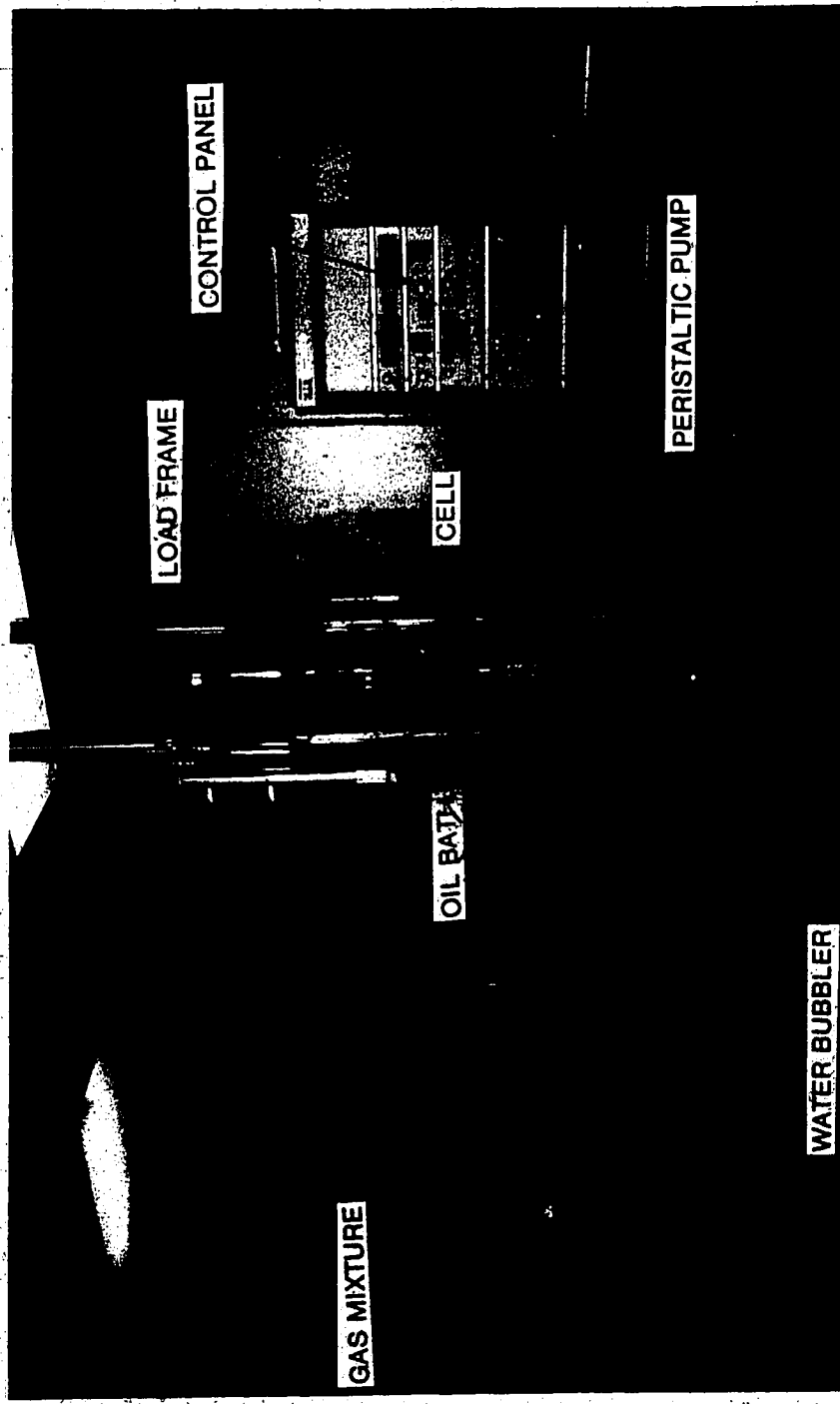


Plate 5.7 Equipment Arrangement for Corrosion Fatigue Testing

### 5.3.1.2 The Cell

The cell, constructed of acrylic, Plate 5.8, was designed to allow axial loading of a threaded tensile specimen in a liquid environment. The assembly consisted of a cylinder with endplates, one of which was removable. To accommodate grip extensions, an opening was made in each end with rubber 'O' rings to provide leak-free operation. Two ports in the side of the cylindrical section served as inlet and outlet for the circulating solution, while a third hole was made available for an optional reference electrode.

### 5.3.1.3 Solution Conditioning And Circulation

Constant test conditions were maintained at all times during a test. In a reservoir outside the cell the solution was aerated by the previously described 'vortex' method and the gas pressure above the solution was set to approximately 1 Pa by a water bubbler. Solution temperature was regulated by immersion in an oil bath.

A peristaltic pump circulated the solution to the cell at a rate of 1 mL per second; return flow was by gravity.

The sample potential was not monitored.

### 5.3.2 Samples

All the specimens were found to have some degree of bend; some more than others. In one case the testing machine grips could not accommodate the bend and the test could not be performed.

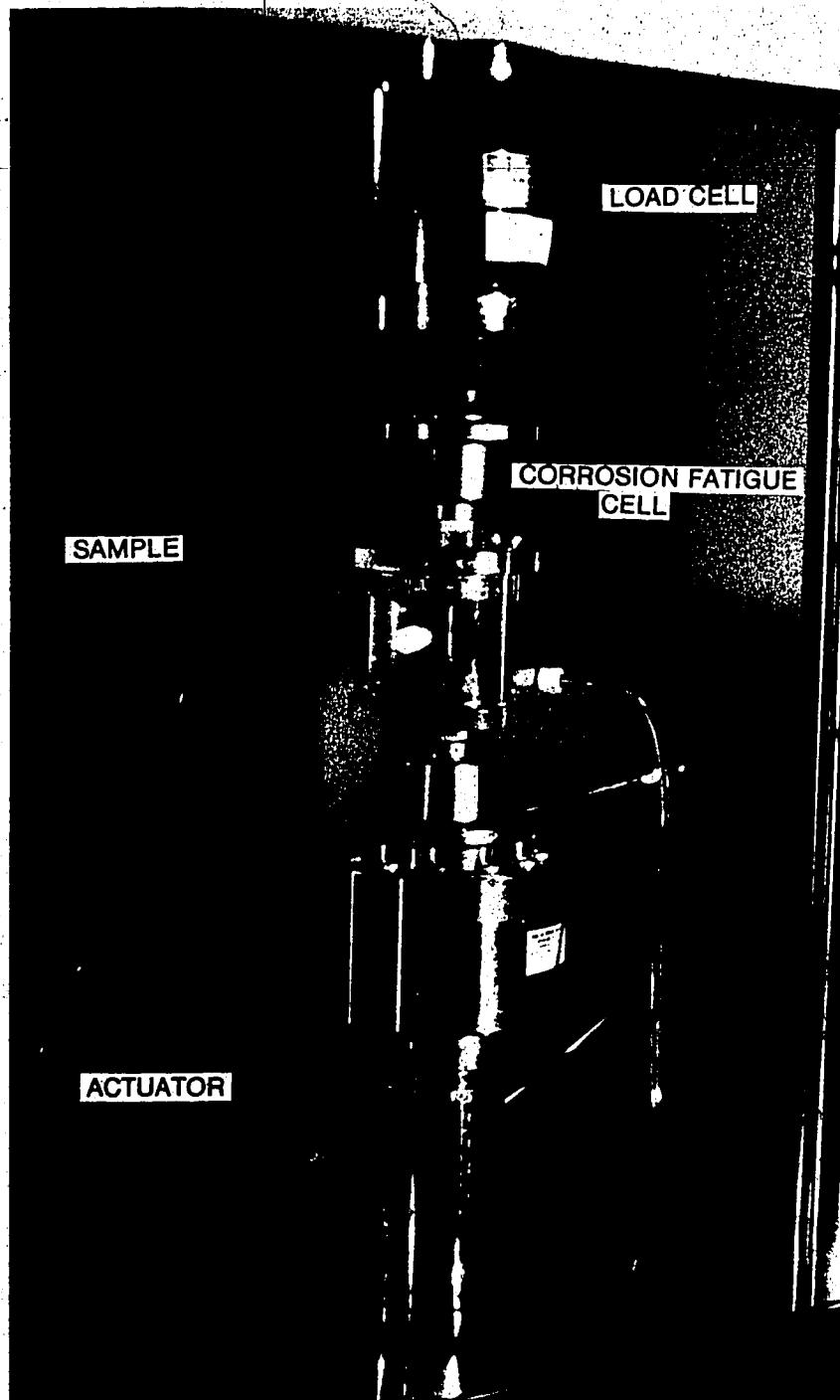


Plate 5.8 The Corrosion Fatigue Cell

The specimens were notched with a low speed diamond wheel to a nominal depth of 0.17 of the diameter. In cases where the bend was noticeable, the notch was made on the concave side. Plate 5.9 shows the typical location of the notches and Plate 5.10 shows a cross section of a typical notch to have a tip radius of approximately 0.25 mm (note porosity).

### 5.3.3 Test Solutions

Solutions consisted only of zero and five percent serum mixed with the other ingredients in the same manner as in the previous tests.

### 5.3.4 Procedures

The specimens were prepared by rinsing them in acetone to remove felt pen markings, followed by washing, rinsing, and drying.

The sample was then threaded into the grip extensions and the crevices at each end covered with Unichrome 'Quick Dry' Stop-Off Lacquer 323 (a fast drying vinyl lacquer produced by M&T Chemicals Inc. for use in the electroplating industry). After the lacquer had dried (one-half hour), the cell was sealed shut, and the solution pumped in.

In order to simulate loading on the hip, fatigue testing involved the use of a sinusoidal load waveform at a frequency of 1 Hz. As the tests were aimed at examining the corrosion fatigue propagation rates and fracture

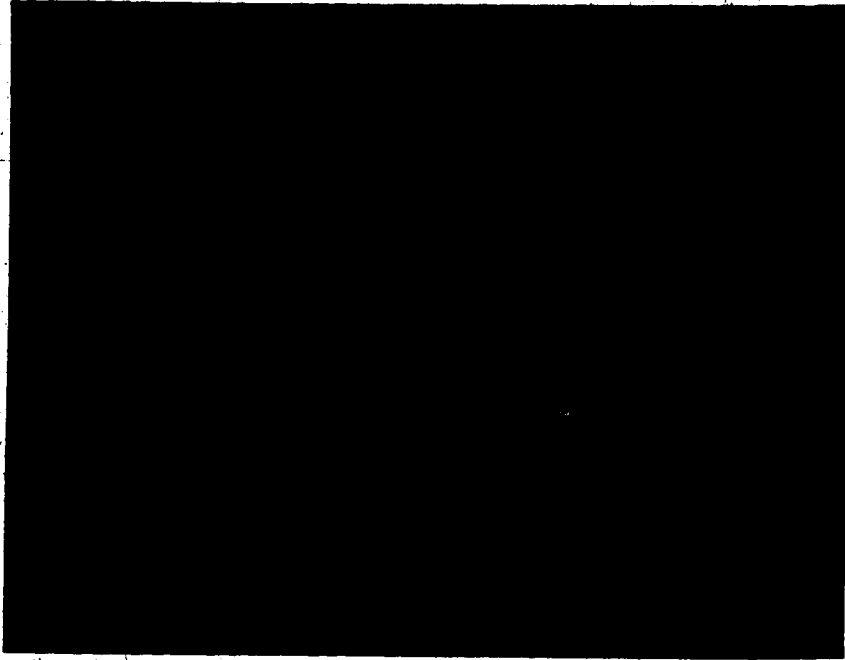


Plate 5.9 Fatigue Specimens showing the Typical Location of the Notch

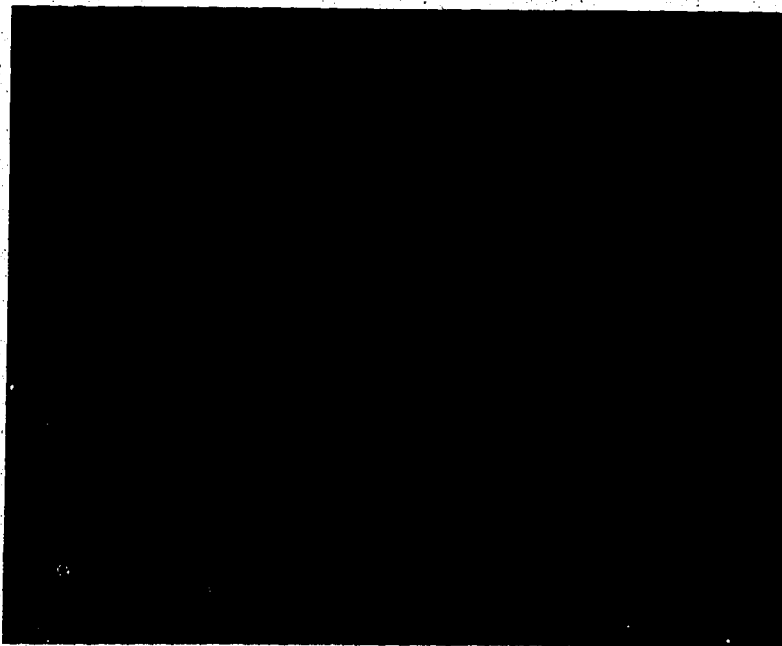


Plate 5.10 Notch Geometry (50X)

morphologies, and not the total fatigue lives, loads were increased well above the endurance limit at  $10^7$  cycles. Selection of the loads was based on the test stress and on the area of the ligament remaining after notching. Minimum and maximum stresses were set at 48.3 and 448.2 MPa (7.0 and 65.0 ksi), for a load ratio of approximately 0.007.

The number of cycles to failure was recorded by a counter panel on the 810 system.

After the samples had failed, the total number of load cycles was recorded and the fracture surfaces were examined by means of a stereo optical microscope and a scanning electron microscope.

#### 4. Conventions

Throughout this thesis all electrical potential differences will be referenced to the Saturated Calomel Electrode (SCE), which is related to the Standard Hydrogen Electrode (SHE) by the following relation:

$$E(\text{SCE}) = 0.244 \text{ V}(\text{SHE}) - 0.00065 \text{ V}/^\circ\text{C}$$

Whenever a potential is calculated by the Nernst Equation the free energy value used will be the reported value at  $25^\circ\text{C}$ , but the temperature will be the test value,  $37^\circ\text{C}$ . Thus:

$$2.303 \text{ RT}/\text{F} = 0.0615 \text{ V}$$

It is considered that the error resulting from this procedure will be insignificant from a practical viewpoint.



## 6. RESULTS AND DISCUSSION

### 6.1 Technique Development

The results of the procedure standardization tests are given in Figure 6.1. Figure 6.2 gives the reference plot taken from ASTM G5-78. Comparison between these curves indicates that the procedure can be used to obtain satisfactory and reproducible results.

### 6.2 316L Stainless Steel and Cast Vitallium in Serum-Free and Glucose-free Solution

In order to obtain a perspective on the corrosion behavior of the cast Vitallium, several tests were also made on 316L stainless steel in glucose and serum-free simulated physiological solution. The results of these potentiostatic polarization tests are presented and discussed below.

#### 6.2.1 Stainless Steel

Three tests were performed on the 316L stainless steel to determine its corrosion behavior in a simulated physiological solution. Parameters of particular interest were the corrosion and passive current densities, and the corrosion, breakdown, and repassivation potentials. In each case the start potentials were within 25 mV of -0.50 V (SCE), and the potential was increased by 50 mV every five minutes.

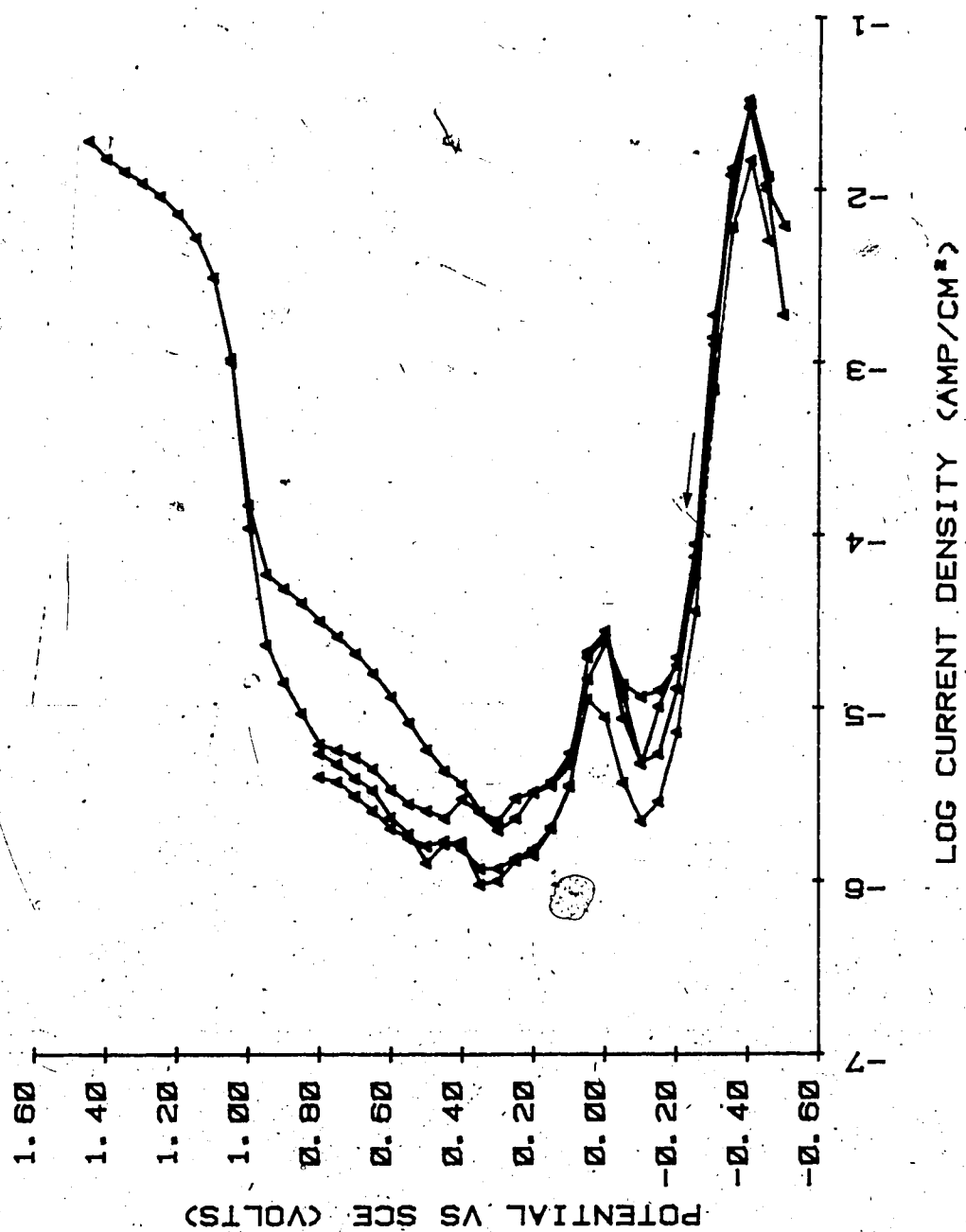


Figure 6.1 Experimental Polarization Plot for 430 Stainless

Steel in 1N H<sub>2</sub>SO<sub>4</sub>

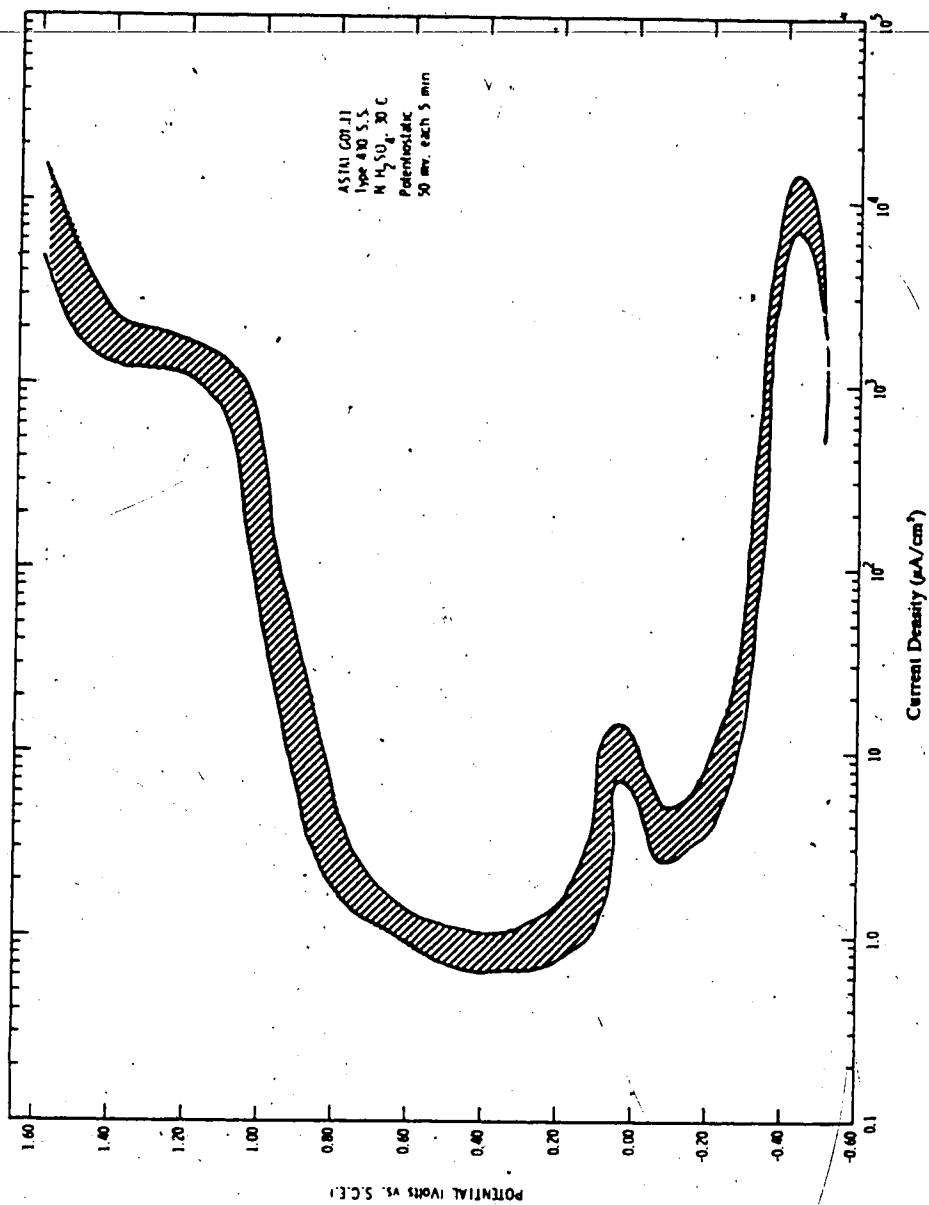


Figure 6.2 Standard Potentiostatic Anodic Polarization Plot for 430 Stainless Steel in 1N H<sub>2</sub>SO<sub>4</sub>. Taken from ASTM G5-78.

The forward anodic scans of all three tests (Figure 6.3) had essentially the same features; the reversible potentials all lay within a narrow range, the corrosion currents ~~were~~ all similar, as were the positions of the cathodic and anodic curves. The average values of the polarization parameters are given in Table 6.1.

Table 6.1  
Polarization Parameters for 316L in Saline  
Solution

|               | Current<br>(A/cm <sup>2</sup> ) | Potential<br>(V) |
|---------------|---------------------------------|------------------|
| Corrosion     | $1.6 \times 10^{-7}$            | -0.26            |
| Passive       | $4.0 \times 10^{-7}$            | ----             |
| Breakdown     | ----                            | 0.15             |
| Repassivation | ----                            | -0.14            |

In the case of scan 1, film breakdown had not occurred at the potential of reversal and the surface passivated to a greater degree than on the forward scan. In the cases of the other two scans breakdown occurred within the range of 0.1 to 0.2 V, whereupon the current increased toward an apparent transpassive region. Following reversal, the currents remained high forming a hysteresis; repassivation was achieved between -0.13 and -0.15 V.

After the latter two of these tests the area beneath the PTFE gasket was corroded. This localized attack was interpreted to be responsible for the hysteresis effect.

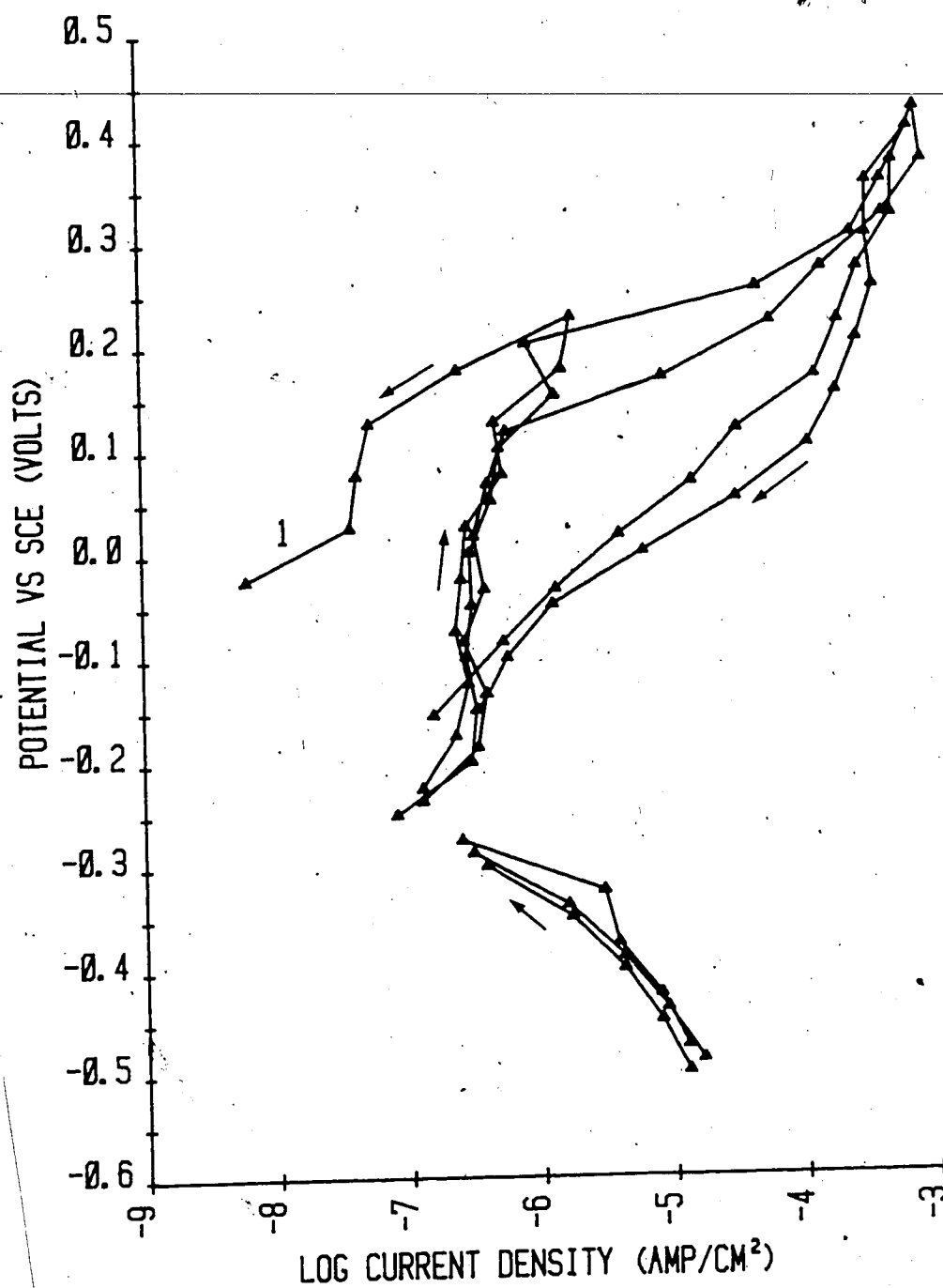


Figure 6.3 Polarization Curves for 316L in Glucose-Free and Serum-Free Simulated Physiological Solution

In order to determine whether or not a higher breakdown potential, due to pitting, existed in the absence of a crevice a further test was performed with the sample only partially submerged; the gasket-sample interface remained above the solution surface. Table 6.2 summarizes the parameters for this test.

Table 6.2  
Corrosion Parameters for 316L without a  
Crevice

|           | Current<br>(A/cm <sup>2</sup> ) | Potential<br>(V) |
|-----------|---------------------------------|------------------|
| Corrosion | $1.6 \times 10^{-7}$            | -0.28            |
| Passive   | $4.4 \times 10^{-7}$            | ----             |
| Breakdown | ----                            | 0.60             |

Figure 6.4 shows that the position of the cathodic curve, the reversible potential, and the passive region for this crevice-free situation to be similar to those of the previous results. However, a higher breakdown potential now exists at 0.5 to 0.6 V, 300 to 400 mV above the previous breakdown position.

According to the polarization curve and the current-time trace (not included), at potentials of approximately 0.1 V, current peaks were experienced, but when 0.2 V was reached the current trace was steady once again. As breakdown previously occurred in this range, the disturbance is considered to have been due to an unstable crevice-like situation, perhaps at the meniscus.

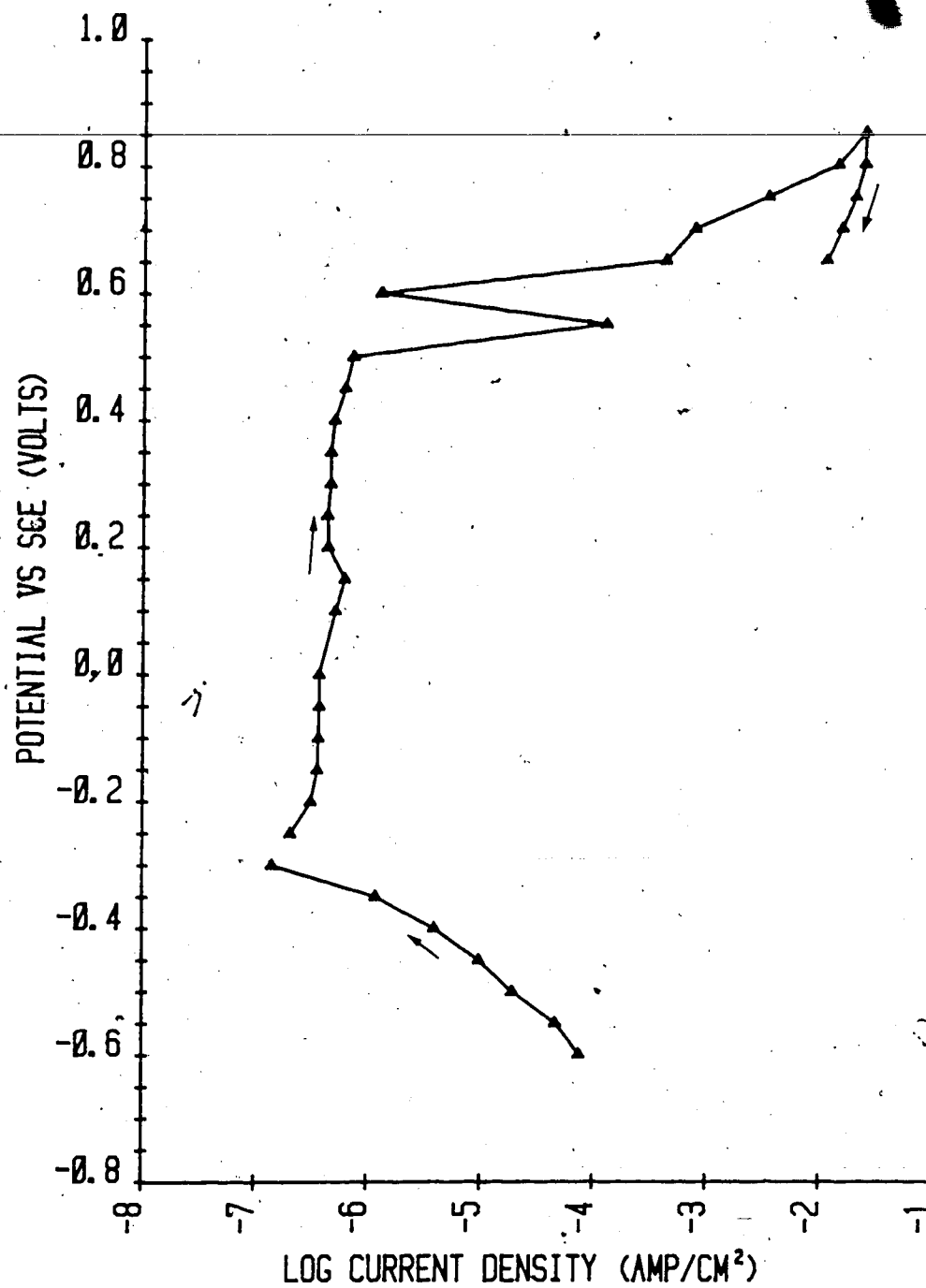


Figure 6.4 Polarization Curve for 316L in Semi-Submerged Position

Although the reverse scan was not extended back to the repassivation potential, enough has been completed to indicate the presence of the hysteresis.

### 6.2.2 Cast Vitallium

In order to evaluate the corrosion behavior of the Vitallium and to compare it with that of the stainless steel, several tests were conducted in identical serum-free and glucose-free solutions as the previous tests. As before the potential was increased in 50 mV steps every five minutes from the starting potentials of -0.40 and -0.60 V. No precautions were taken to avoid the formation of a crevice between the PTFE gasket and the sample.

Samples exhibited self-passivation in every case. The corrosion parameters corresponding to Figure 6.5 are listed below.

Table 6.3  
Polarization Parameters for Vitallium in  
Glucose-Free Saline Solution

|               | Current<br>(A/cm <sup>2</sup> ) | Potential<br>(V) |
|---------------|---------------------------------|------------------|
| Corrosion     | $2.7 \times 10^{-7}$            | -0.38            |
| Passive       | $4.0 \times 10^{-7}$            | ----             |
| Breakdown     | ----                            | 0.38             |
| Repassivation | ----                            | 0.35             |

The material displayed a very small hysteresis which increased slightly as the reverse potential was taken to



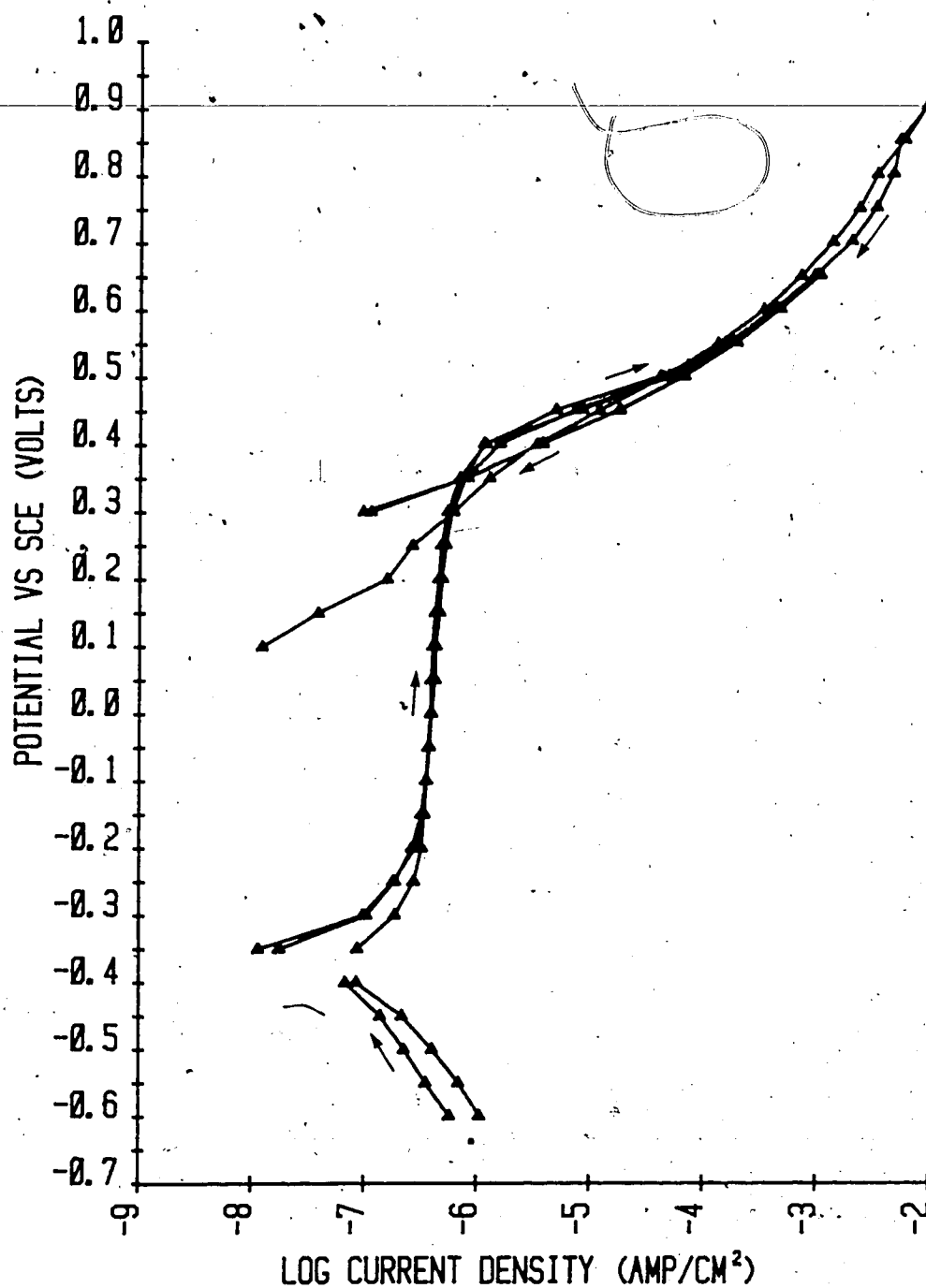


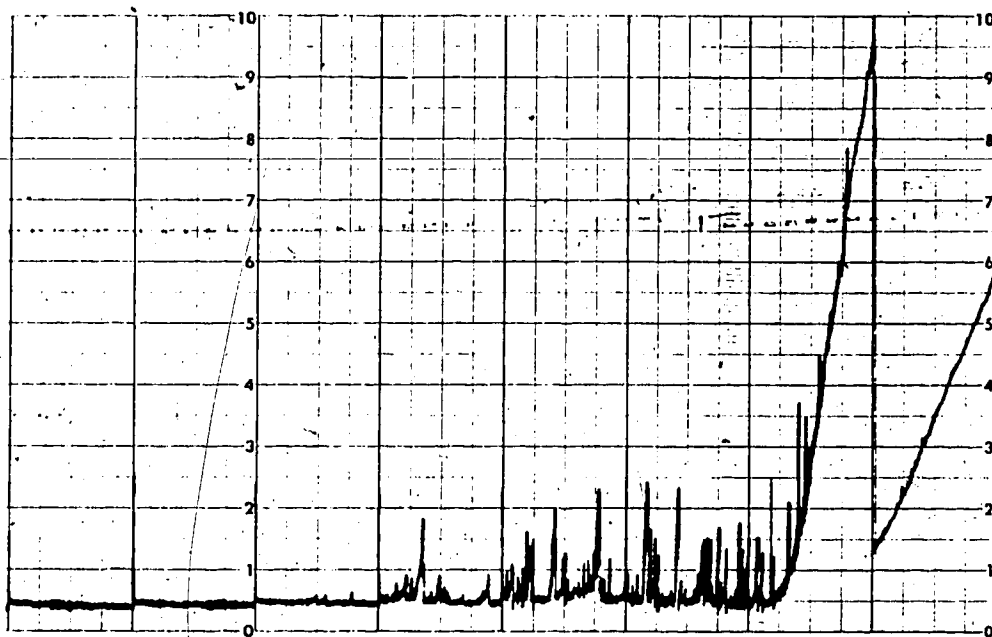
Figure 6.5 Polarization Curves for Vitallium in Glucose-Free and Serum-Free Solution

more positive values, in agreement with the results of Wilde'. No crevice attack or pitting was observed on the sample at the end of any test.

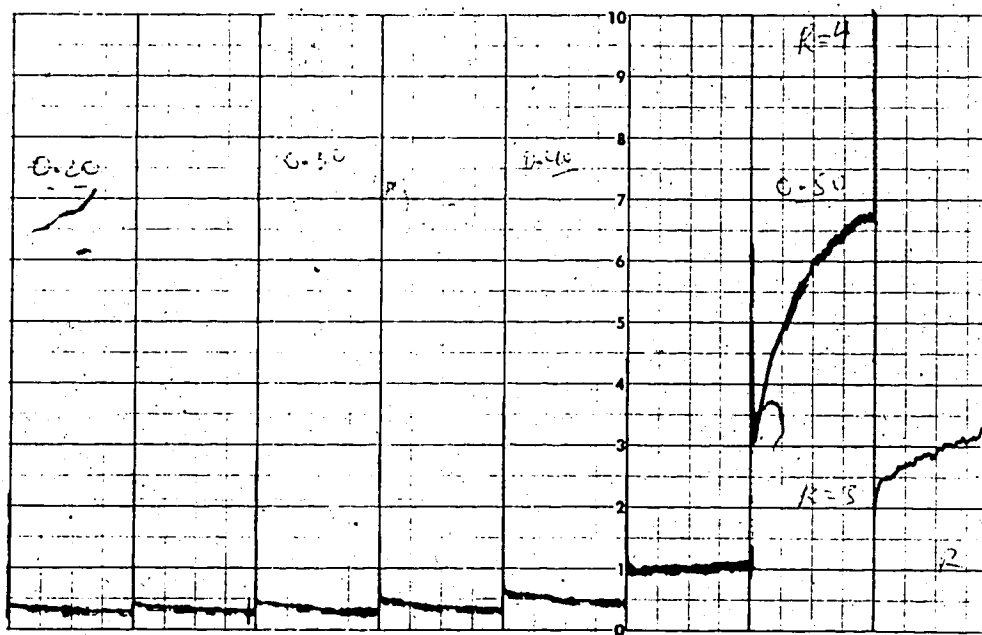
It is also interesting to compare the current-time traces for the stainless steel and the Vitallium, Figure 6.6. In contrast to the instability shown by the stainless steel prior to breakdown the cobalt alloy exhibited a stable low current until the sharp rise occurred at the breakdown potential. This stability would suggest that in the short time it took to perform this test (less than six hours) passive film breakdown and repair did not occur..

#### 6.2.3 316L vs. Vitallium

Although both materials exhibit self-passivation, and the corrosion and passive currents were approximately the same, the relative sizes and positions of the hystereses give a more significant measure of the relative long term corrosion behaviors. Based on the values of the repassivation potentials with respect to the breakdown potentials, it is, therefore, concluded that the cobalt alloy should be more resistant to localized attack than the stainless steel. Quantitatively, this resistance can be expressed in terms of the ratio of the differences between the breakdown and the repassivation potentials and between the breakdown and the reversible potentials. These results indicate that the likelihood of localized attack initiating spontaneously on Vitallium is much less than on 316L. These



316L Stainless Steel



Vitallium

Figure 6.6 Current-Time Traces for 316L and Vitallium

findings are in agreement with those of others including Hoar and Mears<sup>43</sup>.

The relevant parameters of both materials are given below.

Table 6.4  
Anodic Polarization Parameters

| <u>Parameter</u>                    | <u>316L<br/>Stainless Steel</u> | <u>Cast<br/>Vitallium</u> |
|-------------------------------------|---------------------------------|---------------------------|
| $E_{corr}$                          | -0.26 V                         | -0.38 V                   |
| $E_b$                               | 0.15 V                          | 0.38 V                    |
| $(E_b - E_{corr}) / (E_b - E_{rp})$ | 1.4                             | 13.8                      |

The implication of these results is that, from a corrosion point of view, Vitallium is more suitable as an implant material owing to its higher resistance to localized attack, and to its broad passive potential range. Although the stainless steel shows some resistance to localized attack in the absence of crevices, this situation cannot be guaranteed, and even if it could, the current instability, noted in the crevice breakdown potential range, may indicate that the resistance would only have short term value.

### 6.3 The Effects of Organics on the Corrosion of Cast Vitallium

The next series of experiments was conducted to evaluate the effects of combinations of glucose and serum on the corrosion behavior of the cobalt alloy. These tests consisted of two sets: the first was designed to determine whether or not the organics had any major effects on the polarization curves. Tests were made using serum at concentrations of 0%, 0.01%, 0.1%, 5%, and 15%, and at a stepping rate of 50 mV every five minutes in the manner described in the previous chapter. During all of these tests solution samples were drawn at intervals for pH determination.

One test was also performed to monitor the change in corrosion potential with time. A Vitallium sample was immersed in oxygenated saline solution containing glucose but no serum, and the potential was recorded approximately every five minutes over twenty-four hours using the Hewlett-Packard 9825A desktop computer.

When it was found that the organics only affected the position of the cathodic curve and the value of the corrosion potential, the second set of tests was conducted to examine these changes in more detail. Cathodic potentiostatic polarization tests were made with the following glucose-serum combinations:

|                       |       |
|-----------------------|-------|
| No Glucose / No Serum | NG/NS |
| Glucose / No Serum    | G/NS  |
| Glucose / Serum       | G/S   |
| No Glucose / Serum    | NG/S  |

---

In contrast to the first set of tests the potential stepping rate was decreased, in most cases, from 50 mV to 10 mV every five minutes.

In the following section, the results of each set of tests will be presented and discussed. At the end, the overall effects of the organics on the potentiostatic polarization behavior of the alloy will be discussed.

### 6.3.1 Preliminary Tests on the Effects of Organics

#### 6.3.1.1 The Effects of Glucose in the Absence of Serum

The results of the preliminary polarization tests in solutions containing glucose but no serum are given in Figure 6.7 and Table 6.5.

**Table 6.5**  
**Corrosion Parameters in Solution Containing**  
**Glucose but no Serum**

|               | Current<br>(A/cm <sup>2</sup> ) | Potential<br>(V) |
|---------------|---------------------------------|------------------|
| Corrosion     | $2.7 \times 10^{-7}$            | -0.35            |
| Passive       | $4 \times 10^{-7}$              | ----             |
| Breakdown     | ----                            | 0.38             |
| Repassivation | ----                            | 0.35             |

Comparing the results for a solution without glucose (Figure 6.5) and a solution with glucose (Figure 6.7) it is evident that they both have essentially the same characteristics: the values of the corrosion and breakdown potentials, as well as the corrosion and passive currents are not significantly different, and the hystereses are identical. These similarities indicate that, in the absence of serum, glucose does not hinder the formation or short term stability of the passive surface film.

#### The Effects of Serum in the Presence of Glucose

Figure 6.7 gives the results of the preliminary tests using glucose and serum. Table 6.6 summarizes the corrosion parameters.

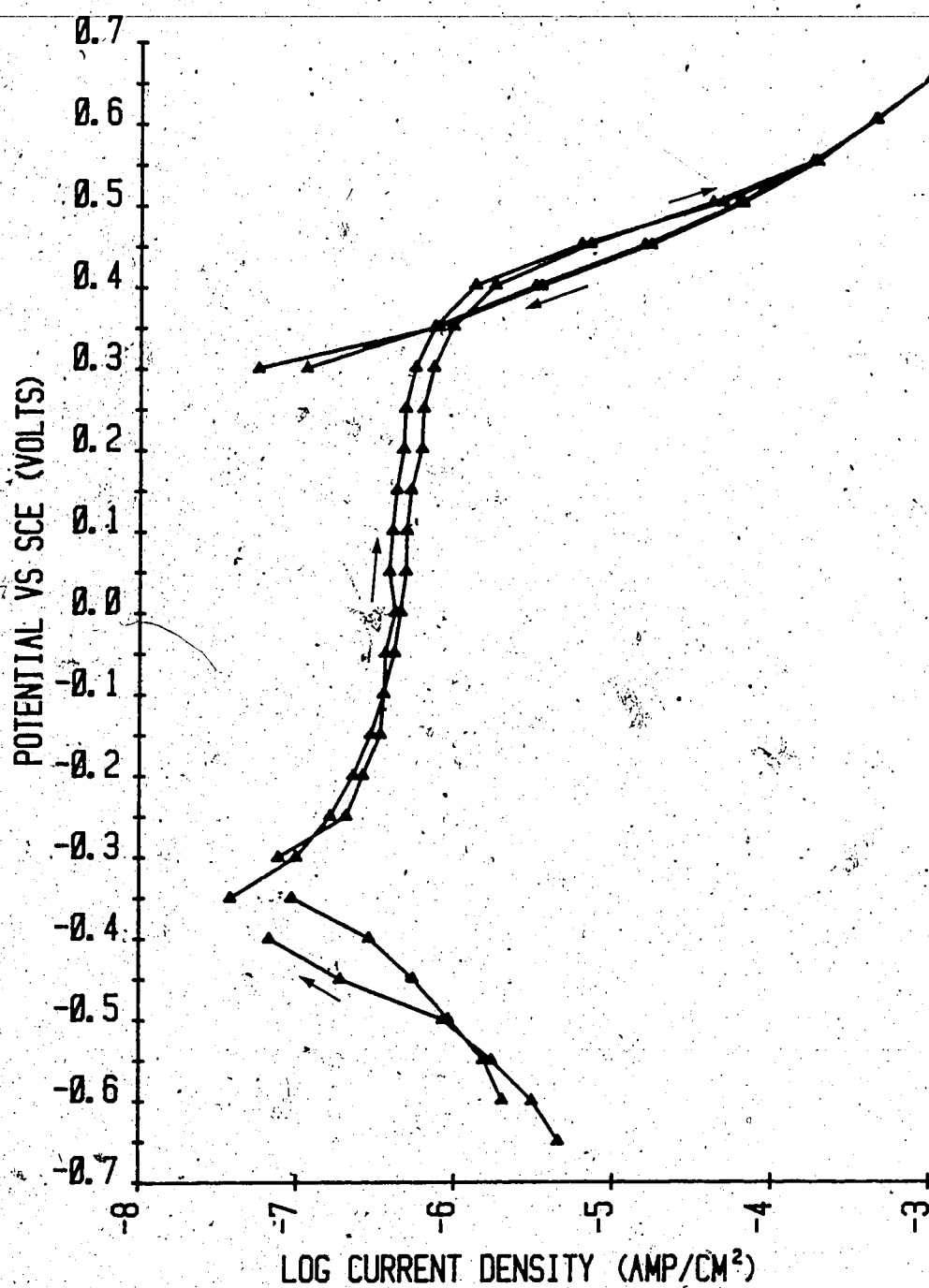


Figure 6.7 Preliminary Polarization Curves for Vitallium in Solution Containing Glucose but no Serum



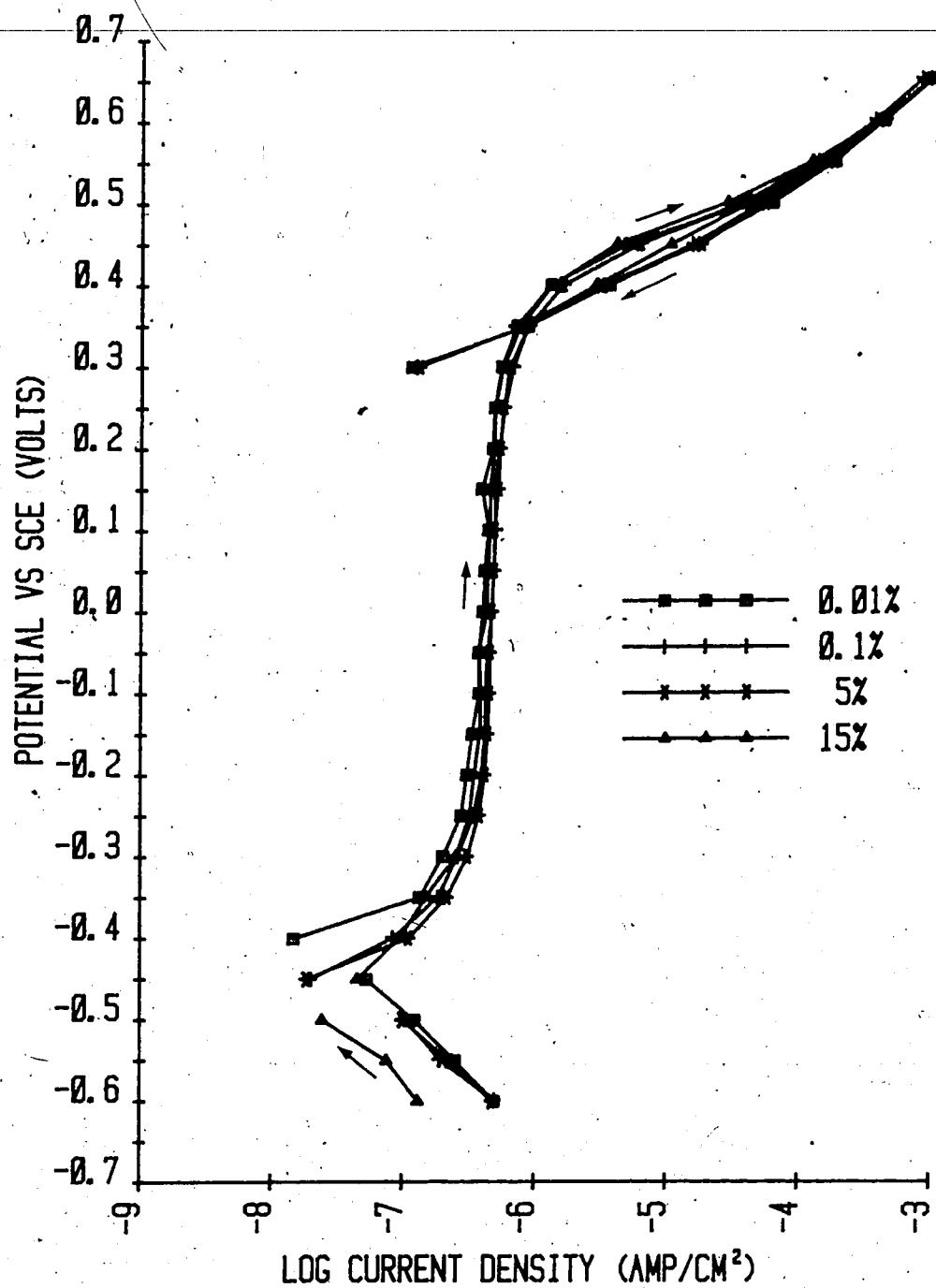


Figure 6.8 Preliminary Polarization Curves for Vitallium in Solution Containing Glucose and Serum

Table 6.6  
Preliminary Polarization Curves for  
Vitalium in Solution Containing Glucose and  
Serum

|               | Current<br>(A/cm <sup>2</sup> ) | Potential<br>(A) |
|---------------|---------------------------------|------------------|
| Corrosion     | $3 \times 10^{-7}$              | Varies           |
| Passive       | $4.5 \times 10^{-7}$            | ----             |
| Breakdown     | ----                            | 0.38             |
| Repassivation | ----                            | 0.35             |

Considering the scans given in Figures 6.7 and 6.8, (G/NS and G/S), it is evident that they all have the same form of anodic polarization curves. The only differences between the scans are in the value of the corrosion potential and, possibly, the position of the cathodic curve. Although only one test was performed at each serum concentration, it appears that as the serum content is increased the corrosion potential is shifted to more negative values. However, while the change in corrosion potential was on the order of 100 mV, the almost vertical slope of the passive region resulted in a negligible decrease in the corrosion current.

#### 6.3.1.2 Solution pH

During these preliminary tests samples of solution were intermittently drawn for pH determination. The results, given below, show no significant differences or trends,

neither from one test to another, nor among the serum-free and serum-containing tests. The overall average pH was

7.7±0.1.

Table 6.7  
pH Readings

| Serum Content | Potential (V) | pH  | Serum Content | Potential (V) | pH  |
|---------------|---------------|-----|---------------|---------------|-----|
| 0%            | -0.40         | 7.8 | 0.01%         | -0.60         | 7.8 |
|               | 0.05          | 7.6 |               | 0.20          | 7.7 |
|               | 0.45          | 7.6 | 0.1%          | -0.60         | 7.8 |
|               | 0.80          | 7.6 |               | 0.15          | 7.8 |
|               | 0.85          | 7.6 |               | 0.65          | 7.7 |
|               | 0.15          | 7.6 |               | 0.15          | 7.7 |
|               | -0.40         | 7.6 |               | -0.45         | 7.7 |
| 0%            | -0.60         | 7.7 |               | -0.25         | 7.7 |
|               | 0.10          | 7.6 | 5%            | -0.60         | 7.7 |
|               | 0.40          | 7.6 |               | 0.10          | 7.7 |
|               | -0.25         | 7.6 |               | 0.55          | 7.7 |
|               | -0.60         | 7.6 |               | 0.00          | 7.6 |
| 0%            | -0.60         | 7.6 | 15%           | -0.35         | 7.7 |
|               | -0.20         | 7.6 |               | 0.20          | 7.7 |
|               | 0.50          | 7.7 |               | 0.65          | 7.8 |
|               | -0.60         | 7.6 |               |               |     |

#### Long Term Corrosion Potential

The variation of corrosion potential with time is shown in Figure 6.9. As indicated, the potential increased over the first eighteen hours from approximately -0.41 V, to a maximum value of -0.15 V, then, after eighteen hours fell to approximately -0.25 V. Both these peak and minimum values are consistent with the potentials measured by Brettle and Hughes<sup>44</sup> within the first ten days of their potential-time tests. Furthermore, as no localized attack was noted at the

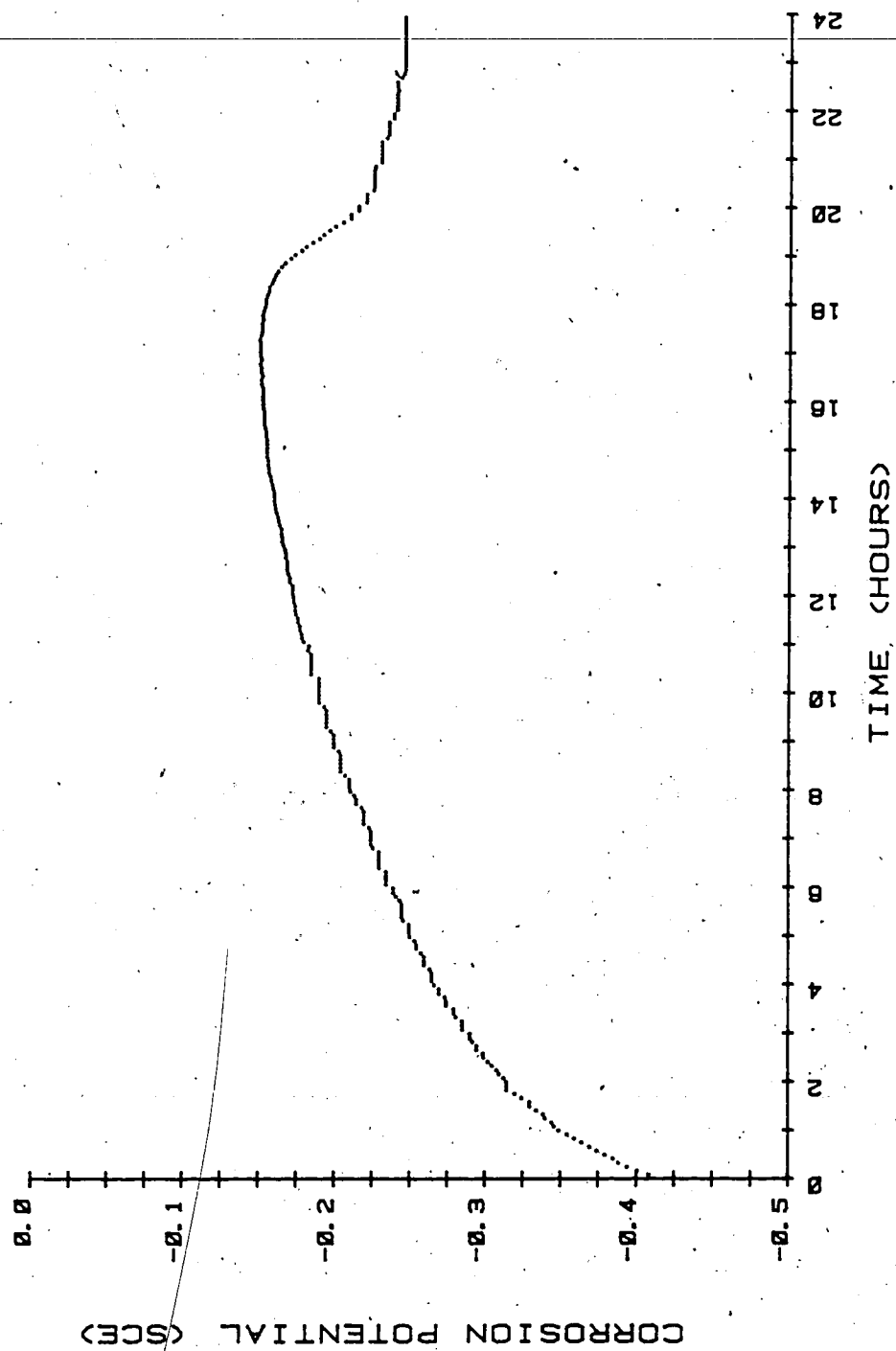


Figure 6.9 Variation of Corrosion Potential of Vitallium in Oxygenated Solution Containing Glucose but no Serum

end of the test, it would seem that these results corroborate the speculation by Hoar and Mears<sup>45</sup> that ~~spontaneous film breakdown is unlikely for this material~~ under these conditions, at least in the short term.

The results of the foregoing tests have indicated that neither the glucose, in the absence of serum, nor the serum, in the presence of glucose, affect the anodic polarization behavior. It is also apparent that the serum, in the presence of glucose, may decrease the corrosion potential, thus making it a possible cathodic corrosion inhibitor.

The following series of tests will concentrate on the effects of glucose and serum on the cathodic polarization behavior of the alloy.

### 6.3.2 The Effects of Glucose and Serum on the Cathodic Polarization Behavior of Vitallium

#### 6.3.2.1 No Glucose and No Serum - NG/NS

The first set of experiments in this series was conducted with no glucose and no serum and gave the results shown in Figure 6.10. As shown the curves have three relative positions, which only in part, reflect variations in procedure. The curves at the left and centre were obtained by the procedure described in the earlier chapter, the only major difference being that the central curve equilibrated for two and one-half hours before starting, whereas those at the left equilibrated for only one hour.

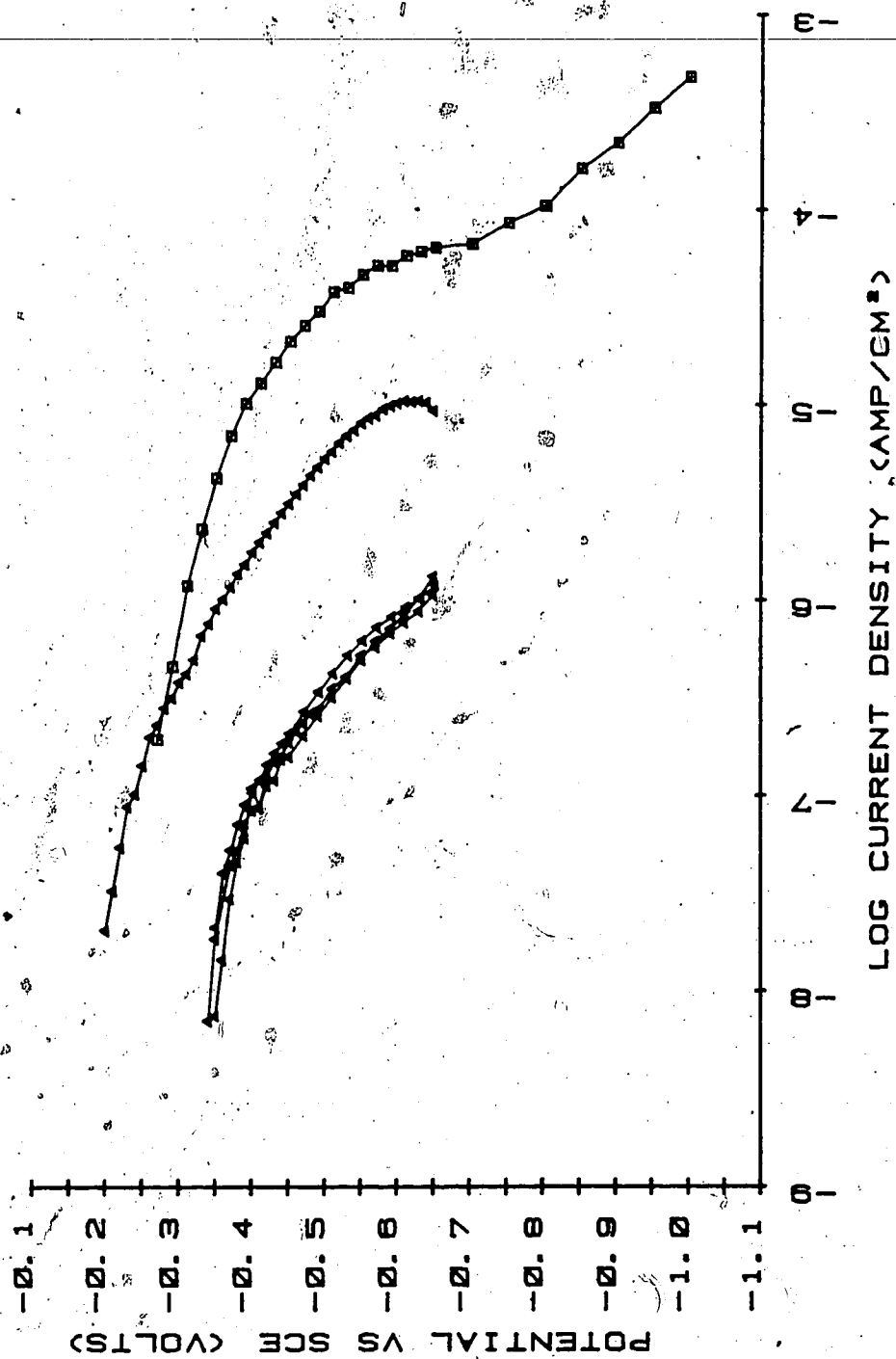


Figure 6.10 Polarization Behavior of Vitallium in  
Glucose-Free and Serum-Free Solution

This difference is considered to explain the higher corrosion potential in the case of the central curve.

~~The procedure leading to the curve at the right varied~~ significantly from the others. Rather than equilibrating at the rest potential, the sample was cathodically charged at -1 V for at least one hour prior to commencing the scan. The higher currents at all potentials, therefore, are a result of the reduced activation energy for the cathodic reaction on a surface whose anodic film has been either partially or completely removed by cathodic charging. Why the corrosion potential of the clean electrode (the curve at the right) should be higher than the filmed electrode (curves at the left) is not known for certain, but may be a result of either a longer equilibration time, or the longer time required to reach a given potential as a result of the lower start potential.

If the film reduction mechanism is also active, at least intermittently, in the region -0.65 to -0.70 V, it might also explain the higher currents in the case of the central curve.

In addition to the effects of variations in procedure these curves exhibit several other interesting features: the central curve exhibits a 'hook' or positive slope near the starting end of the curve, and the curve at the right appears to be formed by the addition of two cathodic curves. The latter of these observations is discussed now, while the former is dealt with later.

### Cathodic Reactions

The curve at the right, in Figure 6.10, consists of two distinct regions, which are interpreted to indicate the presence of two separate cathodic reactions. The first, which dominates from the corrosion potential to the limiting current at approximately -0.7 V, is likely due to the oxygen reduction reaction which can be written as:



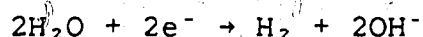
and which has, under these conditions, a redox potential given by:

$$E = E^\circ + 0.861 - 0.062 \text{ pH} + 0.015 \log p\text{O}_2$$

$$= 0.77 \text{ V (SHE), or}$$

$$E = 0.53 \text{ V (SCE)}$$

At potentials below -0.70 V the curve deviates from the limiting current toward higher current values. As the test solutions were neutral, the predominant reaction is expected to be the reduction of water according to the following:



which has a redox potential of:

$$E = -0.062 \text{ pH}$$

$$= -0.48 \text{ V (SHE), or}$$

$$E = -0.71 \text{ V (SCE)}$$

As this potential is within the vicinity of the point of deviation of the second slope, and because the overpotential of hydrogen evolution is small, this water reduction reaction is most likely responsible for the curve form below



-0.7 V.

#### 6.3.2.2 Glucose With and Without Serum - G/S and G/NS

---

Figures 6.11 to 6.15 give the results of the potentiostatic cathodic polarization tests using no serum, and serum at various concentrations in solutions containing glucose. Several features are immediately apparent: the curves for 0%, 0.01%, and 0.1% serum are relatively closely grouped, while those for 5% and 15% have wider variations, and the curves obtained at 0.01% serum consist of two groups, those with and without positive slopes on the cathodic curves. These results will now be considered in more detail.

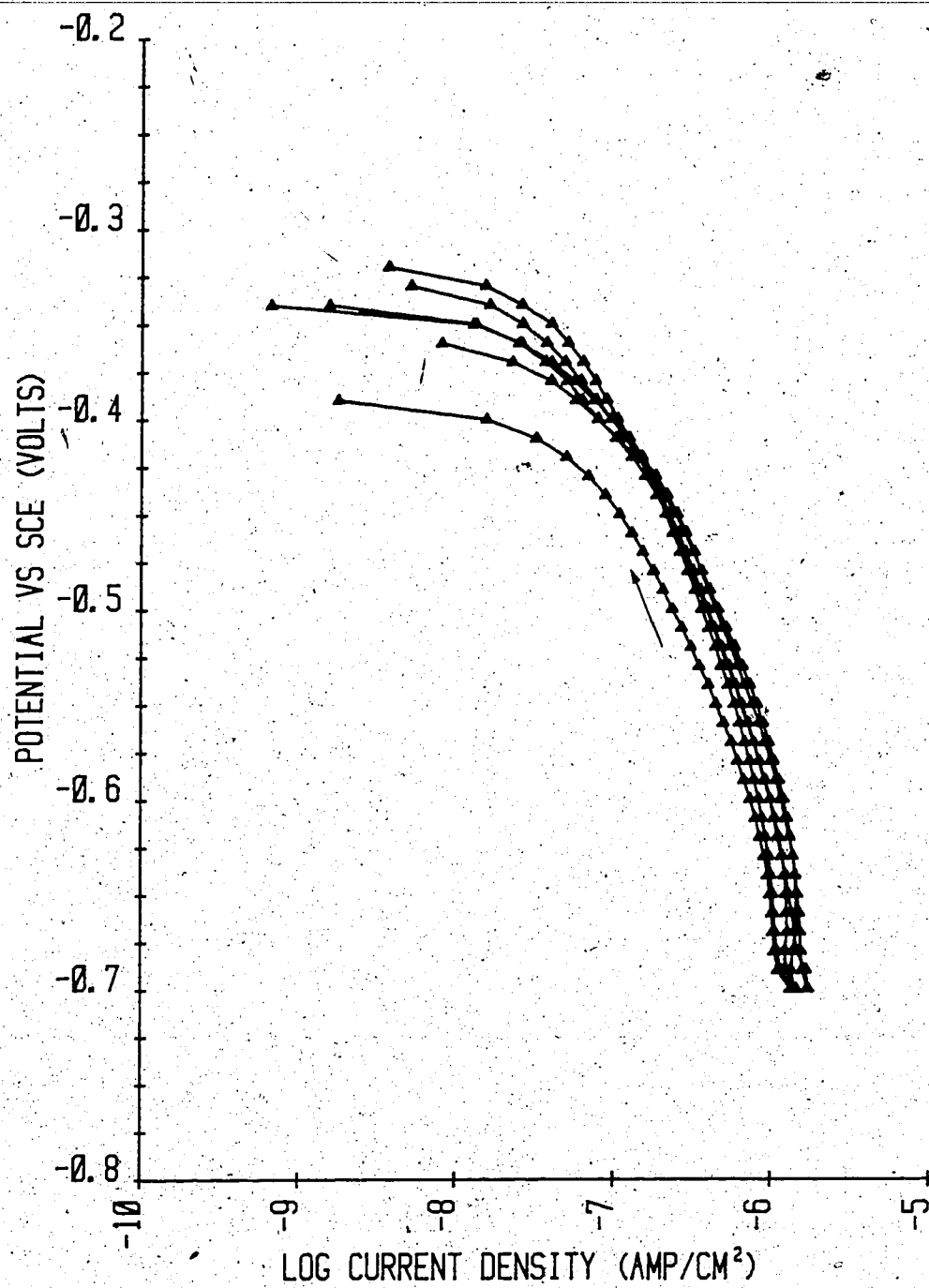


Figure 6.11 Cathodic Polarization of Vitallium in Serum-Free Solution

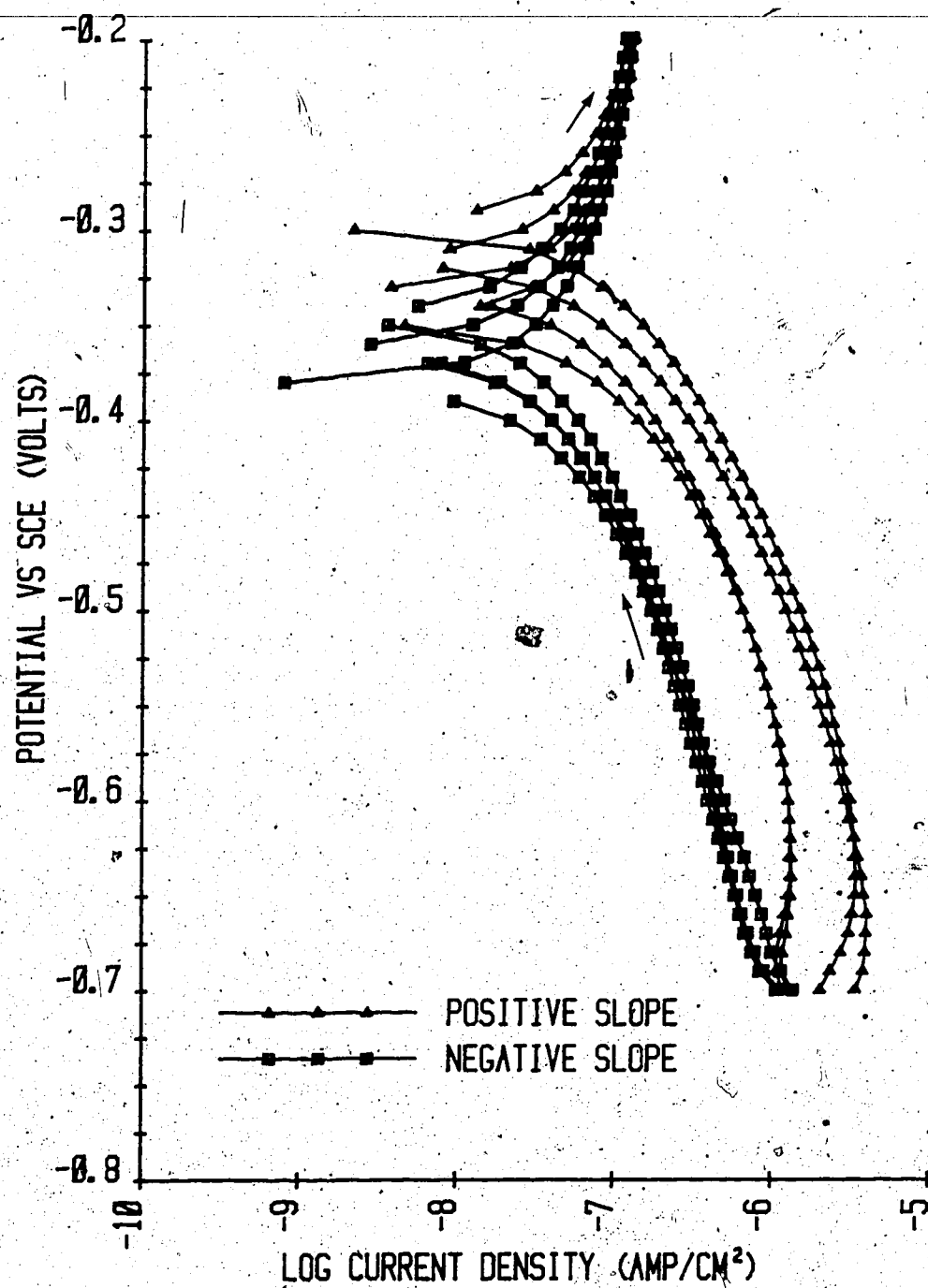


Figure 6.12 Polarization Behavior of Vitallium in Solution Containing 0.01% Serum

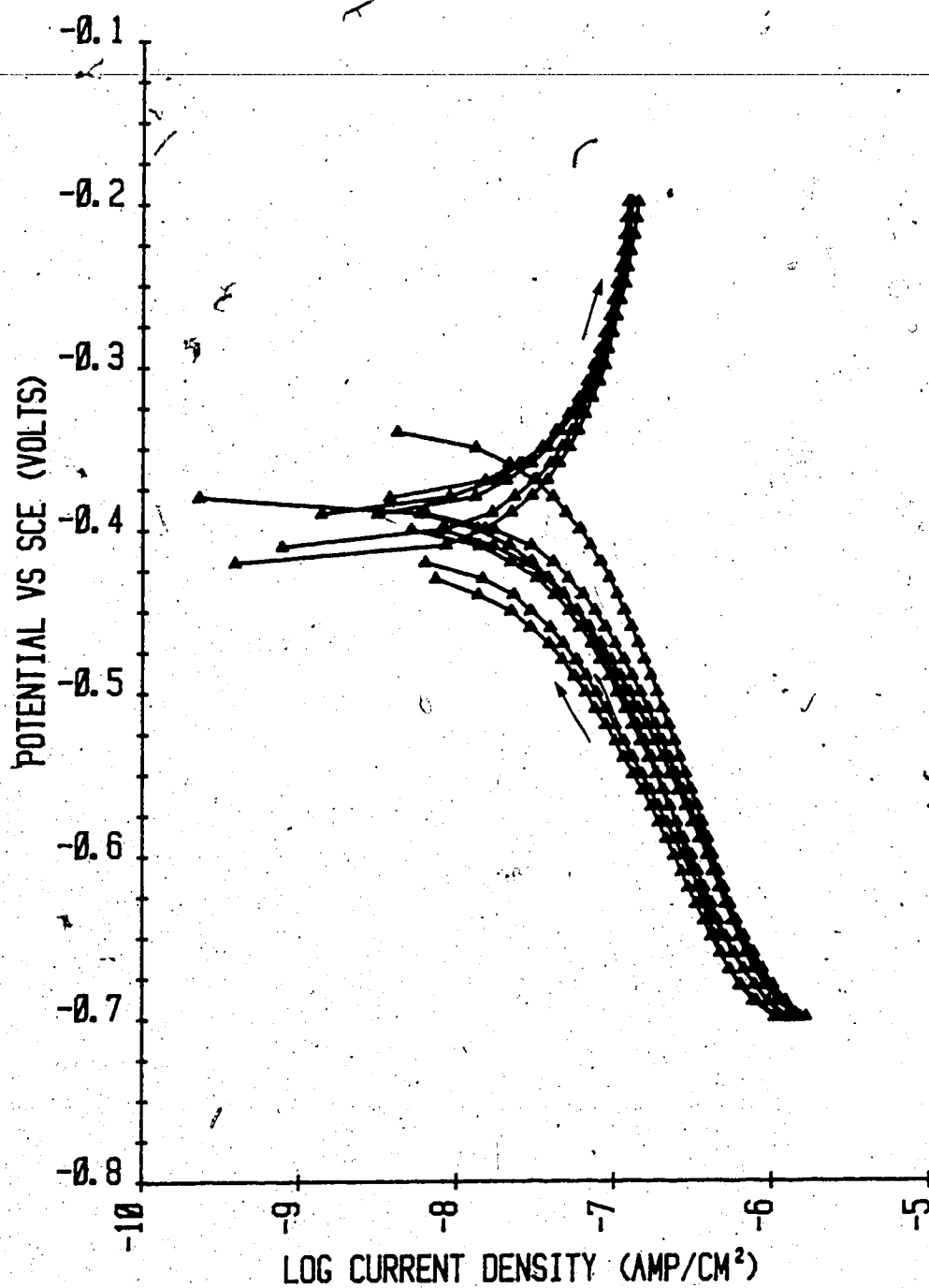


Figure 6.13 Polarization Behavior of Vitallium in Solution Containing 0.1% Serum

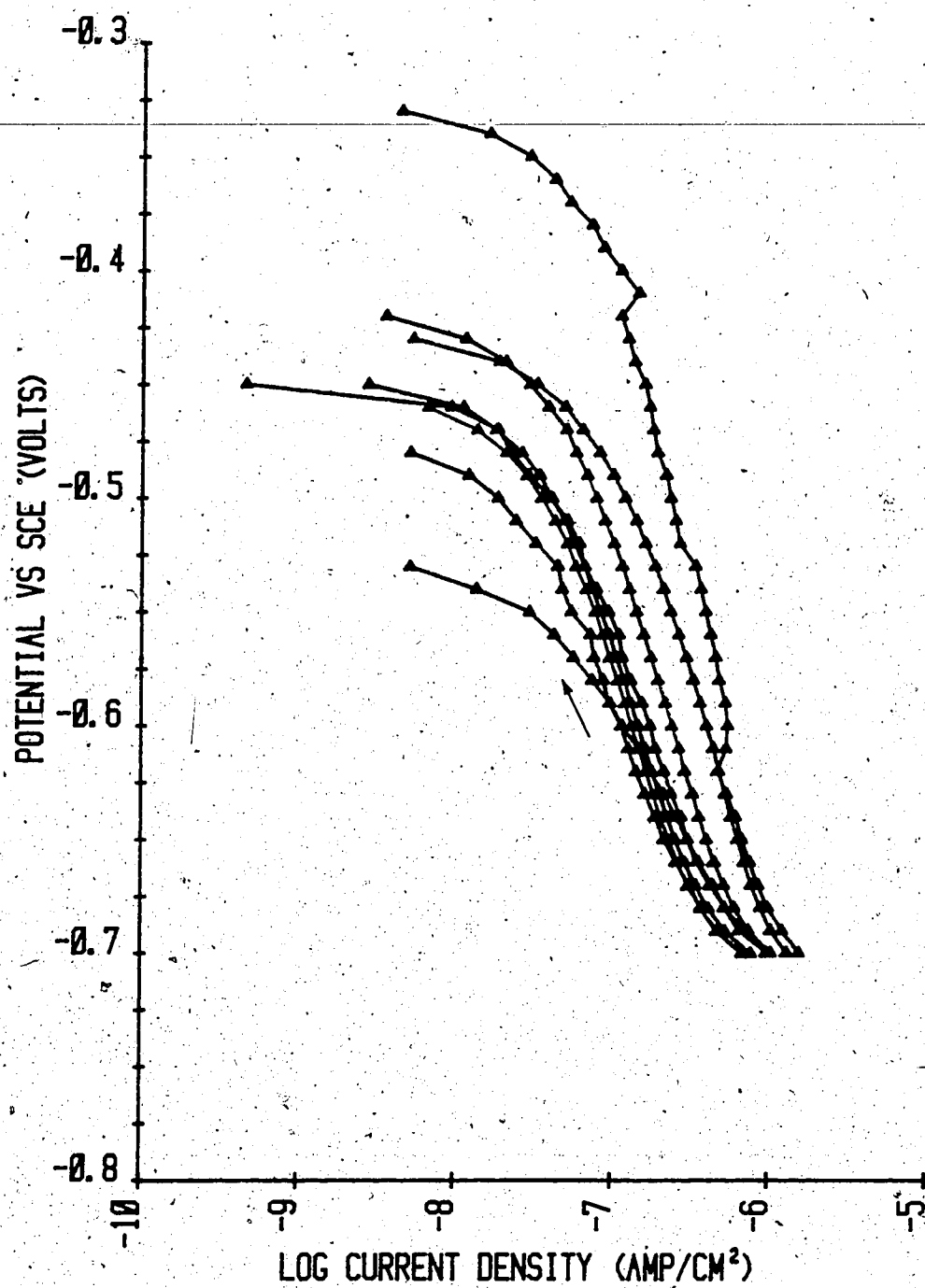


Figure 6.14 Cathodic Polarization Behavior of Vitallium in Solution Containing 5% Serum

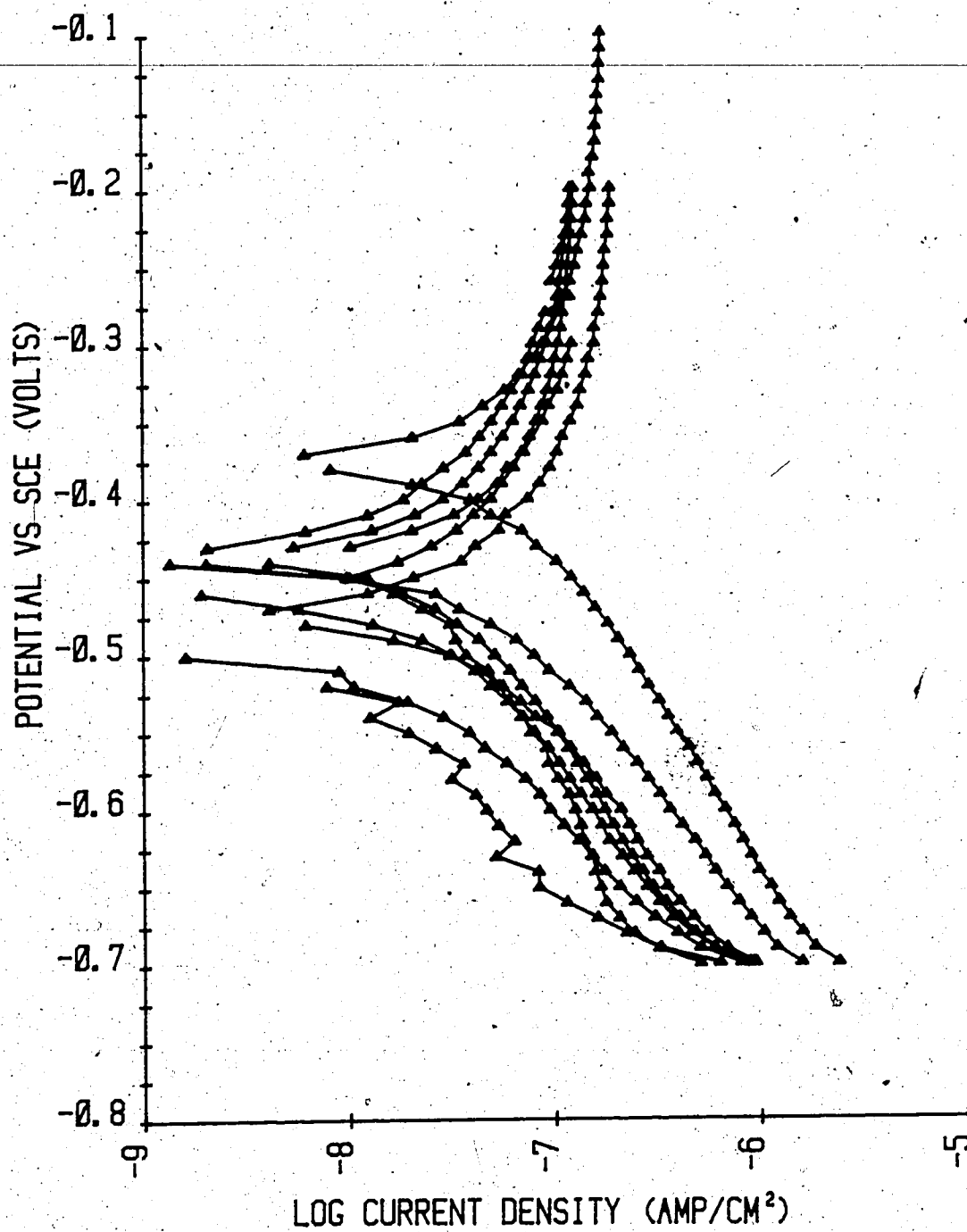


Figure 6.15 Polarization Behavior of Vitallium in Solution Containing 15% Serum

### Effect of Serum on the Corrosion Potential

As was suggested in the preliminary results, the corrosion potential was found to fall with increasing serum contents, Figure 6.16 (the left-most error bar refers to zero serum conditions). As can be seen, the corrosion potential falls perceptibly after 0.01% serum, and may be continuing to fall, albeit at a lower rate, after 15%. Although the mechanism behind the potential change is unknown, it would appear that these results could be grouped with those of Solar et al.<sup>33</sup>, who found that certain organics shifted the corrosion potential of Ti-6Al-4V in the negative (active) direction. Furthermore, these results corroborate the findings of Brown and Merritt<sup>44</sup> who found that the corrosion potential of 316L, a material also protected by a chromium oxide film, was shifted in the same direction by a physiological solution.

The difference in the corrosion potentials between the serum-free and 15% serum situations also resembles the difference reported by Hoar and Mears<sup>45</sup> between in vitro tests in saline and in vivo tests using human subjects. Although the actual potential values depend on the procedures used in each case, the similarity in the differences suggest that the conditions used in these tests simulate the in vivo conditions more accurately than inorganic saline solutions.

In terms of the mechanism involved in shifting the corrosion potential, the results are interpreted to indicate

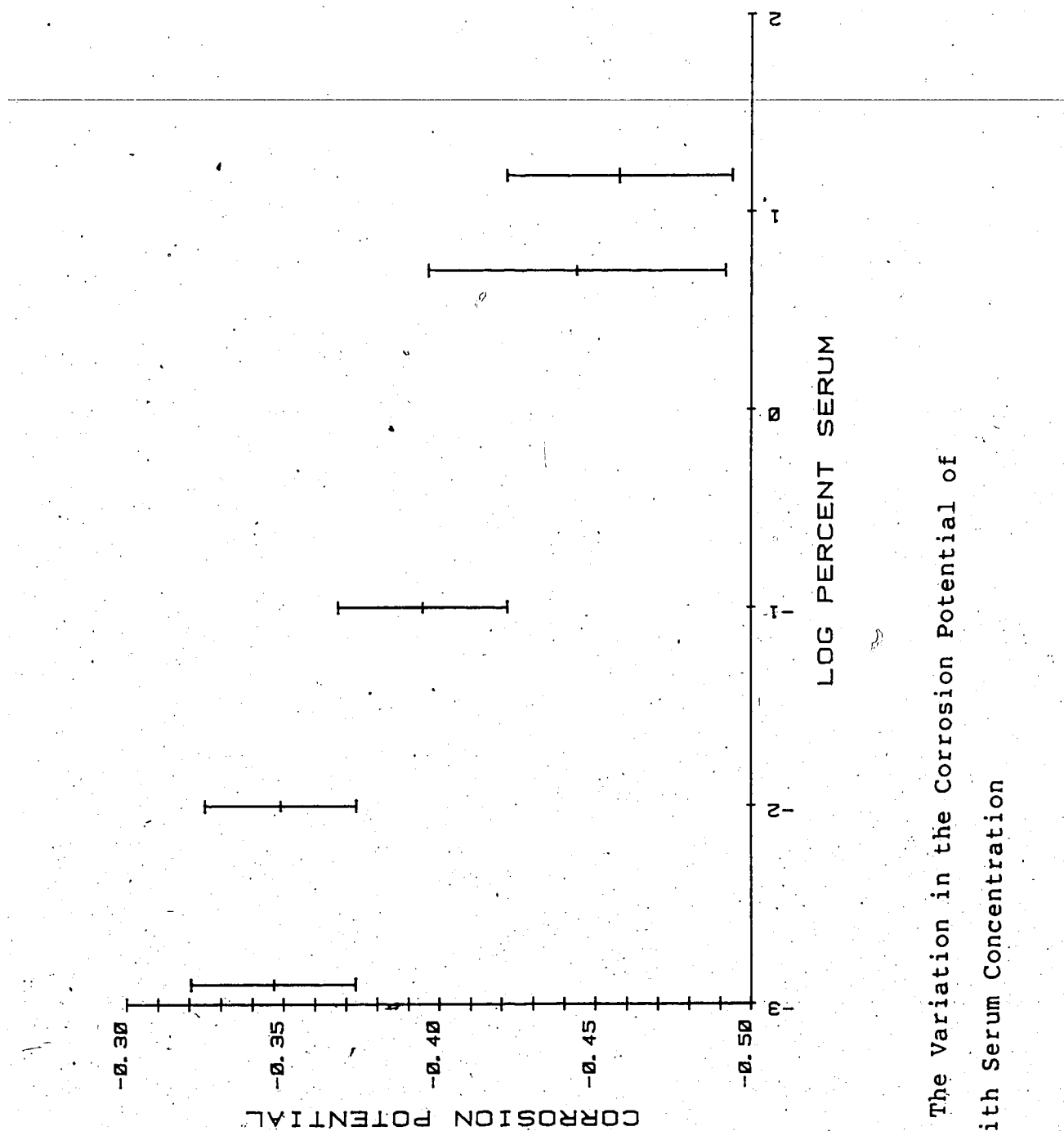


Figure 6.16 The Variation in the Corrosion Potential of Vitallium with Serum Concentration



that the serum hinders the diffusion of oxygen to the metal surface.

#### Effect of Serum on the Corrosion Current

Because the corrosion potentials were remote from the reversible potentials for the anodic and cathodic reactions, no Tafel lines existed in the vicinity, and, therefore, another method was used to estimate the corrosion currents. The preliminary tests showed that the slope of the passive curve was reproducible and independent of the serum content. In tests, therefore, where the scans had been taken into the anodic range (0.01%, 0.1%, and 15% serum), the best fit line describing the passive ranges of the preliminary data was applied to the anodic current values, and the intersection of these lines with the corrosion potentials were taken to be the corrosion currents. Where the scans had been terminated at the corrosion potentials, the corrosion currents were estimated on the basis of the positions of the cathodic curves with respect to the former data. In all cases the estimates of the corrosion currents were essentially equal at  $1 \times 10^{-7}$  A/cm<sup>2</sup>.

#### Positive Cathodic Slopes

During some of the previous tests and these latter tests, regions of positive slope were encountered on the cathodic curves. These include one curve obtained with glucose and serum-free solution, one with serum-free solution, one partially completed curve at 0.001% serum, Figure 6.17, four with 0.01% serum, and one at 5% serum.

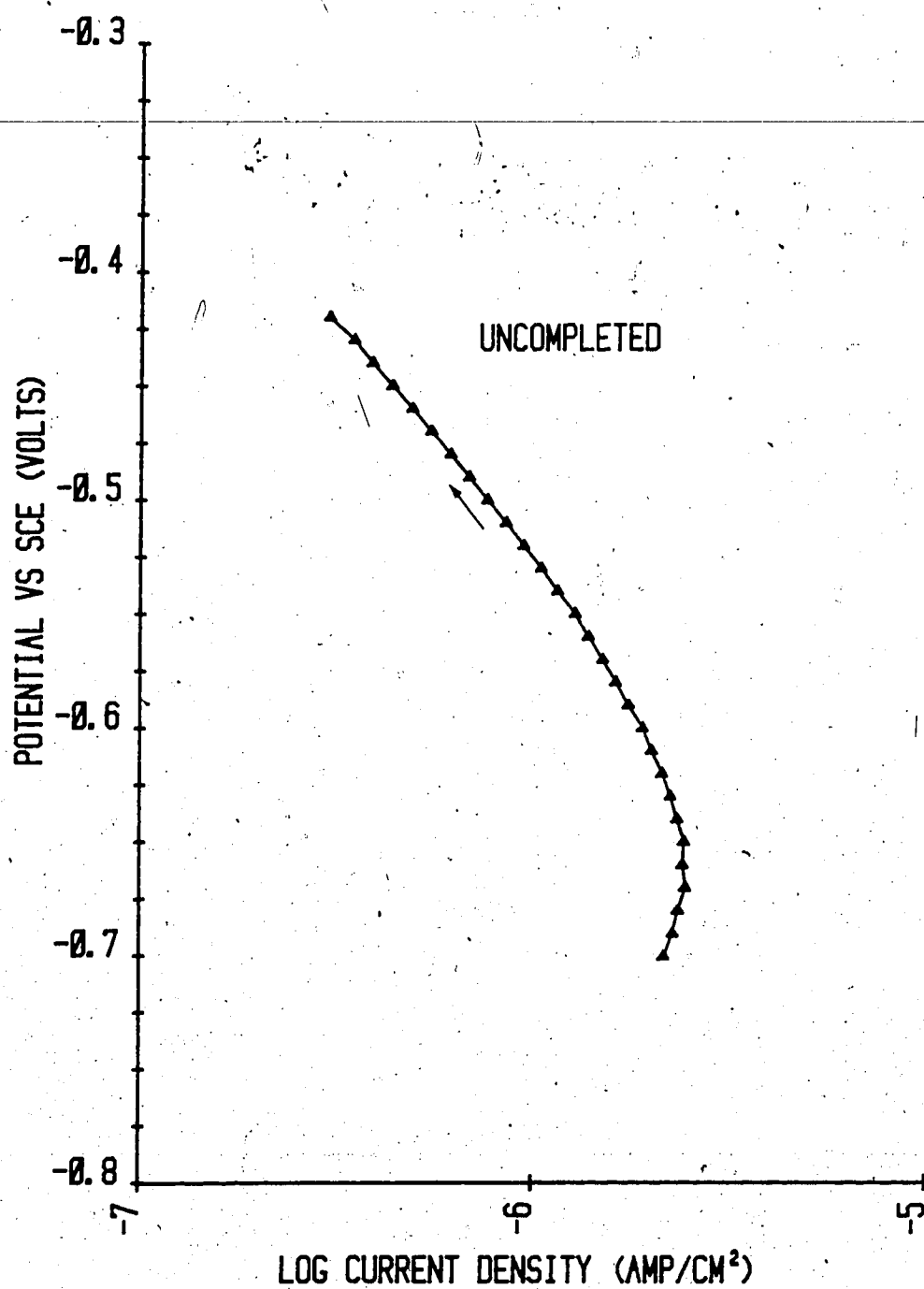


Figure 6.17 Incomplete Cathodic Polarization Curve for Vitallium obtained with 0.001% Serum

where the curve seemed to alternate between two courses. No such positive slopes were observed at 15% serum.

Common to all these curves is the location of the region of positive slope, beginning near the start potential,  $-0.65$  or  $-0.70$  V, and increasing to maximum current values between  $-0.63$  and  $-0.67$  V. The maximum increase in current is only 22%.

Regarding corrosion potentials, values were either higher or the same as in the curves without positive slopes. In the case of the 0.01% serum results, those curves with positive slopes had an average corrosion potential 40 mV higher than the other curves in the same group, and at 5% serum the difference was over 100 mV. In addition, the curve obtained with glucose and serum-free solution was up to 125 mV higher. Perhaps the two most significant observations are that serum and glucose are not necessary for a positive slope to occur, and no positive slope was encountered at 15% serum.

In general several situations can result in positive cathodic slopes: a cathodic curve which closely approaches an anodic critical current peak, a simultaneous oxidation reaction which exhausts its reactant supply, or a second cathodic reaction whose rate increases with time.

The first of these possibilities is not responsible as it has been reported by Lucas et al.<sup>54</sup> that Vitallium exhibits self-passivation in deoxygenated conditions.

Similarly, the simultaneous anodic reaction mechanism is considered unlikely as no such reaction is known to be active under glucose-free and serum-free conditions.

The third situation, however, may be closer to the actual mechanism. Since it is thermodynamically impossible for the kinetics of a reaction to increase as the driving force is reduced, the only explanation for such an observation is that time is the controlling factor. It is possible, therefore, that the increasing current is a result of a partial reduction of the anodic film (a mechanism discussed in the glucose-free and serum-free results, above) whose rate increases with time until the overpotential becomes too low, at approximately  $-0.65$  V, for the reaction to proceed. In addition, the decrease in the frequency of positive slopes as the serum content is increased may indicate that the serum has a stabilizing effect on the film.

#### 6.3.2.3 Glucose-Free Solution Containing Serum - NG/S

Two tests were conducted to determine the polarization behavior of the alloy in glucose-free solutions containing 15% serum.

As Figure 6.18 shows, the two curves were not entirely consistent either with one another or with the previous results. One curve reached its corrosion potential at  $-0.63$  V, while the other reached it at  $-0.69$  V, but without the asymptotic decrease in current normally observed as the corrosion potential is approached. The form and corrosion

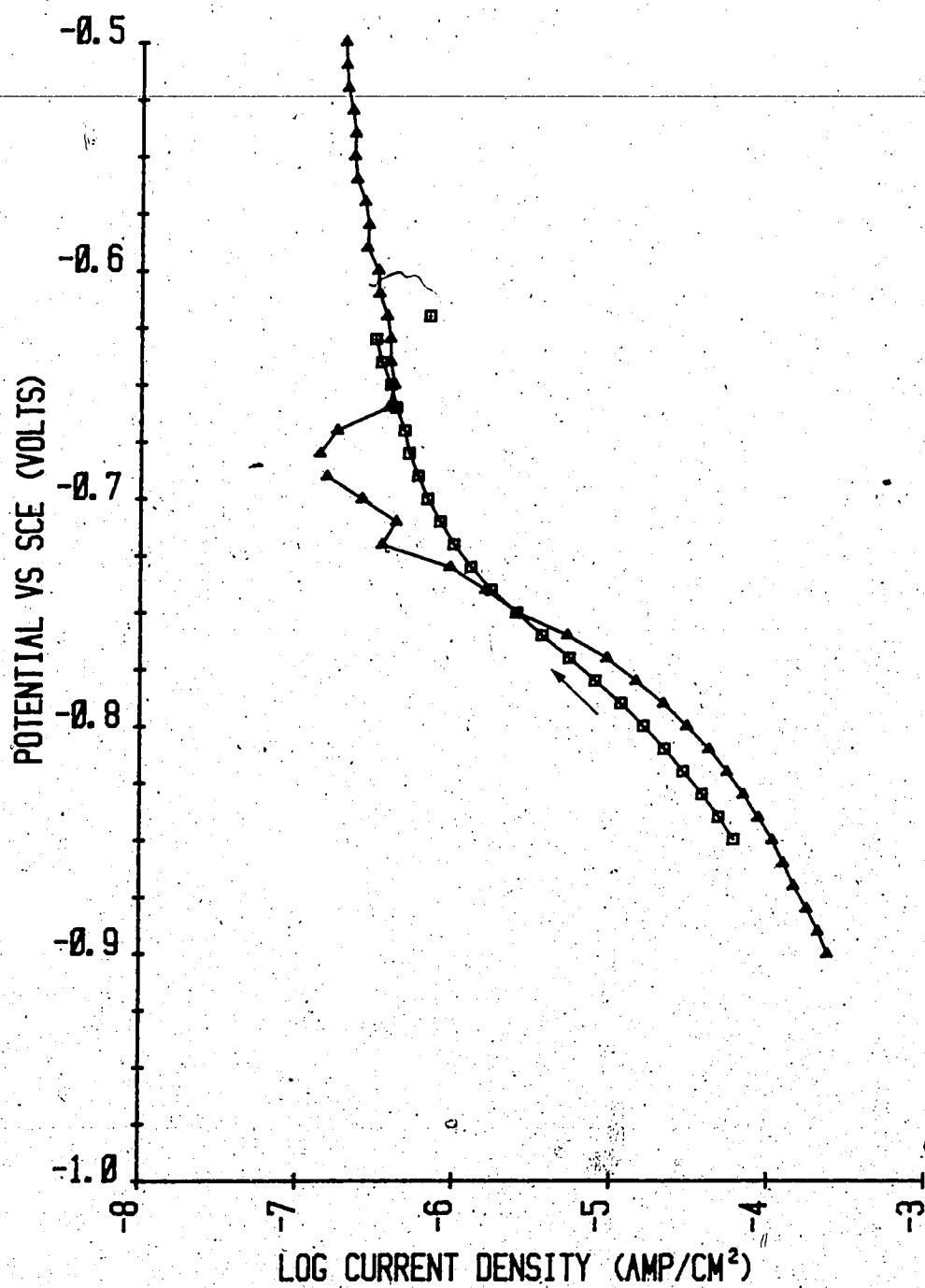


Figure 6.18 Polarization Curves for Vitallium in  
Glucose-Free Solution Containing Serum

potential of the latter of the above mentioned curves would suggest that it was obtained under deaerated test conditions; however this is not considered to have been the case. The following discussion will include a possible explanation for these findings.

### 6.3.3 The Effects of Organic Additions on the Polarization Behavior of Vitallium

As the results show, the most significant effect that the glucose and serum have on the corrosion behavior of Vitallium is to alter the value of the corrosion potential. For this reason the following table summarizes the results of the four glucose/serum combinations in terms of the corrosion potentials:

Table 6.8  
Corrosion Potentials at the Four  
Glucose-Serum Combinations

|          | No Glucose | Glucose |
|----------|------------|---------|
| No Serum | -0.32      | -0.35   |
| Serum    | -0.63      | -0.46   |

According to this summary glucose has little, if any, significant effect on the corrosion potential when serum is absent. However, when serum is present, the corrosion potential is pushed to more negative values, until when glucose is absent the corrosion potentials approach the redox potential for hydrogen reduction. The mechanisms

responsible for these potential shifts almost certainly involve the relative adsorption of the glucose and other serum components, and appear to be dependent on the relative concentrations of the various components.

---

It is believed that, while the glucose competes with the serum for adsorption, its 'adsorbability' is weaker than that of the serum. The fact that the corrosion potential is higher when glucose is present with serum indicates that the glucose is competing for adsorption, but does not hinder the diffusion of oxygen to the cathodic sites. However, when only serum is added the lower glucose content (0.15 g maximum) is not sufficient to produce a significant effect and, as a result, other serum components adsorb and hinder, if not completely block the diffusion of oxygen.

## 6.4 Corrosion Fatigue

The results of the corrosion fatigue tests in serum-free and 5% serum are summarized in Table 6.9.

Table 6.9  
Corrosion Fatigue Lives

| Test | 0% Serum<br>Cycles | 5% Serum<br>Cycles |
|------|--------------------|--------------------|
| 1    | 44000              | 25892              |
| 2    | 29613              | 17410              |
| 3    | 36660              | 28399              |
| 4    | 30710              | 177000†            |
| 5    | 38852              |                    |
| 6    | 26621              |                    |
| 7    | 61845              |                    |

† - Rejected on a statistical basis; refer to Appendix C.

According to ASTM committee E-9 fatigue life data can be considered to be log-normally distributed; that is, the data, itself, is significantly skewed, while the natural logarithm of the data is normally distributed. The above data was analysed on the basis of this assumption (Appendix C).

Table 6.10 summarizes the means and standard deviations of the two data sets in terms of the the log-normal distribution, as well as the 80% confidence limits and other statistical parameters for the two data sets in terms of the arithmetic values.



Table 6.10  
Results of Statistical Analyses of Corrosion  
Fatigue Life Data

|                                       | <u>0% Serum</u>          | <u>5% Serum</u>          |
|---------------------------------------|--------------------------|--------------------------|
| Mean<br>(log-normal)                  | 10.517                   | 10.060                   |
| Standard<br>Deviation<br>(log-normal) | 0.286                    | 0.260                    |
| <u>At 80% Confidence Interval</u>     |                          |                          |
| Lower Limit                           | 10.361<br>(31603 cycles) | 9.777<br>(17622 cycles)  |
| Upper Limit                           | 10.673<br>(43160 cycles) | 10.343<br>(31042 cycles) |
| <u>Arithmetic Statistical Values</u>  |                          |                          |
| Mean                                  | 38432 cycles             | 29194 cycles             |
| Median                                | 36897 cycles             | 23388 cycles             |
| Mode                                  | 34009 cycles             | 21857 cycles             |

According to the statistical analysis, there is a high probability that the two data sets are from different populations' (based on an 80% confidence interval). The fatigue life of Vitallium, therefore, is likely to be less when tested in a 5% serum solution, as opposed to when tested in serum-free solution.

While the standard deviations for the two data sets are very similar, which may reflect similar basic fracture mechanisms, no solid fatigue life data indicates a possible cause for the detrimental effect of the serum.

#### 6.4.1 Fractographic Results

Several of the fatigued samples were examined in the scanning electron microscope to determine if the fracture morphologies changed with the introduction of serum. Photomicrograph composites of the fracture surfaces of one specimen from each group are enclosed in an envelope at the back. As these composites illustrate, the fracture surfaces typically consist of two regions: a flat transgranular region adjacent to the notch, interpreted to be the extent of corrosion fatigue crack propagation, and a second mixed trans- and intergranular, likely final, fracture over the remaining ligaments. Both these regions were examined at higher magnifications and are dealt with as follows.

##### 6.4.1.1 Flat Fracture

As the composites illustrate the flat fracture regions typically consisted of cleavage steps, and porosity and/or

incoherent inclusions. Plate 6.1 from the serum-free group shows the surface adjacent the notch to be generally flat with cleavage steps beginning at the notch. This micrograph

shows both porosity, labelled 'P', and holes from where inclusions had been pulled out, labelled 'I'.

Plate 6.2 illustrates the change in pattern of the cleavage steps which resulted when the crack propagated across a grain boundary.

Much of the flat fractures consisted of the type of cleavage steps shown in Plate 6.3. In all cases, either subsidiary cleavage cracks or dissolved slip planes<sup>14</sup> intersected the surface, while inclusions pock-marked the surface. A qualitative X-ray analysis of one such precipitate revealed it to be high in niobium.

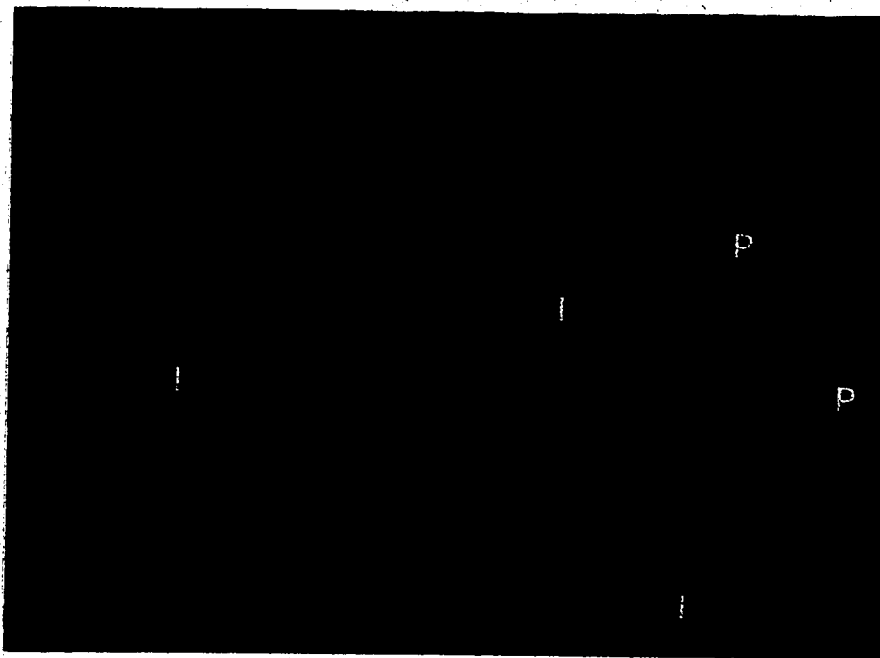


Plate 6.1 Fracture Surface Adjacent to the Notch on a Specimen Tested in Serum-Free Solution (1000X)

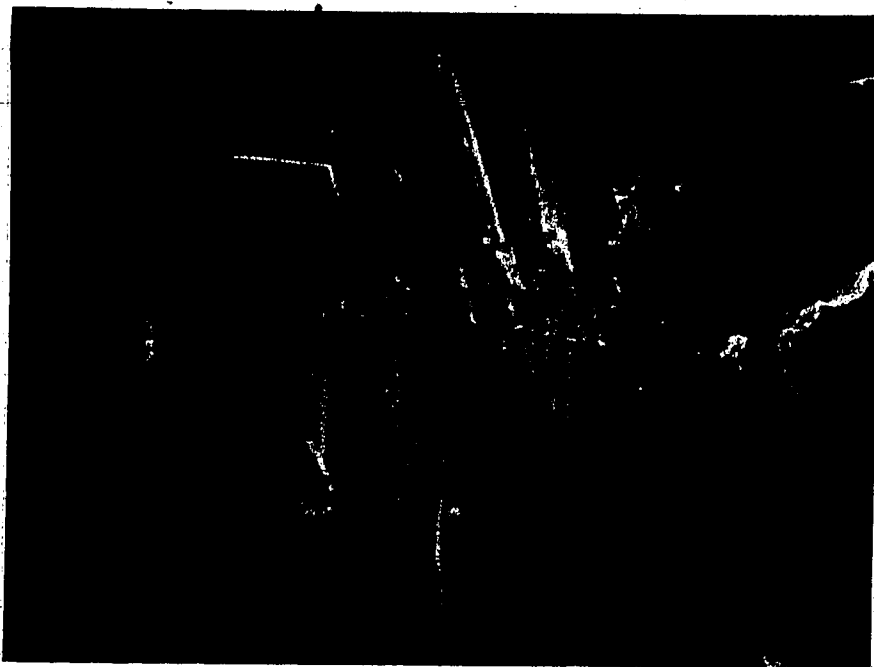


Plate 6.2 Cleavage in Two Adjacent Grains (1200X)

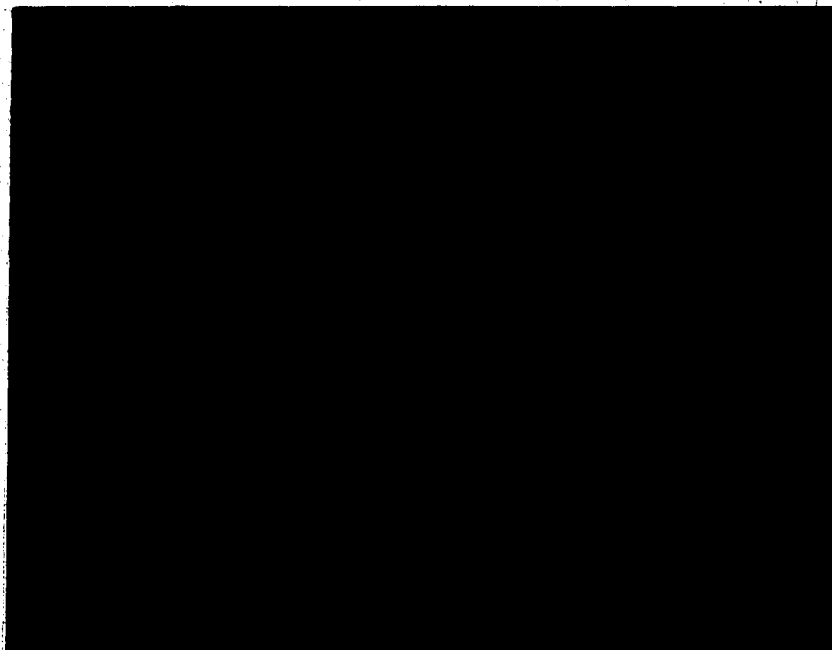


Plate 6.3 Typical Cleavage Fracture near the Final Fracture Zone (900X)

#### 6.4.1.2 Mixed-Mode Fracture

This second fracture zone was typically brittle, showing very little plastic deformation. The fact that the path of least resistance included interdendritic and grain boundary porosity indicates that the fracture involved the expenditure of less energy. This would suggest, therefore, that the material would have a greater fatigue life if such defects were not present.

#### 6.4.2 The Effects of Organics on the Corrosion Fatigue

##### Behavior of Vitallium

At a confidence interval of 80% the corrosion fatigue life of the Vitallium is significantly less in saline solution containing serum, than in serum-free saline. However, the fracture modes encountered in both sets of tests were identical. While the results indicate no cause for the reduction in fatigue life with the introduction of serum, the mechanism of propagation does not change. Therefore, the serum must alter, by degree only, some rate controlling step or property within the material.

According to Tyson and Alfred<sup>5</sup>, "Propagation of a truly brittle cleavage crack through a crystal is possible only if the stress required to rupture atomic bonds at the crack tip is reached before the shear strength of the lattice is exceeded." Therefore, if adsorption of some serum component reduces the cohesion between strained crystal planes at the tip, the fatigue life would be reduced.

Another possibility is that the serum affects the dissolution rate at the tip. If, as Woodson et al.<sup>54</sup> suggest (that organics can lead to an autocatalytic corrosion mechanism), an increased dissolution rate may be responsible for the reduction in life.

## 7. CONCLUSIONS

The effects of serum and glucose additions on the corrosion and corrosion fatigue behavior of a cast CoCrMo alloy have been investigated with the following conclusions:

---

### 7.1 Potentiostatic Polarization Tests

1. Both the 316L stainless steel and the cobalt alloy, machined from the prostheses, exhibited self-passivation with similar values of corrosion and passive currents in the oxygenated, neutral saline solution.
2. 316L stainless steel is highly susceptible to spontaneous passive film breakdown and crevice corrosion in these chloride solutions.
3. The cobalt alloy tested here is highly resistant to passive film breakdown.
4. Glucose and other serum components compete for adsorption on the cobalt alloy in simulated physiological solutions.
5. Neither glucose nor serum have any effect on the anodic polarization behavior of the Vitallium.

6. While glucose does not appear to alter the corrosion potential, serum tends to shift it in the negative (active) direction. It is possible that this shift is a result of lower oxygen reduction rates caused by low diffusion rates through an adsorbed serum film. By this argument, it would appear that the glucose does not hinder oxygen diffusion.

#### 7.2 Corrosion Fatigue Tests

7. Fatigue cracks in the cobalt alloy, from which the fatigue samples were cast, propagate by a cleavage mechanism.
8. According to the fatigue life data and a confidence interval of 80%, the corrosion fatigue life of cast Vitallium is less when tested in 5% serum than when tested in serum-free solution. However, the means by which this reduction occurs, without changing the basic fracture mechanism, is not known.
9. Casting porosity is believed to have been, at least, partially responsible for reducing the fatigue lives of all samples.



## 8. RECOMMENDATIONS

Tests have been conducted to evaluate the effects of serum and glucose on the corrosion of a cast CoCrMo alloy in solutions approximating the physiological conditions of healthy tissue. Results have indicated that while glucose and serum compete for adsorption on the metal surface, only the serum has any significant effect on the corrosion process. It has, furthermore, been demonstrated that the addition of serum to inorganic simulated physiological solution results in test conditions which approximate more accurately the in vivo conditions than do many of the traditional inorganic test media.

Several important questions concerning the effects of organics on the corrosion and corrosion fatigue, however, have not been addressed. The following questions are suggested as topics of further research:

- Are any physiological organics involved in electrochemical reactions?
- What specific organics are responsible for the effects noted above, and is the adsorption potential dependent?
- What is the effect of physiological organics in healing tissue where the conditions are significantly different from those used in this study?
- What is the effect of the organics in crevice situations?

Potentiostatic polarization is an accelerated corrosion testing technique the results of which only indirectly forecast the long term behavior of a system. It is

---

suggested, therefore, that long term tests be conducted to examine the effects of physiological organics. In addition to studying the variation of the corrosion potential and current with time, the following questions might also be addressed:

- What is the nature of the adsorbed and anodic films, and how do they change with time?
- Are specific constituents of the alloy selectively leached and, if so, what is the role of the organics?

Regarding the corrosion fatigue aspect, this research indicated there to be a high possibility that serum reduces the corrosion fatigue life of Vitallium. However, the means by which the reduction is produced is not known. It is, therefore, suggested that more extensive studies be conducted to investigate the effects of serum on the initiation and propagation phases, with the aim of determining the mechanism by which the serum shifts the corrosion potential and reduces the corrosion fatigue lives.

## REFERENCES

1. C.S. Venable and W.G. Stuck, *The Internal Fixation of Fractures*, Charles C. Thomas at Bannerstone House, Springfield, Illinois, p.3 (1947)
2. D.F. Williams and R. Roaf, *Implants in Surgery*, W.B. Saunders Co. Ltd., Philadelphia, (1973)
3. A.C. Guyton, *Textbook of Medical Physiology*, Sixth Ed., W.B. Saunders Co. Ltd., Philadelphia, (1981)
4. N.W. Rydell, "Forces Acting on the Femoral Head-Prosthesis", *Acta. Orthop. Scand. Suppl.* v.37, no.88, pp.1-132 (1966)
5. J.P. Paul, "Forces Transmitted by Joints in the Human Body", *Symposium on Lubrication and Wear in Living and Artificial Human Joints*, Institute of Mechanical Engineers, London (1967)
6. I. Langmuir, *Trans. Electrochem. Soc.*, v.29, p.260 (1916)
7. R.P. Frankenthal, "On the Passivity of Iron-Chromium Alloys. I. Reversible Primary Passivation and Secondary Film Formation", *J. Electrochem. Soc.*, v.114, pp.542-547 (1967)
8. B. Agius and J. Siejka, "Investigations of the Passivity of Iron by Nuclear Microanalysis Using Stable Oxygen Isotopes", *J. Electrochem. Soc.*, v.120, pp.1019-1025 (1973)
9. T.S. DeGromoboy and L.L. Shreir, "The Formation of Nickel Oxides During the Passivation of Nickel in Relation to the Potential-pH Diagram", *Electrochimica Acta*, v.11,

pp.895-904 (1966)

10. E.D. Verink, Jr., "Applications of Electrochemical Techniques in the Development of Alloys for Corrosive Service", *Electrochemical Techniques for Corrosion Testing*, R. Baboian, ed., NACE, Katy, Texas, p.43-51 (1977)
11. B.E. Wilde, "A Critical Appraisal of Some Popular Laboratory Tests for Predicting the Localized Corrosion Resistance of Stainless Alloys in Sea Water", *Corrosion*, v.28, p.283 (1972)
12. T.S. Lee, "A Method for Quantifying the Initiation and Propagation Stages of Crevice Corrosion", *Electrochemical Corrosion Testing; ASTM STP 727*, Florian Mansfeld and U. Bertocci, eds., ASTM, pp.43-68 (1981)
13. S.W. Dean Jr., R. Derby, and G.T. Von Dem Bussche, "Inhibitor Types", *Materials Performance*, v.20, no.12, pp.47-51 (1981)
14. M.O. Speidel, *The Theory of Stress Corrosion Cracking in Alloys*, J.C. Sculley, ed., NATO, Brussels, Belgium, (1971), p.289
15. C. Laird, "Fatigue Crack Propagation", *ASTM STP 415*, pp.131-168, (1967)
16. W. Elber, "Fatigue Crack Closure Under Cyclic Tension", *Engineering Fracture Mechanics*, v.2, pp.37-45 (1970)
17. J. Maarse, "Crack Closure Related to Fatigue Crack Propagation", *Advances in Research on the Strength and*

- Fracture of Materials*, v.2B, pp.1025-1034 (1977)
18. M. Kikukawa, M. Jono, K. Tanaka, and Y. Kondo, *Advances in Research on the Strength and Fracture of Materials*, v.2B, pp.1109-1116 (1977)
19. M.W. Mahoney and N.E. Paton, *Advances in Research on the Strength and Fracture of Materials*, v.2B, pp.1081-1089 (1977)
20. R.P. Wei and M.O. Speidel, "Phenomenological Aspects of Corrosion Fatigue, Critical Introduction", *Nace-2; Corrosion Fatigue: Chemistry, Mechanics, and Microstructure*, pp.379-380 (1972)
21. J.M. Barsom, "Effect of Cyclic Stress Form on Corrosion Fatigue Crack Propagation below  $K_{ISCC}$  in a High Yield Strength Steel", *Corrosion Fatigue: Chemistry, Mechanics, and Microstructure; NACE-2*, Houston, Texas, pp.424-436 (1972)
22. J.D. Atkinson and T.C. Lindley, "Effect of Stress Waveform and Hold-Time on Environmentally Assisted Fatigue Crack Propagation in C-Mn Structural Steel", *Metals Sci.*, pp 444-448, July (1979)
23. C.E. Feltner and C. Laird, Scientific Report Nos. SL-66-93 and SL-66-115, Ford Motor Co., 1966
24. C. Laird, "The Influence of Metallurgical Structure on the Mechanism of Fatigue Crack Propagation", *Fatigue Crack Propagation*, ASTM STP 415, pp.131-168 (1967)
25. P. Haasen, *Physical Metallurgy*, Cambridge University Press, Cambridge, 1978, p.295

26. B.I. Sandor, *Fundamentals of Cyclic Stress and Strain*, University of Wisconsin Press, Madison, Wisc., 1972
27. J.O. Galante, W. Rostoker, and J.M. Doyle, "Failed Femoral Stems in Total Hip Prostheses", *J. Bone J. Surg.*, v.57A, pp.230-236 (1975)
28. J.R. Cahoon and H.W. Paxton, "Metallurgical Analyses of Failed Orthopedic Implants", *J. Biomed. Mater. Res.*, v.2, pp.1-22 (1968)
29. W.E. White, J.H. Wedge and C.M. Sargent, "Failure Analysis of a Charnley-Muller Total Hip Replacement Prosthesis", *Microstructure Science*, Elsevier North Holland Inc., v.7, pp.27-39 (1979)
30. W.E. White and I. LeMay, "Optical and Electron Fractographic Studies of Fracture in Orthopaedic Implants", *Microstructural Science*, Elsevier, v.3, pp.911-930 (1974)
31. A.N. Hughes and B.A. Jordan, "Metallurgical Observations on Some Metallic Surgical Implants Which Failed in Vivo", *J. Biomed. Mater. Res.*, v.6, pp.33-48 (1972)
32. R.J. Gray, "Metallographical Examinations of Retrieved Intramedullary Bone Pins and Bone Screws from the Human Body", *J. Biomed. Mater. Res. Symp.*, no.5, Part 1, pp.27-38 (1974)
33. W. Rostoker, E.Y.S. Chao, and J.O. Galante, "Defects in Failed Stems of Hip Prostheses", *J. Biomed. Mater. Res.*, v.12, pp.635-651 (1978)
34. Ducheyne, P. DeMeester, E. Aernoudt, M. Martens, and

- J.C. Mulier, "Fatigue Fracture of the Femoral Component of Charnley and Charnley-Muller Type Total Hip Prostheses", *J. Biomed. Mater. Res. Symp.*, v.6, pp.199-219 (1975)
- 
35. V.J. Colangelo and N.D. Greene, "Corrosion and Fracture of Type 316 SMO Orthopedic Implants", *J. Biomed. Mater. Res.*, v.3, pp.247-265 (1969)
36. R.T. Holt and W. Wallace, "Failure Analysis of Some Orthopedic Implants", National Research Council Canada, NRC No. 18397, Ottawa, (1980)
37. C.S. Venable and W.G. Stuck, "A General Consideration of Metals for Buried Appliances in Surgery", *International Abstract of Surgery*, v.76, no.4, pp.297-304 (1943)
38. M.A. Streicher, "Analysis of Crevice Corrosion Data From Two Seawater Exposure Tests On Stainless Alloys", *Materials Performance*, v.22, no.5, pp.37-50 (1983)
39. H.P. Hack, "Crevice Corrosion Behavior of Molybdenum-Containing Stainless Steels In Seawater", *Materials Performance*, v.22, no. 6, pp.24-30 (1983)
40. D.C. Bennett and C.J. Federowicz, "Prediction of Localized Corrosion of Stainless Steels in White Water", *Materials Performance*, v.21, no.4, pp.39-43 (1982)
41. R. Bandy and J.R. Cahoon, "Effect of Composition on the Electrochemical Behavior of Austenitic Stainless Steel in Ringer's Solution", *Corrosion*, v.33, pp.204-208 (1977)

42. H.J. Mueller and E.H. Greener, "Polarization Studies of Surgical Materials in Ringer's Solution", *J. Biomed. Mater. Res.*, v.4, pp.29-41 (1970)
- 
43. D.L. Levine and R.W. Staehle, "Crevice Corrosion in Orthopaedic Implant Metals", *J. Biomed. Mater. Res.*, v.11, pp.553-561 (1977)
44. J. Brettell and A.N. Hughes, "The Corrosion Properties of Currently Used and Potentially Useful Surgical Implant Materials", *Engineering in Medicine*, v.7, no.3, pp.142-150 (1978)
45. T.P. Hoar and D.C. Mears, "Corrosion Resistant Alloys in Chloride Solutions: Materials for Surgical Implants", *Proceedings of the Royal Society, Series A*, v.294, pp.486-510 (1966)
46. B.C. Syrett, "The Applications of Electrochemical Techniques to the Study of Metallic Implant Materials", *Electrochemical Techniques for Corrosion*, R. Baboian, ed., NACE, Katy, Texas, pp.93-100 (1978)
47. M.H. Samitz and S.A. Katz, "Nickel Dermatitis Hazards from Prostheses", *Brit. J. Dermat.*, v.92, pp.287-290 (1975)
48. S.A. Brown, K. Merritt, "In Vivo and In Vitro Considerations of Corrosion Testing", *Biomater. Med. Dev. Art. Org.*, v.9, no.1, pp.57-63 (1981)
49. S.A. Brown and K. Merritt, "Fretting Corrosion in Saline and Serum", *J. Biomed. Mater. Res.*, v.15, pp.479-488 (1981)



50. J.R. Cahoon, R. Bandyopadhia, and L. Tennesse, "The Concept of Protection Potential Applied to the Corrosion of Metallic Orthopedic Implants", *J. Biomed. Mater. Res.*, v.9, pp.259-264 (1975)
- 
51. P. Sury, "Corrosion Behavior of Cast and Forged Implant Materials for Artificial Joints, Particularly with Respect to Compound Designs", *Sulzer Research Number*, pp.39-50 (1974)
52. H.H. Uhlig and A.I. Asphahani, "Corrosion Behavior of Cobalt Alloys in Aqueous Media", *Materials Performance*, v.18, no.11, pp.9-20, (1979)
53. J.W. Pugh, W. Jaffe, F.J. Kummer, and J.C. Runkle, "Corrosion Behavior of a Metallic Implant: A Scanning Electron Microscope Study", *Proc. of the Second Annual New England Bioengineering Conference*, pp.15-30 (1974)
54. L.C. Lucas, R.A. Buchanan, and J.E. Lemons, "Investigations on the Galvanic Corrosion of Multialloy Total Hip Prostheses", *J. Biomed. Mater. Res.*, v.15, pp.731-747 (1981)
55. C.G.F. Clark and D.F. Williams, "The Effects of Protein on Metallic Corrosion", *J. Biomed. Mater. Res.*, v.16, pp.125-134 (1982)
56. S.L. Woodman, J. Black, and D.M. Nunamaker, "Release of Cobalt and Nickel from a new Total Finger Joint Prosthesis Made of Vitallium", *J. Biomed. Mater. Res.*, v.17, pp.655-668 (1983)
57. A.B. Ferguson, Y. Akahoshi, P.G. Laing, and E.S. Hodge,

- "Characteristics of Trace Ions Released From Embedded Metal Implants in the Rabbit", *J. Bone J. Surg.*, v.44-A, pp.323-336 (1962)
58. S.M. Weinzierl and M. Webb, "Interaction of Carcinogenic Metals with Tissue and Body Fluids", *Brit. J. Cancer*, v.26, pp.279-291 (1972)
59. A.S. Dobbs and M.J. Minski, "Metal Ion Release After Total Hip Replacement", *Biomaterials*, v.1, pp.193-198 (1980)
60. C.P. Sharma, G.C.F. Clark, and D.F. Williams, "The Adsorption of Proteins on Metal Surfaces", *Engineering in Medicine*, v.10, no.1, pp.11-16 (1981)
61. N. Niazy, R.B. Beard, H.M. Carim, and A.S. Miller, "Comparison of In-Vitro and In-Vivo Passivation Studies of Implantable Anodes", *Sixth New England Bioengineering Conference*, Pergamon Press, pp.321-324 (1978)
62. C.W. Svare, G. Belton, and E. Korostoff, "The Role of Organics in Metallic Passivation", *J. Biomed. Mater. Res.*, v.4, pp.457-467 (1970)
63. R.J. Solar, S.R. Pollack, and E. Korostoff, "In Vitro Corrosion Testing of Titanium Surgical Implant Alloys: An Approach to Understanding Titanium Release from Implants", *J. Biomed. Mater. Res.*, v.13, pp.217-250 (1979)
64. P.J. Aragon<sup>B</sup> and S.F. Hulbert, "Corrosion of Ti-6Al-4V in Simulated Body Fluids and Bovine Plasma", *J. Biomed.*

- Mater. Res.*, v.6, pp.155-164 (1972)
65. H.A. Luckey, "Corrosion Fatigue of Biomedical Engineering Alloys", *Proc. of the Fourth New Eng. Bioeng. Conf.*, S. Saha, ed., Pergamon Press, pp.119-122 (1976)

---

  66. H.L. Miller, W. Rostoker, and J.O. Galante, "A Statistical Treatment of Fatigue of the Cast Co-Cr-Mo Prosthesis Alloy", *J. Biomed. Mater. Res.*, v.10, pp.399-412 (1976)
  67. P. Ducheyne, M. Wevers, and P. DeMeester, "Fatigue Properties of Implant Materials in Hip Prosthesis Form: A Standardized Test", *J. Biomed. Mater. Res.*, v.17, pp.45-57 (1983)
  68. L.N. Gilbertson, "Accelerated Fatigue Testing of the Femoral Component of Mueller Type Total Hips", *Proc. of the Fourth New Eng. Bioeng. Conf.*, S. Saha, ed., Pergamon Press, pp.109-112 (1976)
  69. M. Lorenz, M. Semlitsch, B. Panic, W. Weber, and H.G. Willert, "Fatigue Strength of Cobalt-Base Alloys with High Corrosion Resistance for Artificial Hip Joints", *Engineering in Medicine*, v.7, no.4, pp.241-250 (1978)
  70. M. Semlitsch, "Implant Metals for Plates, Screws, and Artificial Joints in Bone Surgery", *Sulzer Technical Review*, v.3, pp.245-254 (1972)
  71. J.G. Parr and A. Hanson, *An Introduction to Stainless Steel*, American Society for Metals, Metals Park, Ohio,

(1965)

72. R.L. Chance, R.G. Ceselli, and M.S. Walker, "A Comparison of Deaerating Gases for Electrochemical Tests ", *Corrosion*, v.35, pp.327-328 (1979)
- 
73. N.D. Greene, *Experimental Electrode Kinetics*, Rensselaer Polytechnic Institute, Troy, N.Y., 1965
74. J.D. Harston and J.C. Scully, *Corrosion*, v.25, p.493 (1969)
75. W.R. Tyson and L.C.R. Alfred, "Crack Propagation on an Atomic Scale", *Corrosion Fatigue: Chemistry, Mechanics, and Microstructure*, NACE, 1972, p.287
76. D.C. Mears, "Metals in Medicine and Surgery", *Internat. Metals Revs.*, pp.119-155, June, (1977)
77. J.R. Cahoon and L.D. Hill, "Evaluation of a Precipitation Hardened Wrought Cobalt-Nickel-Chromium-Titanium Alloy for Surgical Implants", *J. Biomed. Mater. Res.*, v.12, pp.805-821 (1978)
78. A. Hald, *Statistical Theory with Engineering Applications*, John Wiley and Sons, pp.160-174 (1952)

## APPENDIX A

---

### Test Solutions

The following solutions have been used as simulated physiological saline solutions:

Table A.1  
Compositions of Various Inorganic Test  
Solutions

| Substance                        | Hank's''<br>(g/l) | Ringer's''<br>(g/l) |
|----------------------------------|-------------------|---------------------|
| NaCl                             | 8.0               | 6.3                 |
| CaCl <sub>2</sub>                | 0.14              | ----                |
| KCl                              | 0.40              | 0.37                |
| KH <sub>2</sub> PO <sub>4</sub>  | 0.06              | ----                |
| NaHCO <sub>3</sub>               | 0.35              | 2.4                 |
| Na <sub>2</sub> HPO <sub>4</sub> | 0.05              | 0.07                |
| NaH <sub>2</sub> PO <sub>4</sub> | ----              | 0.06                |
| MgCl <sub>2</sub>                | 0.05              | 0.10                |
| MgSO <sub>4</sub>                | 0.03              | 0.06                |
| Sodium<br>Lactate                | ----              | 3.10<br>(Optional)  |

## APPENDIX B

---

Alberta Research Council  
Chemical Analysis Results

REPORT OF ANALYSIS

Laboratory Sample Number: 1662-83G to 1664-83G

**DESCRIPTION**

Three samples of metal submitted September 1, 1983 by the University of Alberta, Mineral Engineering, 89th Avenue and 114th Street, Edmonton, Alberta, Attention: Mr. Bob Sutherby with request for the following analyses.

RE: PO# 18553NC

**ANALYSIS**

| Laboratory Sample Number:<br>Reference | 1662-83G<br>Implant | 1663-83G<br>Fatigue | 1664-83G<br>Stainless |
|--|---------------------|---------------------|-----------------------|
|--|---------------------|---------------------|-----------------------|

Elements detected by  
Induction Coupled Plasma,  
wt% (SL-ARC)

|                 |      |      |      |
|-----------------|------|------|------|
| Cobalt (Co)     | 58.6 | 51.5 | 0.31 |
| Chromium (Cr)   | 27.1 | 24.0 | 18.0 |
| Copper (Cu)     | 0.05 | 0.05 | 0.21 |
| Iron (Fe)       | 0.18 | 0.17 | 67.2 |
| Manganese (Mn)  | 2.3  | 2.2  | 4.7  |
| Molybdenum (Mo) | 6.05 | 5.35 | 2.55 |
| Nickel (Ni)     | 2.10 | 0.16 | 14.0 |
| Phosphorus (P)  | 0.70 | 0.61 | 0.40 |
| Sulfur (S)      | 0.16 | 0.15 | 0.15 |
| Silicon (Si)    | 0.82 | 0.99 | 1.46 |

DATE September 20, 1983

SIGNED

Gasoline & Oil Laboratory  
Alberta Research Council



## APPENDIX C

---

### Statistical Analyses of Corrosion Fatigue Life Data

The purposes of these analyses were as follows:

- A. To determine the acceptability of the high data point in the 5% serum results,
- ~~B. To determine if the two data sets are from different~~  
populations; that is, to determine if the serum had any statistical effect on the corrosion fatigue life, and
- C. To determine the upper and lower limits of the data populations, and to determine the statistical parameters of the arithmetic data values.

The statistical analyses were made based on the following two assumptions:

1. That the corrosion fatigue life data is log-normally distributed, and
2. While the means of the data may be shifted, the variance of the 5% serum data is equal to that of the 0% serum data. This assumption would be justified if the basic cracking mechanisms were the same in both cases.

Table C.1  
Fatigue Life Data in Natural Logarithm Form

| 0% Serum | 5% Serum |
|----------|----------|
| 10.692   | 10.162   |
| 10.296   | 9.765    |
| 10.509   | 10.254   |
| 10.332   | 12.084   |
| 10.568   |          |
| 10.189   |          |
| 11.032   |          |

If  $E(\ln x) = \lambda$ , and  $(\text{VAR}(\ln x))^{1/2} = \xi$

then  $\lambda_0 = 10.517$  and  $\xi_0 = 0.286$

and  $\lambda_5 = 10.566$  and  $\xi_5 = \xi_0$

#### A. High Data Value in 5% Serum Results

Based on the assumptions listed above, what is the upper limit for the 99.8% confidence interval based on a t-distribution with 3 degrees of freedom?

$$1 - \alpha = 0.998$$

$$\therefore 1 - (\alpha/2) = 0.999 \Rightarrow t = 10.2$$

$$\therefore \text{Upper limit} = \lambda_5 + t[\xi_5/(n^{1/2})]$$

$$= 10.566 + 10.2 (0.286/(4^{1/2}))$$

$$= 12.025$$

Since  $\ln(177000) = 12.084 > 12.025$ , then the data point can be rejected at a confidence interval of 80%.

Based on the rejection of this data point, the statistical parameters of the remaining data become as follows:

$$\lambda_s = 10.060; \zeta_s = 0.260$$

Although assumption 2, above, indicates that the standard deviation of the two sets shall be considered to be the same ( $\lambda = 0.286$ ), it is interesting to note how closely the actual standard deviation values compare. This similarity may indicate that the cracking mechanisms active in both test sets are, in fact, fundamentally the same.

#### B. Statistical Effect of the Serum

To determine if the serum had any statistical effect, a t-test is performed to test the following hypothesis:

$$\text{If } \lambda_o \neq \lambda_s, \text{ then } T \geq t.$$

With 2 degrees of freedom, and a confidence interval of 80%:

$$1 - \alpha = 0.80$$

$$\therefore 1^{\alpha} - (\alpha/2) = 0.90 \Rightarrow t = 1.886$$

$$\begin{aligned} T &= (\lambda_o - \lambda_s) / (\zeta / (n^{1/2})) \\ &= (10.517 - 10.060) / (0.286 / (3^{1/2})) \\ &= 2.768 \end{aligned}$$

Since T is, in fact, greater than t, the hypothesis is valid at the 80% confidence interval.

### C. Statistical Parameters

Based on the confidence intervals used in the above analyses, the total confidence interval is:

$$(0.80)(0.998) \cong 0.80 \text{ or } 80\%$$


---

#### 0% Serum

degrees of freedom = 6

$$\lambda_0 = 10.517$$

$$\xi_0 = 0.286$$

$$t = 1.440$$

$$\text{lower limit} = 10.361 \text{ (31603 cycles)}$$

$$\text{upper limit} = 10.673 \text{ (43160 cycles)}$$

#### 5% Serum

degrees of freedom = 2

$$\lambda_5 = 10.060$$

$$\xi_5 = 0.260$$

$$t = 1.886$$

$$\text{upper limit} = 9.777 \text{ (17622 cycles)}$$

$$\text{lower limit} = 10.343 \text{ (31042 cycles)}$$

Based on the equations given by Hald<sup>11</sup>, the statistical parameters of the original data (assuming the log-normal distribution) are:

#### 0% Serum

$$\text{median } x_0 = \text{anti-ln } (\lambda_0)$$

$$= 36897 \text{ cycles}$$

$$\text{mode } x_0 = \text{anti-ln } (\lambda_0 - 2.030\xi_0^2)$$

$$= 34009 \text{ cycles}$$

$$\begin{aligned}\text{mean } x_0 &= \text{anti-ln } (\lambda_0 + 1.1513\lambda_0^2) \\ &= 38432 \text{ cycles}\end{aligned}$$

5% Serum

---

Similarly:

median  $x_5$  = 23388 cycles

mode  $x_5$  = 21857 cycles

mean  $x_5$  = 24194 cycles